MICROTUBULE ASSEMBLY AND TRANSLOCATION DYNAMICS DURING AXONAL ELONGATION

by

Kristi McElmurry

A Dissertation

Submitted to the Faculty of Purdue University

In Partial Fulfillment of the Requirements for the degree of

Doctor of Philosophy

Department of Biological Sciences

West Lafayette, Indiana

May 2019

THE PURDUE UNIVERSITY GRADUATE SCHOOL
STATEMENT OF COMMITTEE APPROVAL

Dr. Daniel Suter, Chair
Department of Biological Sciences
Dr. Peter Hollenbeck
Department of Biological Sciences
Dr. R. Claudio Aguilar
Department of Biological Sciences
Dr. Fang Huang
Department of Biomedical Engineering

Approved by:

Dr. Janice Evans
Head of the Graduate Program

This work is dedicated to Mom, Dad, Ryan, and Kim who are the bedrock of my being.

ACKNOWLEDGMENTS

I am grateful to the countless number of people who have supported me personally and professionally throughout my life. This work is a result of your kindness, mentorship, and encouragement.

I am thankful for those who specifically contributed to this work. Dr. Daniel Suter guided me through the doctoral process. His generous gifts of thoughtfulness, patience, and time made this project possible. Additionally, I am grateful to committee members Dr. Peter Hollenbeck, Dr. Claudio Aguilar, and Dr. Fang Huang who provided their knowledge, expertise, and resources. I am also thankful for Dr. Donghan Ma, Dr. Yuan Ren, Dr. Kyle Miller, Aslihan Terzi, Jessica Stone, and Yueyun Zhang who took the time to mentor me and collaborate with me on the front lines.

PREFACE

The views expressed in this thesis are those of the author and do not reflect the official policy or position of the United States Air Force, Department of Defense, or the United States Government.

TABLE OF CONTENTS

LIST OF TABLES

LIST OF FIGURES

ABSTRACT

Author: McElmurry, Kristi. PhD
Institution: Purdue University
Degree Received: May 2019
Title: Microtubule Assembly and Translocation Dynamics During Axonal Elongation
Committee Chair: Dr. Daniel Suter

The urgency for deeper knowledge about nervous system function and dysfunction has never been greater. With increasing rates of mental disorders and expanding healthcare costs, deciphering details of axonal development is essential to meeting this imperative. Models of neuronal growth are improving as roles of microtubules and motor proteins surface. However, traditional motor protein studies focus on intracellular cargo transport, leaving deficits in knowledge about how these proteins organize cytoskeletal filaments in the axon and growth cone during neuronal development. Inconsistent findings on microtubule activity in growing axons also leave gaps in quantitative assessments of microtubule translocation and assembly, limiting the ability to construct a comprehensive model of axonal elongation.

The goal of this study was to provide a more complete neuronal growth cone model by determining how individual microtubule translocation and assembly, mass microtubule movements, and motor protein activity contribute to axonal elongation. The underlying mechanisms of these processes were investigated by testing the roles of dynein and microtubule dynamics in axonal elongation of *Aplysia californica* neurons using transillumination, fluorescent speckle, and super-resolution microscopy. Pharmacologically inhibiting either dynein activity or microtubule assembly reduced both bulk and individual microtubule anterograde translocation and neurite elongation rates. Suppressing both processes simultaneously had compensatory rather than additive effects. Super-resolution imaging also revealed fewer dynein motors co-localized with microtubules when microtubule assembly was inhibited. These results strongly suggest that disrupting microtubule assembly blocks neurite outgrowth partly because it inhibits dynein-mediated bulk microtubule translocation.

CHAPTER 1. INTRODUCTION

1.1 Imperative for Greater Knowledge of Growth Cones and Microtubules

Post-traumatic stress disorder (PTSD), major stress disorder, and traumatic brain injury (TBI) affect 31% of previously deployed service members. However, they represent only a portion of the 43 million Americans suffering from mental health conditions and cognitive impairment (Tanielian et al., 2008). Moreover, the World Economic Forum reports mental health disorders as the largest health care expenditures at $2.5 trillion annually with projections to exceed $6 trillion by 2030, and these costs do not account for associated biological, emotional, social, or health deficits (Candeias and Diabo, 2018; Insel, 2015; Insel, 2008; Tanielian et al., 2008). These data emphasize the urgency for greater knowledge of nervous system intricacies and impairments to prevent, diagnose, and treat the 450 million people living with mental disorders across the globe (Candeias and Diabo, 2018). Achieving a more comprehensive understanding of axonal growth cone and microtubule dynamics serves as a foundation to meet this imperative because targeting them holds promise for designing neuronal regeneration strategies for treating neurological damage and disorders, including Parkinson's disease, Alzheimer's disease, and amyotrophic lateral sclerosis (Hur et al., 2012; Kapitein and Hoogenraad, 2015; McMurray, 2000; Millecamps and Julien, 2013).

1.2 Growth Cones and Microtubules

Santiago Ramon y Cajal's investigations into the central nervous system inspired the modern era of neuroscience research (Stahnisch and Nitsch, 2002). His discovery of neuronal growth cones in 1890 sparked diverse inquiries into the mechanisms governing their behavior and provided the basis for contemporary theories of neuronal development (Tamariz and Varela-Echavarria, 2015). Despite decades of discovery, the intricacies of growth cone guidance and migration continue to provide exciting, unexplored frontiers.

Growth cones are highly motile sensory structures at the distal tips of elongating axons that migrate microns to meters to connect with precise targets (Dent and Gertler, 2003; Lowery and Van Vactor, 2009; Omotade et al., 2017; Pollard et al., 2017). They steer, advance, and retract

by processing soluble and insoluble cues to continuously reorganize the primary cytoskeletal components, microtubules and filamentous actin (F-actin), which are essential for coordinated growth cone motility and guidance (Geraldo and Gordon-Weeks, 2009; Gomez and Letourneau, 2014; Lowery and Van Vactor, 2009; Suter and Forscher, 1998; Suter and Forscher, 2000). These polymers drive proper neurite elongation and synapse formation via specific arrangements and behaviors that vary across the three growth cone domains: central (C), transitional (T), and peripheral (P) (Fig. 1.1) (Davenport et al., 1993; Miller and Suter, 2018). Dense microtubule bundles splay as they extend into the growth cone C domain where they contact F-actin arcs (Dent and Kalil, 2001; Marx et al., 2013; Miller and Suter, 2018; Schaefer et al., 2002; Tanaka and Kirschner, 1991). Microtubule looping and catastrophe limit extension beyond this domain, but some pioneering microtubules advance into the growth cone periphery where they encounter F-actin matrices (Marx et al., 2013; Miller and Suter, 2018; Schaefer et al., 2002). In the P domain, F-actin bundles guide trailblazing microtubules to the cell boundary and push the membrane forward to form filopodia and lamellipodia, two fundamental structures for motility (Fig. 1.1) (Gallo, 2011; Lewis and Bridgman, 1992; Mallavarapu and Mitchison, 1999; Miller and Suter, 2018; Suter et al., 2004). F-actin acts as a microtubule polymerization guide and pushes the cell edge forward while generating tension (Korobova and Svitkina, 2008; Medeiros et al., 2006; Schaefer et al., 2002). It also sweeps microtubules backward as it recycles materials during retrograde flow (Korobova and Svitkina, 2008; Medeiros et al., 2006; Schaefer et al., 2002; Suter and Miller, 2011). The complex interplay of actin dynamics, microtubule dynamics, microtubule translocation, and related forces are required for neurite outgrowth but are poorly understood.

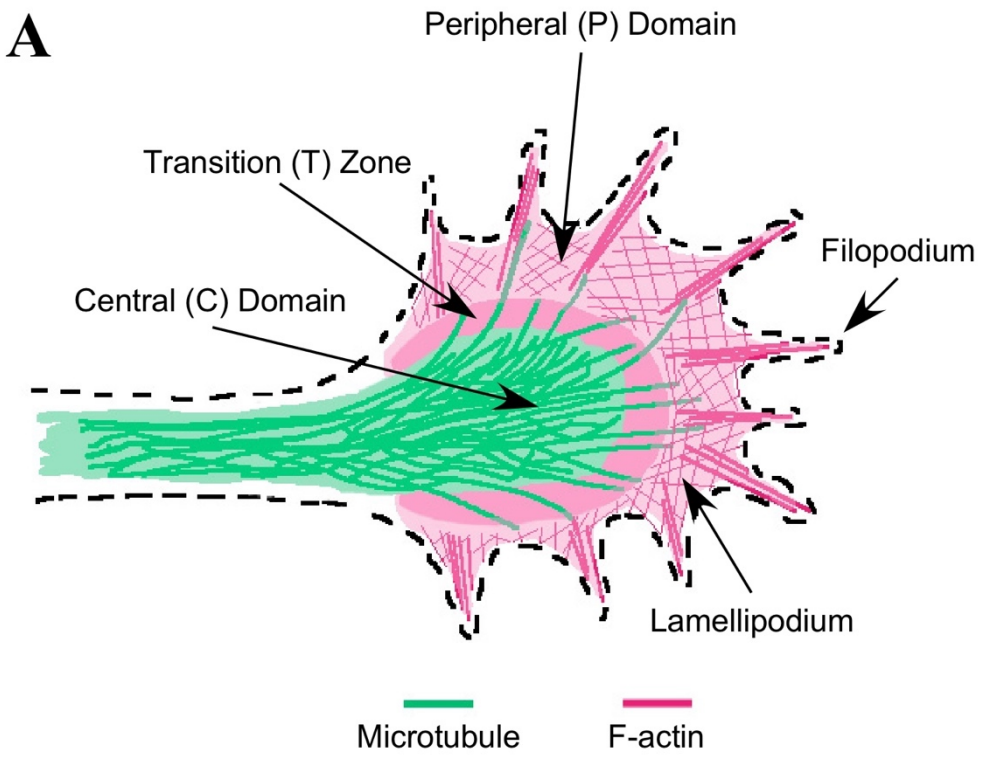

Figure 1.1. Growth cone domains

Growth cones are highly motile sensory structures at the distal tips of maturing neurites. (A) The diagram depicts microtubules densely packed in the axon and growth cone central domain. Pioneering microtubules explore the transition zone and peripheral domain, but actin filaments are primarily found in these regions. Actin acts as a microtubule polymerization guide, but it also sweeps them rearward as it recycles organelles and materials. (B) The image displays growth cone domains in an *Aplysia californica* bag cell neuron. Scale: 10 μm.

Dynamic microtubules with diverse lengths, varying stability, and specific orientations are among the multitudinous requisites for neuronal motility (Baas et al., 2016). Microtubules are more stable and uniformly oriented, with plus-ends directed away from the cell body, in axons than in dendrites (Baas et al., 1988; Baas and Lin, 2011; Baas et al., 2016; Burton and Paige, 1981; Heidemann et al., 1981; Kapitein and Hoogenraad, 2015). These hollow structures range from less than 1 μm to greater than 100 μm in length and contain 10-15 protofilaments of α-tubulin and β-tubulin heterodimers (Fig. 1.2) (Baas and Lin, 2011; Baas et al., 2016; Bray and Bunge, 1981; Conde and Caceres, 2009; Yu and Baas, 1994). A γ-tubulin complex caps the slow-growing microtubule minus end and serves as a template for proper nucleation and assembly, ensuring β-tubulin monomers point toward the plus end and α-subunits point toward the minus end (Conde and Caceres, 2009). The microtubule plus end is typically capped by a ring of several hundred β-tubulin subunits bound to guanosine triphosphate (GTP) (Bieling et al., 2007; Brouhard and Rice, 2018; Inoue and Salmon, 1995). This ring forms when β-tubulin-GTP dimers are incorporated into the microtubule before GTP is hydrolyzed to guanosine diphosphate (GDP) (Inoue and Salmon, 1995; Jordan and Kamath, 2007). GTP hydrolysis produces a GDP-bound β-subunit that remains in place until the cap is lost through the action of microtubule-associated proteins (MAPs) and other regulatory molecules (Akhmanova and Steinmetz, 2008; Akhmanova and Steinmetz, 2015; Brouhard and Rice, 2018; Howard and Hyman, 2007; Rochlin et al., 1996). Microtubules are intrinsically polar due to differences in tubulin dimers (Baas et al., 2016). Tubulin addition is less favored at the generally stable minus ends, where α-tubulin is exposed, while it is favored at fast-growing plus ends, where β-tubulin is exposed (Akhmanova and Steinmetz, 2010; Baas et al., 2016). Because of differences in α- and β-tubulin, the length of the microtubule polymer is also polar (Baas et al., 2016).

1.2.1 Microtubule dynamics

Dynamic instability describes the random nature of microtubule polymerization that results in continuous cycles of growth and shrinkage at microtubule plus ends (Baas and Black, 1990; Bamburg et al., 1986; Kalil and Dent, 2014; Mitchison and Kirschner, 1984a). These dynamics are characterized by four phases: slow growth, catastrophe, rapid depolymerization, and recovery (Fig. 1.2) (Desai and Mitchison, 1997; Mitchison and Kirschner, 1984a; Mitchison and

Kirschner, 1988). Catastrophe marks the abrupt transition from elongation to depolymerization, and rescue denotes the transition from shortening back to growth (Coombes et al., 2013; Walker et al., 1988). Although evidence shows that dynamics and translocation enable microtubules to reorganize and explore the growth cone periphery, the mechanisms underlying transitions between rescue and catastrophe are complex and unclear (Akhmanova and Steinmetz, 2015; Kalil and Dent, 2014; Lee and Suter, 2008; Tanaka et al., 1995; Tanaka and Kirschner, 1991).

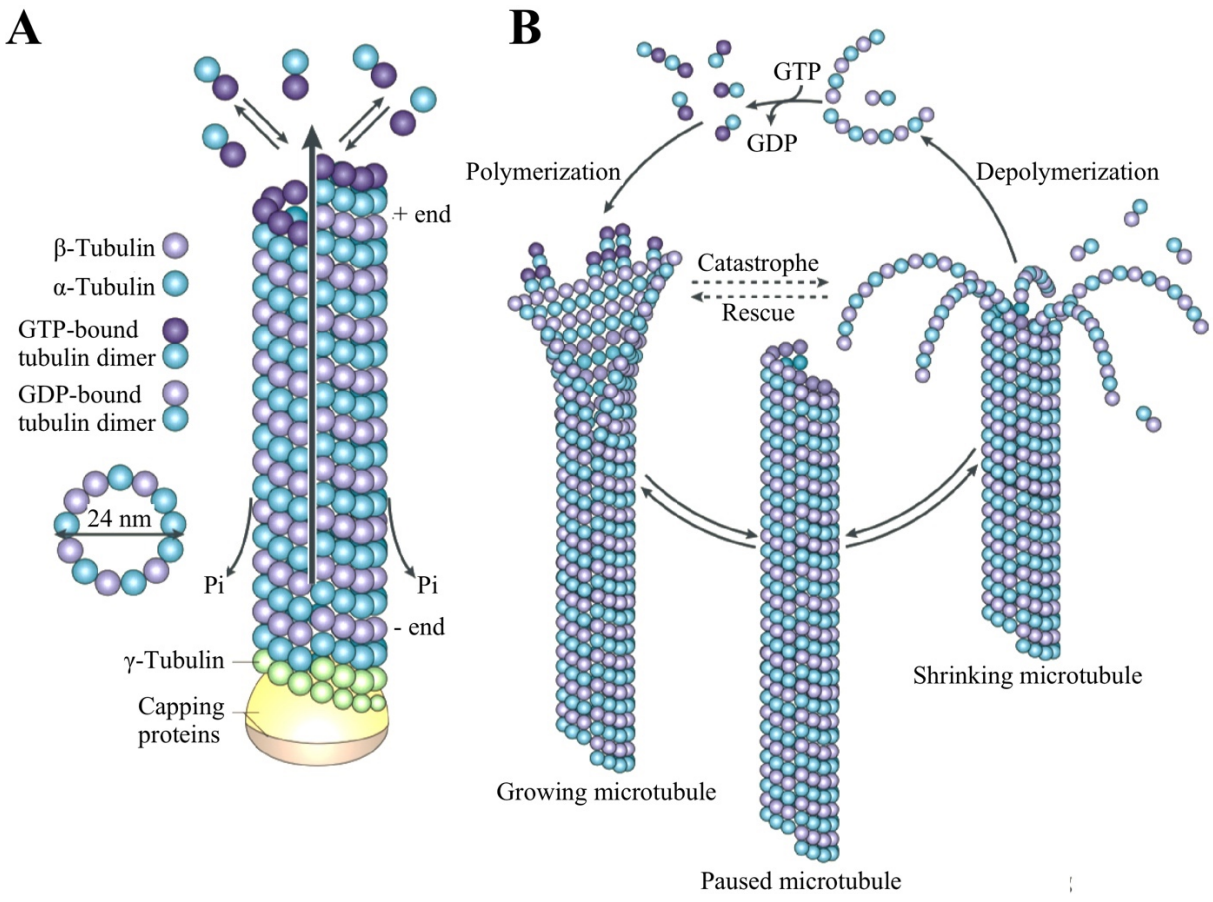

Figure 1.2. Microtubule dynamics

Microtubules contain 10-15 protofilaments of α- and β-tubulin heterodimers (Conde and Caceres, 2009). A γ-tubulin network caps the microtubule minus end and provides a template for microtubule nucleation and assembly (Conde and Caceres, 2009). GTP hydrolysis controls tubulin addition and integration as microtubules cycle independently through polymerization, catastrophe, depolymerization, and rescue. This figure is reprinted from Conde and Caceras (2009) with minor alterations in accordance with permission granted by Springer Nature (license number 4571401511337) (Conde and Caceres, 2009).

1.2.2 Tubulin and microtubule post-translational modifications

A number of soluble tubulin and microtubule post-translational modifications (PTMs) have been documented (Song and Brady, 2015). Although it is well established that PTMs influence microtubule dynamics and protein interactions, their precise impacts remain unclear (Song and Brady, 2015; Wloga et al., 2017). Examining details of detyrosination, acetylation, and polyglutamylation provides a glimpse into the broad influences PTMs have on microtubules (Hubbert et al., 2002; Janke and Bulinski, 2011; North et al., 2003; Song and Brady, 2015; Szyk et al., 2014; Van Dijk et al., 2008; Webster et al., 1990; Wloga and Gaertig, 2010).

During detyrosination, cytosolic carboxypeptidase (CCP) removes a terminal tyrosine on tyrosinated (Tyr) α-tubulin to expose a glutamate and convert it to detyrosinated (Glu) tubulin (Gundersen et al., 1987; Song and Brady, 2015). Conversely, tubulin tyrosine ligase (TTL) tyrosinates Glu-tubulin (Ersfeld et al., 1993; Raybin and Flavin, 1975; Wloga et al., 2017). Detyrosination is characteristic of aged microtubules but does not directly alter microtubule polymerization or stabilization (Khawaja et al., 1988; Webster et al., 1990). End-binding protein (EB) 1, a microtubule plus-end tracking protein (+TIP), is also unaffected by detyrosination (Song and Brady, 2015). However, cytoskeleton-associated proteins with a glycine-rich (CAP-Gly) domain, such as cytoplasmic-linker protein (CLIP)-170 and $p150^{Glued}$, require both EB1 and Tyr-tubulin to interact with microtubule plus ends and mediate microtubule rescue and catastrophe (Akhmanova and Steinmetz, 2015; Bieling et al., 2008; Komarova et al., 2002; Lazarus et al., 2013; Song and Brady, 2015). Although experimental results vary, tubulin detyrosination and tyrosination have been shown to influence motor proteins (Song and Brady, 2015). For example, studies on hippocampal neurons from TTL-knockout mice have shown kinesin-1 accumulates in axons and somatodendritic regions when Glu-tubulin levels increase (Konishi and Setou, 2009).

Tubulin acetylation occurs primarily on α-tubulin lysine 40 (Lys40) residues throughout the lumen of microtubules (Ledizet and Piperno, 1987; Song and Brady, 2015; Wloga et al., 2017). Acetylation α-acetyltransferase 1 (αTAT1), the primary acetyltranferase, appears to access the lumen of microtubules by diffusion (Szyk et al., 2014). Whereas αTAT1 acts slowly, two deacetylases, sirtuin 2 (SIRT2) and histone deacetylase 6 (HDAC6), quickly convert tubulin dimers upon incorporation into microtubules; therefore, acetylation increases with microtubule

age, but it has not been shown to indicate microtubule stability or affect polymerization rates after microtubule formation (Hubbert et al., 2002; North et al., 2003; Portran et al., 2017; Song and Brady, 2015; Wloga et al., 2017). Experiments with rat hippocampal neurons have demonstrated katanin preferentially binds to acetylated tubulin to increase microtubule severing, which strengthens the possibility that severing proteins are targeted to microtubules with abundant PTMs (Sudo and Baas, 2010).

Both α- and β-tubulin undergo polyglutamylation and polyglycylation, whereby enzymes with a TTL-related domain add glutamate or glycine to tubulin C-terminal side chains (Janke and Bulinski, 2011; Van Dijk et al., 2008; Wloga and Gaertig, 2010). Polyglutamylation, the major neuronal PTM, reduces the affinity of most MAPs for tubulin (Bonnet et al., 2001). However, it promotes spastin-mediated microtubule severing and differentially regulates MAP1 and MAP2 (Bonnet et al., 2001; Lacroix et al., 2010). Polyglycylation regulates cilia assembly and is confined to ciliary microtubules (Wloga et al., 2009).

Along with a number of additional PTMs, detyrosination, acetylation, and polyglutamylation, significantly influence microtubule dynamics and behavior (Song and Brady, 2015; Wloga et al., 2017). The number and complexity of possible tubulin and microtubule PTM combinations present challenges in understanding the unique impacts they have on cellular processes. Nevertheless, PTMs are integral to microtubule dynamics, organization, and interactions with other proteins (Song and Brady, 2015).

1.2.3 Mechanics of microtubule dynamics

In vitro reconstitution experiments have demonstrated that stable microtubules are more prone to catastrophe than newer, more dynamic microtubules (Howard et al., 2011). This aging behavior implies several molecular changes occur before microtubules transition from polymerization to depolymerization (Akhmanova and Steinmetz, 2015; Howard et al., 2011). Some studies have shown catastrophe is induced by an accumulation of microtubule lattice defects (Akhmanova and Steinmetz, 2015; Howard et al., 2011). Studies employing 3D mechanochemical simulations indicate catastrophe initiation involves tapering at the microtubule growth end and changes to GTP-tubulin cap size (Coombes et al., 2013). Furthermore, simulations and experiments in live cells suggest mechanical stress, such as pushing forces on the growth ends of microtubules, destabilizes the GTP-cap, which leads to its eventual loss and

subsequent microtubule catastrophe (Hunyadi et al., 2005; Janson et al., 2003). Less is known about rescue, but *in vivo* experiments using recombinant antibodies that bind to GTP-tubulin in microtubules have revealed rescue may depend upon microtubule lattice features, such as the presence of GTP-tubulin at the tip of a depolymerizing microtubule (Dimitrov et al., 2008).

Cryo-EM reconstructions and protein crystallography demonstrate that tubulin dimers undergo conformational changes from curved, to expanded, to compacted during growth and shrinkage (Alushin et al., 2014; Brouhard and Rice, 2018; Ravelli et al., 2004; Zhang et al., 2015). Mammalian studies have shown GTP-rich tubulin dimers are curved in the free state, expand and straighten following microtubule binding, and compact into the microtubule lattice following phosphate release (Alushin et al., 2014; Buey et al., 2006; Nawrotek et al., 2011; Rice et al., 2008). It remains unclear whether compaction is conserved across species, but cryo-EM studies have revealed GDP-tubulin relaxes to its curved conformation after catastrophe (Brouhard and Rice, 2018; Mandelkow et al., 1991). Microtubules store and release strain energy due to tubulin conformational changes; tubulin binding and straightening induces strain energy in the microtubule lattice, and tubulin relaxation and curving releases energy during catastrophe (Brouhard and Rice, 2018; Coue et al., 1991; Hyman et al., 1995; Koshland et al., 1988; Mandelkow et al., 1991). These conformational and energy changes are directly related to microtubule mechanics measured by *in vitro* purified tubulin and microtubule seed assays which demonstrated that microtubule movements generate and respond to changes in energy and forces (Dogterom and Yurke, 1997; Koshland et al., 1988). These examinations showed that growing microtubules generate pushing forces when they encounter a barrier and that shrinking microtubules generate pulling forces on objects coupled to them (Dogterom and Yurke, 1997; Koshland et al., 1988). Changes in microtubule dynamics in response to compressive and tensile stresses indicate microtubules also react to pushing and pulling forces exerted upon them (Brouhard and Rice, 2018; Dogterom and Yurke, 1997; Miller and Suter, 2018; Rice et al., 2008).

Pushing and pulling forces are known to influence microtubule dynamics but little is known about how forces generated by microtubule assembly affect axonal elongation. Early studies employing microtubule assembly inhibitors and stabilizers suggested microtubule assembly was the driving force behind growth cone motility and axonal elongation (Bamburg et al., 1986; Letourneau and Ressler, 1984). However, more recent investigations revealed individual and

bulk microtubule movements play strong roles in neurite outgrowth (Athamneh et al., 2017; Lee and Suter, 2008; Schaefer et al., 2002). Delineating the contributions of such movements complicates emerging questions about whether microtubule assembly or microtubule translocation is more influential during axonal elongation. Previous studies have indicated individual microtubule translocation initiates neurites, whereas mass microtubule movements drive subsequent neurite outgrowth (Athamneh et al., 2017; Baas and Yu, 1996; Chang et al., 1998; Lee and Suter, 2008; Lu et al., 2013; Lu and Gelfand, 2017). Further defining differences between these movements and fully deciphering how microtubule dynamics, individual translocations, and mass movements alter neuronal force balance and neurite behavior requires continued measurements of these activities and their relationships to one another (Miller and Suter, 2018).

1.3 Microtubule-Associated Proteins

MAPs regulate microtubule dynamics, translocation, and organization to mediate distinct cellular functions, including growth cone steering and advance; they include stabilizing, severing, destabilizing, and plus-end tracking proteins (Brouhard et al., 2008; Desai and Mitchison, 1997; Kalil and Dent, 2014; Kapitein and Hoogenraad, 2015; McNally and Vale, 1993; van der Vaart et al., 2009; Wiese and Zheng, 2006; Wong and Hashimoto, 2017). MAPs perform unique functions in growth cone motility and axonal branching, and they play important roles in regulating microtubule transitions from growth to shrinkage (Akhmanova and Steinmetz, 2015; Kalil and Dent, 2014). Microtubule polymerases, including members of the XMAP215 +TIP family, are important regulators that bind to microtubule plus ends, recruit tubulin subunits, and promote tubulin addition at growing tips (Al-Bassam et al., 2012; Brouhard et al., 2008). EBs are polymerases that promote microtubule assembly and suppress catastrophe in part by modulating the structure of microtubule ends (van der Vaart et al., 2011). Depolymerases, such as mitotic centromere-associated kinesin (MCAK), induce catastrophes by removing tubulin subunits through adenosine triphosphate (ATP) hydrolysis (Desai et al., 1999; Hunter et al., 2003; Moores et al., 2002; van der Vaart et al., 2011). Live-cell imaging and gliding assays indicate other kinesins stabilize microtubules by decreasing tubulin turnover at the plus tip to inhibit microtubule growth and catastrophe (Du et al., 2010; Hafner et al., 2014; Stumpff et al.,

2008). CLIPs and CLIP-associated proteins (CLASPS) also suppress catastrophes and stimulate rescues by binding to microtubule lattices and recruiting tubulin dimers (Al-Bassam et al., 2010; Komarova et al., 2002; Mimori-Kiyosue et al., 2005; van der Vaart et al., 2011). The CAP-Gly domain proteins CLIP-170 and $p150^{Glued}$ promote rescue and suppress catastrophe, respectively (Akhmanova and Steinmetz, 2015; Komarova et al., 2002; Lazarus et al., 2013). Largely through interactions with $p150^{Glued}$, the motor protein dynein regulates microtubule dynamics by capturing and anchoring microtubules at the cell cortex, where it exerts pulling forces and grasps shrinking plus ends to reduce depolymerization (Hendricks et al., 2012; Laan et al., 2012). MAPs also include linker proteins, such as actin cross-linking factor 7 (ACF7), also known as microtubule-actin-crosslinking-factor (MACF) 1, and bullous pemphigoid antigen (BPAG), that are responsible for anchoring microtubules to the cytoskeletal network and the plasma membrane (Houseweart and Cleveland, 1999).

Several MAPs exploit tubulin structural changes to regulate microtubule dynamics by selectively binding to specific tubulin conformations (Brouhard and Rice, 2018). EBs mediate changes from expanded to compacted conformations along the microtubule while other MAPs, such as stathmin (STMN1), regulate transitions between curved and straight tubulin heterodimer conformations at the growing microtubule end (Belmont and Mitchison, 1996; Steinmetz et al., 2000). Preferential binding of MAPs to curved tubulin heterodimers has been shown to promote both microtubule depolymerase and polymerase activity, which emphasizes the complexity of MAP-tubulin relationships in microtubule dynamics. This is evidenced by studies that show kinesin-related protein 3 (KIP3) promotes microtubule catastrophe by binding preferentially to curved tubulin heterodimers (Gupta et al., 2006; Varga et al., 2006; Varga et al., 2009). Meanwhile, other investigations show that polymerases from the suppressor of tubulin 2 (Stu2)/XMAP215 family also preferentially bind to curved tubulin heterodimers via tumor-overexpressed gene (TOG) domains to promote microtubule assembly (Ayaz et al., 2014; Ayaz et al., 2012; Brouhard et al., 2008; Hussmann et al., 2016).

+TIPs accumulate at the ends of growing microtubules and regulate interactions with cellular structures, responses to signals, and reactions to forces (Akhmanova and Steinmetz, 2008). They form networks via protein modules and linear sequence motifs to mediate associations with each other and microtubules, and they serve as adaptors for actin-binding proteins (Akhmanova and Steinmetz, 2010; Marx et al., 2013). Although many +TIPs can associate directly with

microtubules, most interact with microtubule plus ends by binding to EBs, the master +TIP regulators (Akhmanova and Steinmetz, 2008; van der Vaart et al., 2011).

EBs regulate microtubule dynamics and mediate most +TIP-microtubule interactions, including CLIP-170, MCAK, MACF, stromal interaction molecule 1 (STIM1), and CLASP2 (Bieling et al., 2008; Dixit et al., 2009; Gouveia et al., 2010; Honnappa et al., 2009; Kumar et al., 2012; Kumar and Wittmann, 2012). They recognize both ends of microtubules and preferentially bind to newly polymerized microtubule plus ends (Akhmanova and Steinmetz, 2015; Kumar and Wittmann, 2012). EBs contain an N-terminal calponin homology (CH) domain, a variable linker region, a coiled-coil domain, and a C-terminal dimerization domain with +TIP binding sites (Buey et al., 2006; De Groot et al., 2010; Hayashi and Ikura, 2003; Slep et al., 2005). The CH domain is responsible for microtubule interactions; phosphorylated Ser, Thr, and Tyr residues in the linker region regulate EB functions (Ferreira et al., 2013; Iimori et al., 2012; Komarova et al., 2009; Slep et al., 2005; Xia et al., 2014; Zimniak et al., 2009). Interactions between the CH-linker region and the C-terminal domain refine EB specificity toward microtubule tips (Buey et al., 2006).

EBs recruit proteins with serine-X-isoleucine-proline (SxIP) motifs and CAP-Gly domains to growing microtubule ends (Almeida et al., 2017; Duellberg et al., 2014; Honnappa et al., 2009). The SxIP motif and CAP-Gly domains enable transient interactions between +TIPs and the formation of flexible networks around elongating microtubules (Akhmanova and Steinmetz, 2015). They also prompt competition among +TIPs due to the limited number of specific binding sites (Duellberg et al., 2014). *In vitro* reconstitution studies reveal layers of regulation are required to control +TIP organizational hierarchies (Duellberg et al., 2014). Some studies support the idea that strictly regulated +TIP networks promote microtubule assembly by restricting conformation changes at the microtubule plus end (Gupta et al., 2014).

1.3.1 Microtubule-actin cross-linking factor

MACF is a 608 kDA +TIP spectraplakin that associates with actin and microtubules (Leung et al., 1999; Sun et al., 2001; Wu et al., 2008) (Fig. 1.3). Spectraplakins regulate cytoskeletal reorganization during development and following injury (Broderick and Winder, 2005; Liem, 2016; Roper et al., 2002; Zhang et al., 2017). They are large, evolutionarily conserved proteins from the spectrin superfamily that bind to cytoskeletal networks to mediate cytoskeletal

dynamics (Broderick and Winder, 2005; Liem, 2016; Roper et al., 2002). MACF1 and BPAG1, also known as dystonin (DST), encode mammalian spectraplakins (Zhang et al., 2017).

Spectraplakin domains include a central rod domain with 23 dystrophin-like spectrin repeats, calponin actin-binding domains, and a plakin domain (Fig. 1.3) (Gouveia and Akhmanova, 2010; Sun et al., 2001). Spectraplakins also have two EF-hand calcium-binding motifs, a region homologous to the microtubule-binding growth arrest specific 2 (GAS2) and GAS-related (GAR) 22 proteins, and an ATPase domain (Fig. 1.3) (Gouveia and Akhmanova, 2010; Sun et al., 2001; Suozzi et al., 2012; Wu et al., 2008; Zhang et al., 2017). The C-terminus is basic and serine rich (Gouveia and Akhmanova, 2010; Leung et al., 1999; Sun et al., 2001; Wu et al., 2008).

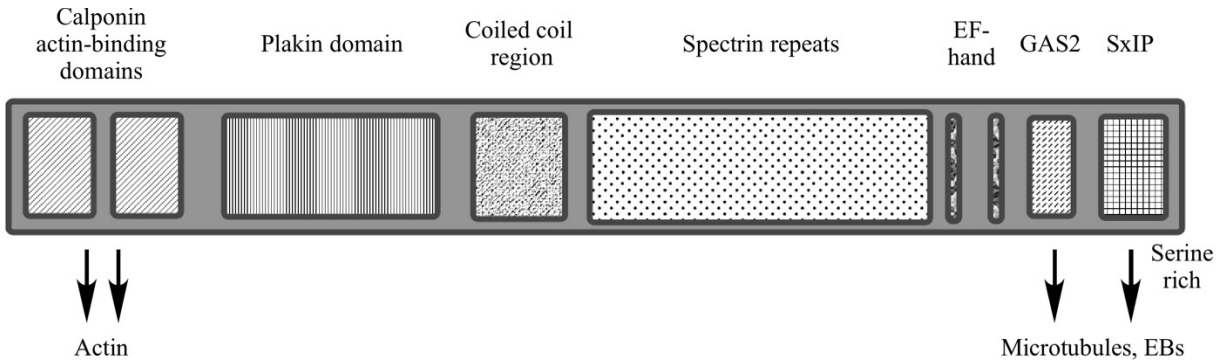

Figure 1.3. Microtubule-actin cross-linking factor

MACF is a +TIP spectraplakin that associates with microtubules and actin. Spectraplakin N-terminal regions consist of a calponin actin-binding domain, a plakin domain, a central rod with spectrin repeats, an EF-hand motif, microtubule-binding GAS2 domains, and a serine-rich C-terminus (Gouveia and Akhmanova, 2010; Leung et al., 1999; Suozzi et al., 2012).

Due to their structure and function, spectraplakins are involved in numerous physiological pathways. The plakin domain facilitates binding to intermediate filaments to link them to membrane proteins and adhesive junctions (Jefferson et al., 2004). Spectrin repeats are spacers between the N- and C-termini that enable elastic responses in proteins subject to mechanical force (Djinovic-Carugo et al., 2002; Roper and Brown, 2003; Sonnenberg et al., 2007). MACF1 spectrin repeats associate with proteins in the Wnt signaling pathway and bind to calmodulin-regulated spectrin-associated protein 3, a microtubule minus-end-binding protein (Chen et al.,

2006; Noordstra et al., 2016; Zhang et al., 2017). Adjacent EF-hand and GAR domains are encoded in the C-terminal of spectraplakins (Zhang et al., 2017). The EF-hand motifs are involved in microtubule-BPAG1 binding (Kapur et al., 2012). Studies indicate that the GAR domain plays an accessory role in microtubule interactions (Alves-Silva et al., 2012; Applewhite et al., 2010).

Spectraplakins interact with EB1 to regulate microtubule dynamics and recruit +TIPs by associating with CAP-Gly or SxIP motifs (Akhmanova and Steinmetz, 2008; Gouveia and Akhmanova, 2010; Honnappa et al., 2009; Nehlig et al., 2017). MACF43, a 43-residue fragment of MACF2, contains an SxIP motif that interacts with EB1 and tracks growing microtubules (Gouveia and Akhmanova, 2010; Honnappa et al., 2009; Slep et al., 2005). It displays characteristic +TIP behavior by concentrating at the plus ends of polymerizing microtubules and dissociating exponentially as microtubules age (Gouveia and Akhmanova, 2010). This tendency for localization and dispersion results in comet patterns at microtubule plus ends (Gouveia and Akhmanova, 2010). The +TIP properties of MACF prompted the use of green fluorescent protein (GFP)-MACF43 as a +TIP tracker and marker for microtubule growth during this project.

1.3.2 Microtubule motor proteins

Microtubule motor proteins recognize polarity, which drives their directionality (Vale, 2003). Each of the two families of microtubule motor proteins, dyneins and kinesins, have a conserved motor domain that hydrolyses ATP to generate movement (Carter, 2013). Dynein moves toward the microtubule minus end, and most kinesins move toward the plus end, generating forces relative to microtubules (Ahmad et al., 2000; Roossien et al., 2015; Stiess et al., 2010).

Conventional motor protein studies have uncovered important details about cargo transport and have stirred curiosity about the additional roles motors play in microtubule processes. *Drosophila* neuronal studies show that kinesin-1 crosslinks microtubules and slides them along one another (Lu et al., 2013; Lu et al., 2015). Combining outcomes from experiments with chick dorsal root ganglia (DRG) neurons and COS-7 cells produces a model in which dynein pushes microtubules forward by simultaneously anchoring to stable structures, such as actin or the cell cortex, and binding to microtubules (Dehmelt et al., 2006; Roossien et al., 2014). Dynein may

also bind to two microtubules concurrently to slide them apart (Lu and Gelfand, 2017; Tanenbaum et al., 2013). A unified framework for kinesin and dynein microtubule sliding is that kinesin slides microtubules to initiate neurite outgrowth, and dynein transports microtubules from the centrosome or acentrosomal nucleation sites into axons and dendrites during development (Baas et al., 2016; Lu et al., 2013; Lu and Gelfand, 2017; Roossien et al., 2015; Stiess et al., 2010).

1.4 Dynein

All nine dynein subfamilies in eukaryotic cells move toward the microtubule minus end (Wickstead and Gull, 2007). Axonemal dyneins comprise seven subfamilies that slide microtubules past one other to produce beating motions in cilia and flagella (Carter, 2013). The remaining two subfamilies, cytoplasmic dynein 1 and 2, transport cargo (Carter, 2013). Cytoplasmic dynein 2 carries material into the axoneme within cilia and flagella; cytoplasmic dynein 1 (henceforth referred to as dynein) transports most non-axoneme, minus-end-bound cargo in cilia and flagella and most minus-end-directed cargo in other cells (Carter, 2013; Cole, 2003; Vale, 2003; Vallee et al., 2012).

Dynein is a 1.4 MDa, multi-subunit complex with a 380 kDa, AAA+ ATPase motor domain (Fig 1.4) (McKenney et al., 2014; Pfister et al., 2006; Urnavicius et al., 2015; Vallee et al., 2012). The complex contains two motor domain heavy chains (dynein heavy chains (DHCs)) and multiple additional subunits, including two intermediate chains (ICs) that bind to DHCs and three unique light chains (LCs) that bind to ICs (Fig. 1.4) (Allan, 2011; Vallee et al., 2012). Although ICs and light intermediate chains (LICs) are confined to the dynein complex, LCs interact with numerous partners (Allan, 2011; King et al., 1996; Pfister et al., 2006).

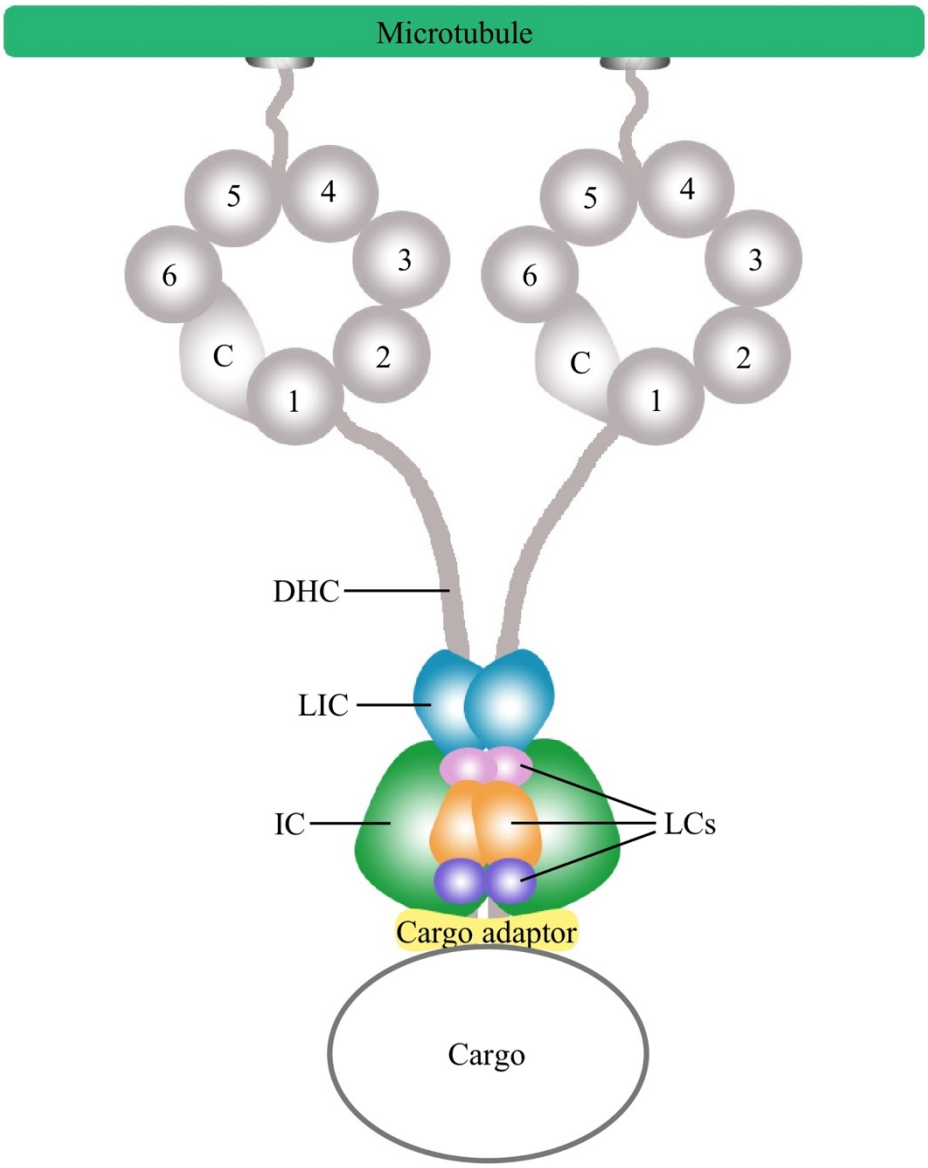

Figure 1.4. Dynein

AAA domains are numbered. C denotes the C-terminus of the heavy chain. The dynein complex contains two dynein heavy chains (DHCs) and several subunits, including two intermediate chains (ICs), and three light chains (LCs). LCs bind to ICs and interact with multiple partners, whereas ICs and light intermediate chains (LICs) are confined to the dynein complex. For simplification, many dynein mediators are not depicted. This figure was inspired by the representation in Pfister et al. (2006); this adaptation is depicted in accordance with the Creative Commons Attribution License (Pfister et al., 2006).

Two regulators, lissencephaly 1 (Lis1) and dynactin, generally govern dynein motility (McKenney et al., 2014). Lis1 cooperates with NudE, another regulator, to suppress dynein activity by preventing the motor domain from transmitting a detachment signal to the microtubule-binding domains (Fig. 1.4) (Huang et al., 2012). Lis1 thereby acts as a clutch that prolongs microtubule binding (Huang et al., 2012; McKenney et al., 2014; McKenney et al., 2010). Dynactin, a 1.0 MD protein complex with over 20 subunits, coordinates with dynein during active motor cycling (Siglin et al., 2013). Dynein IC and dynactin p150^{Glued} subunits are the principal mediators in dynein-dynactin interactions, but a stable complex forms only in the presence of a cargo adaptor (Siglin et al., 2013; Urnavicius et al., 2015). Thus, dynein is largely inactive, but motility is induced when an adaptor links it to cargo and dynactin (McKenney et al., 2014). Lis1 and p150^{Glued} promote dynein cargo loading and motility by recruiting it to microtubule plus ends via interactions with the +TIP CLIP-170 (Coquelle et al., 2002; Lansbergen et al., 2004; Watson and Stephens, 2006).

Dynein has substantial impacts on microtubules, including regulating dynamics, modulating movements, and tethering them to actin, other microtubules, and the cellular membrane (Duellberg et al., 2013; Grabham et al., 2007; Hendricks et al., 2012; Perlson et al., 2013; Roberts et al., 2013; Roossien et al., 2014; Yogev et al., 2017). It also counters forces generated by the actin motor non-muscle myosin II to indirectly affect growth cone advance (Vallee et al., 2009). Non-muscle myosin II localizes in the transition zone and in the growth cone neck (Fig. 1.5) (Suter and Miller, 2011; Vallee et al., 2009). It pulls in the retrograde direction to reorganize actin filaments as they extend rearward during polymerization (Vallee et al., 2009). Conversely, dynein pushes microtubules toward the distal edge, creating tension for microtubules to resist actin-generated forces in the growth cone and powering transport of short microtubules along the axon (Fig. 1.5) (Grabham et al., 2007; Myers et al., 2006; Roossien et al., 2014). Dynein also pushes microtubules forward *en masse* to reorganize the cytoskeletal network during neurite elongation (Roossien et al., 2014). This coordinated interplay of motor-generated actin pulling forces and microtubule pushing forces is integral to neuronal elongation (Heidemann et al., 1990).

Although knowledge of motor protein force generation has improved dramatically during the past few decades, subcellular mechanisms behind these forces remain undefined (Lamoureux et al., 1989; O'Toole et al., 2015). Relationships between motor-generated cytoskeletal movements

and microtubule dynamics must be quantified to produce more comprehensive models of neuronal development (Miller and Suter, 2018). The present study investigated the role of dynein in microtubule translocation and assembly to provide a baseline for quantifying these relationships.

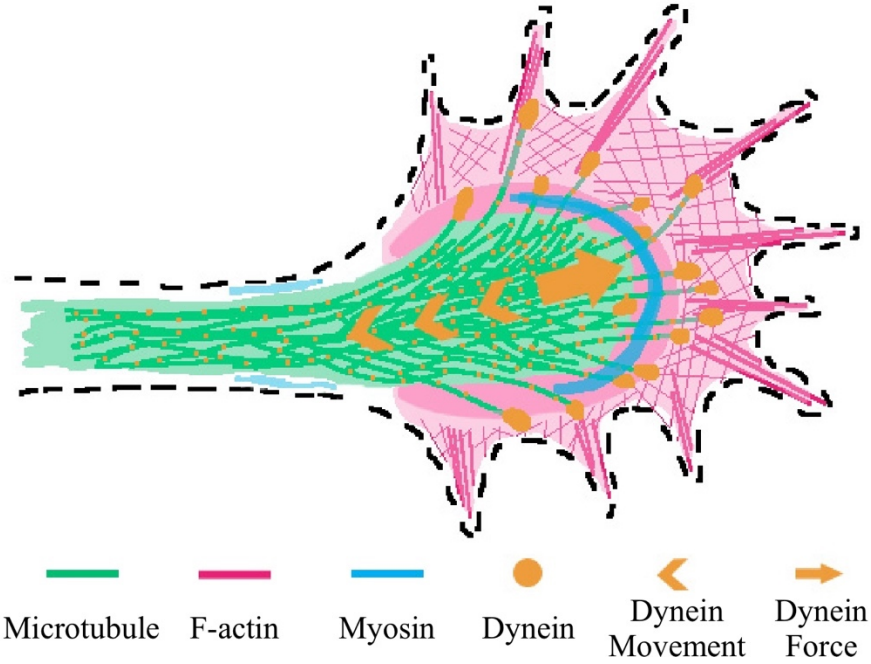

Figure 1.5. Dynein and non-muscle myosin II in the growth cone

Non-muscle myosin II localizes in the transition zone and the growth cone neck. Dynein localizes on plus ends of growing microtubules where it tethers them to the cortex, actin filaments, and other microtubules. As dynein transports materials toward the soma, it generates forces in the opposite direction that counter actin retrograde flow.

1.5 Microtubule Assembly, Translocation, and Mass Movement

Mass microtubule movements that drive cellular motility occur in a slow, unidirectional manner, differing from individual microtubule movements that initiate new neurites and contribute to axonal polarity establishment (Athamneh et al., 2017; Baas and Ahmad, 1993; Baas and Yu, 1996; Chang et al., 1998; Grego et al., 2001; Hutchins and Wray, 2014; Pfister, 2016). They are also distinct from microtubule assembly, which is important for axonal elongation, transport of materials, and structural support for translocation (Athamneh et al., 2017; Roossien et al., 2013; Tanaka and Kirschner, 1991). Independent inquiries into microtubule dynamics,

treadmilling, and translocation have employed a variety of pharmacological tools, such as microtubule assembly enhancers and inhibitors, and an array of isolated microscopy techniques, including phase microscopy, differential interference contrast (DIC) microscopy, and fluorescence speckle microscopy (FSM) (Ahmad et al., 2000; Mitchison and Kirschner, 1984b; Walker et al., 1988; Waterman-Storer and Salmon, 1998). These prior studies indicate microtubule dynamics, bulk motion, and individual movements are important for neurite growth (Fig. 1.6) (Roossien et al., 2013). They also emphasize the need to better understand the relative contributions of microtubule assembly and dynein-driven microtubule transport to axonal elongation. This project integrated previously isolated investigations by merging assembly, translocation, and dynein studies to clarify subcellular relationships contributing to neurite growth. Results strongly suggest microtubule dynamics and dynein-driven translocation are interdependent activities required for neurite growth.

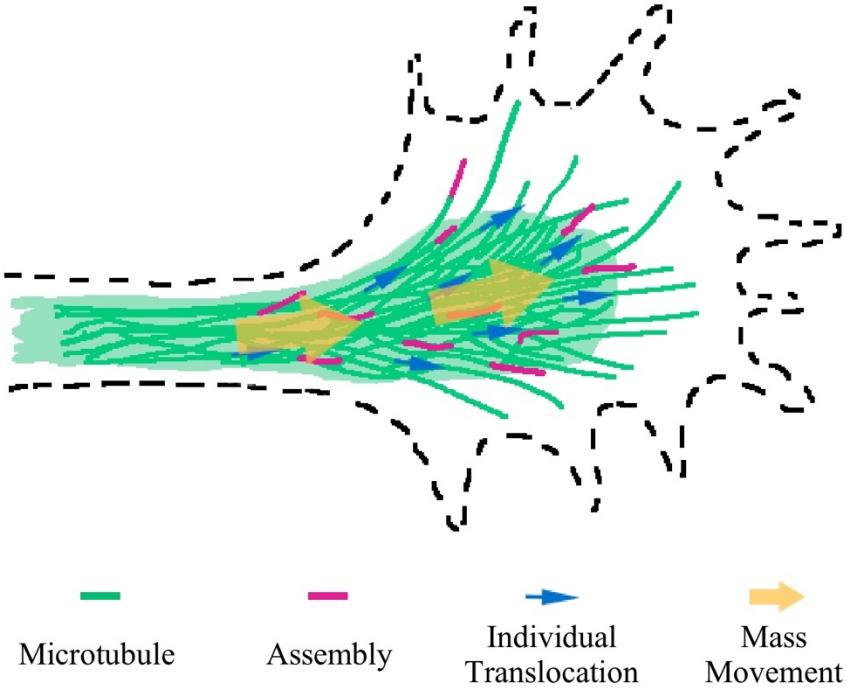

Figure 1.6. Microtubule assembly, translocation, and mass movement

Microtubule assembly and dynein-driven translocation are important for axonal elongation. Quantifying the relative contributions of these processes will enable more comprehensive models of neuronal development. Although depicted activities occur in all directions, the figure displays only anterograde assembly and movement in the growth cone to conceptualize the primary foci of this project.

CHAPTER 2. METHODOLOGY

2.1 Model System

The *Aplysia californica* is a marine mollusk with a simple nervous system comprised of approximately 20,000 neurons (Fig. 2.1 A, B) (Yali et al., 2009). *Aplysia* neurons are easily extracted from clearly discernable ganglia distributed throughout the body (Fig. 2.1 B). They are the largest neurons found in nature, making them ideal for cytoskeletal studies employing fixed and live-cell imaging techniques (Moroz, 2011).

Bag cell neurons responsible for egg-laying behavior are found in paired clusters of 200 to 400 cells in the abdominal ganglion (Magoski, 2017). These neuroendocrine cells range from 40 to 100 μm and extend processes in all directions (Conn and Kaczmarek, 1989) (Fig. 2.1 C). *Aplysia* bag cell neurons serve as a classical neuroscience model and were studied exclusively during this project.

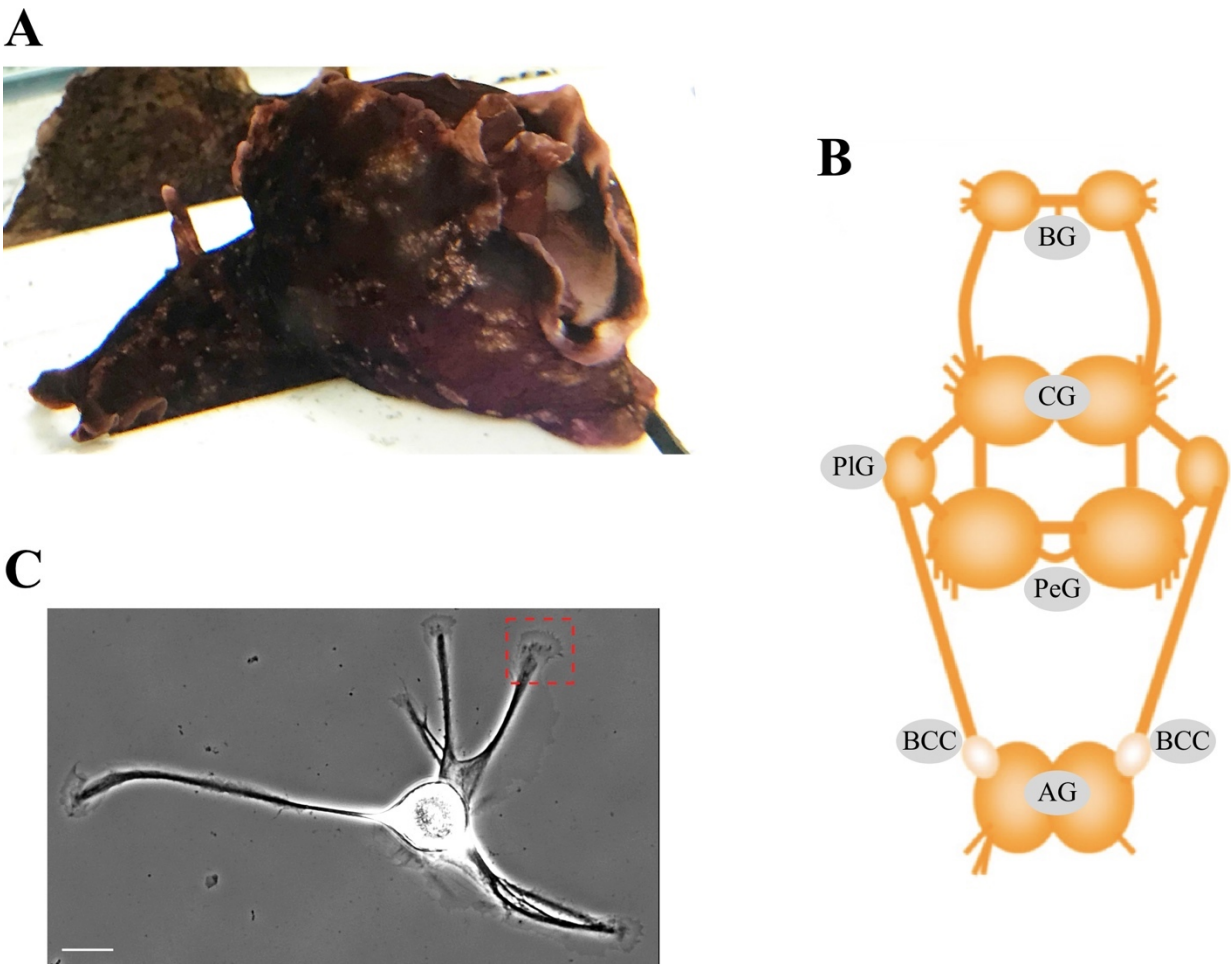

Figure 2.1. *Aplysia californica* bag cell model

(A) *Aplysia californica*. (B) *Aplysia* nervous system reprinted from Moroz et al. (2006) with minor adaptations in accordance with permission granted by Elsevier (license number 4572660328665) (Moroz et al., 2006). The bag cell cluster (BCC) and the buccal (BG), cerebral (CG), pleural (PlG), pedal (PeG), and abdominal (AG) ganglia are depicted. (C) Bag cell neuron. The boxed region outlines a growth cone at the tip of a neurite. Scale: 80 μm.

2.2 Pharmacological Tools

Taxol and nocodazole (Noc) were employed to modulate microtubule dynamics, and ciliobrevin D (CilD) was used to inhibit dynein activity. Taxol binds to β-tubulin subunits along the interior of microtubules to stabilize them against depolymerization without affecting structural integrity (Baas and Black, 1990; Jordan and Kamath, 2007; Suter et al., 2004). Low taxol concentrations promote microtubule assembly by dampening dynamics (Alushin et al.,

2014). High concentrations prohibit dynamics and destabilize microtubules, causing them to buckle and break under actomyosin retrograde forces (Dehmelt et al., 2003; Letourneau et al., 1987; Waterman-Storer and Salmon, 1997). Noc attenuates microtubule assembly by binding to free α-tubulin (Baas and Ahmad, 2013). Low doses of the drug stabilize microtubules by suppressing rapid polymerization and catastrophic shortening, and high concentrations dramatically reduce free tubulin availability and induce depolymerization (Baas et al., 2016; Rochlin et al., 1996; Vasquez et al., 1997). Ciliobrevins are specific, small-molecule dynein antagonists that inhibit ATPase activity and prevent the motor from cycling (Firestone et al., 2012; Sainath and Gallo, 2015; Ye et al., 2001). CilD reduces dynein function most effectively among this group of inhibitors (Firestone et al., 2012; Roossien et al., 2014).

2.3 Materials and Methods

2.3.1 Neuronal cell culture

Aplysia californica bag cell neurons were cultured in L-15 medium with artificial sea water (ASW) (400 mM NaCl, 9 mM $CaCl_2$, 27 mM $MgSO_4$, 28 mM $MgCl_2$, 4 mM l-glutamine, 50 μg/ml gentamicin, 5 mM 4-(2-hydroxyethyl)-1-piperazineethanesulfonic acid, pH 7.9) on coverslips or glass dishes coated with 20 μg/ml poly-L-lysine (P6282, Sigma-Aldrich, Inc.) in hemolymph after overnight digestion in dispase (D4693, Sigma-Aldrich, Inc.), as reported previously (He et al., 2015). Neurons were incubated overnight at 14°C before experimentation.

2.3.2 Pharmacological treatments

Cells were treated with 0.1% DMSO (controls), 1 μM Noc (M1404, Sigma-Aldrich, Inc.), 10 μM CilD (250401, Sigma-Aldrich, Inc.), or a combination of 10 μM CilD and 1 μM Noc in L-15 medium at 23°C. CilD was applied for 5 min before Noc to ensure dynein inhibition before microtubule assembly inhibition during combination treatments. Treated cultures were maintained at 14°C for 6 h during chronic studies. For acute studies, treatments were applied 5 min before imaging and cells were maintained at 23°C for the duration of the experiment. Immunostaining studies followed the 5 min acute treatment scheme before fixation.

Taxol studies followed similar protocols for chronic and acute treatments. Cells were treated with 1, 5, 10, 50, or 100 nM or 1 μM taxol (T1912, Sigma-Aldrich, Inc.) concentrations for 4 to 24 h for chronic studies. Taxol was applied to achieve 5 nM concentrations 30 min before imaging during acute studies.

2.3.3 Microtubule labeling for live-cell recordings

Aplysia neurons were injected with 1 mg/ml X-rhodamine tubulin in buffer (TL620M-A, BST01-001; Cytoskeleton, Inc.) one day after plating, as described previously (Lee and Suter, 2008). Tubulin was spun at 13,000 g for 30 min and stored on ice before injections. Microinjection pipettes (1B100F-4, World Precision Instruments) were prepared using a Narishige PP830 vertical system and chilled to 4°C before use. Cells recovered for a minimum of 1 h at 14°C before drug treatments.

2.3.4 Immunostaining

Aplysia cells were fixed with 3.7% formaldehyde in ASW with 400 mM sucrose for 15 min. They were permeabilized with 0.05% saponin in fixative for 10 min before washing in 0.005% saponin in phosphate-buffered saline (PBS). Blocking was performed with 10% bovine albumin serum in 0.005% saponin-PBS for 1 h. Samples were incubated for 3 h with antibodies against the 532 kDa dynein heavy chain-1 (DHC1) (DHC1 rabbit polyclonal antibody, 101452, GeneTex, Inc.) and the 52 kDa α-tubulin subunit (α-tubulin rat monoclonal antibody, MA1-80189, Thermo Fisher Scientific, Inc.) in blocking buffer at 1:250 dilution. Preparations were washed prior to incubating with Alexa Fluor 568-conjugated anti-IgG antibodies (goat anti-rat polyclonal antibodies, A-11077, Invitrogen) to label microtubules and Alexa Fluor 647-conjugated anti-IgG antibodies (goat anti-rabbit polyclonal antibodies, A-21244, Invitrogen) to label dynein at 1:250 in 0.005% saponin-PBS for 1 h. Samples were washed, and post-fixation was performed with 3.7% formaldehyde in ASW with 400 mM sucrose for 5 min before a final wash. All immunostaining procedures were conducted at room temperature.

Experiments using rabbit polyclonal non-muscle-myosin II heavy chain (NMIIHC) antibodies (a gift from the Forscher Lab, Yale University, New Haven, CT) followed DHC labeling procedures with minor alterations. Incubation time was 1 h with NMIIHC antibodies

rather than 3 h. Triton X-100 (9002-93-1, Sigma-Aldrich, Inc.) was used in place of saponin: 1.0% Triton was used for permeabilization and 0.1% Triton was used for washes.

For dynein IC experiments, sample preparation followed the DHC immunolabeling protocol, except samples were sequentially incubated with each antibody. Neurons were incubated with mouse monoclonal antibodies against two isoforms of 74 kDA dynein ICs (MA1-070, Thermo Fisher, Inc.) in blocking buffer for 3 h, then washed and incubated with Alexa Fluor 647-conjugated anti-IgG antibodies (goat anti-mouse polyclonal antibodies, A-21235, Invitrogen) in 0.005% saponin-PBS for 1 h. Dynein IC-labeled samples were washed, then incubated with α-tubulin rat monoclonal antibodies (MA1-80189, Thermo Fisher Scientific, Inc.) for 3 h in blocking buffer before washing and incubating with secondary antibodies for 1h. All antibodies were diluted to 1:250 for dynein IC studies.

Sample preparation for DNA points accumulation for imaging in nanoscale topography (DNA-PAINT) experiments followed dynein IC protocol. However, DNA-labeled secondary antibodies were used instead of Alexa Fluor-conjugated anti-IgG secondary antibodies in accordance with published procedures (Agasti et al., 2017; Jungmann et al., 2014; Wang et al., 2017). Donkey-α-rat P7 and donkey-α-mouse P1 antibodies (a gift from the Yin Lab, Harvard University, Cambridge, MA) were used to label tubulin and dynein IC, respectively.

2.3.5 Conventional imaging

A Nikon TE2000 E2 Eclipse inverted microscope with an iXon Ultra 888 electron multiplying charge coupled device (EMCCD) camera (Oxford Instruments) was utilized to image *Aplysia* neurons at room temperature. Live cells were imaged in L-15 with ASW, and fixed cells were imaged in 0.005% saponin-PBS. For chronic treatment studies, neurons were imaged using a 10× phase objective with an additional 1.5× magnification lens before drug applications and approximately 6 h afterward to obtain neurite growth data. Cells were similarly imaged immediately following microtubule time-lapse recordings and approximately 1.5 h later to obtain neurite growth data for acute treatment investigations. Time-lapse recordings were obtained on the same system using a 60× 1.4 numerical aperture (NA) oil immersion DIC objective with 1.5× additional magnification for 15 min at 15 s intervals. MACF recordings were conducted in accordance with the time-lapse protocol, except images were acquired for 5 min at 3 s intervals. Stained cells were imaged using the 60× 1.4 NA oil immersion DIC

objective with 1.5× additional magnification. Fluorescent images were acquired using an X-Cite 120 halide lamp (Excelitas Technologies Corp.) with the following excitation (EX) and emission (EM) filters (Chroma Technology Corp.): 555 nm EX/610 nm EM for X-rhodamine tubulin, 480 nm EX/535 nm EM for GFP, 655 nm EX/710 nm EM for Alexa Fluor 647 probes, and 575 nm EX/610 nm EM for Alexa Fluor 568 probes.

2.3.6 Single-molecule switching nanoscopy

Super-resolution imaging and reconstructions were performed by Dr. Donghan Ma (Huang Lab, Purdue University, West Lafayette, IN) via a custom-built apparatus on an Olympus IX-73 microscope stand (IX-73, Olympus America, Inc.) with a 100× 1.35 NA silicone oil-immersion objective lens (FV-U2B714, Olympus America, Inc.) and a PIFOC objective positioner (ND72Z2LAQ, Physik Instrumente). Samples were excited with a 642 nm laser (2RU-VFL-P-2000-642-B1R, MPB Communications, Inc.) or a 560 nm laser (2RU-VFL-P-500-560, MPB Communications, Inc.). Both lasers were focused to the back aperture of the objective lens and offset from the optical axis to illuminate the sample in highly inclined thin illumination mode (Tokunaga et al., 2008). The filter turret contained a quad band dichroic mirror (Di03-R405/488/561/635-t1, Semrock, Inc.). Relay lenses in 4f alignment produced a final magnification of 52.7 at a scientific complementary metal-oxide-semiconductor (sCMOS) camera (Orca-Flash4.0v3, Hamamatsu Photonics) with an effective pixel size of 120 nm. A filter wheel containing two bandpass filters (FF01-731/137-25 and FF01-600/52-25, Semrock, Inc.) was placed just before the camera. Single-molecule localization was performed, as described previously (Huang et al., 2013). Imaging was conducted for approximately 20 cycles for microtubules and 5 cycles for dynein with 2,000 frames per cycle.

For dual channel alignment, coverslips with immunostained cells were incubated for 20 min with 100 nm red fluorescent beads (F8801, Thermo Fisher Scientific, Inc.) diluted to 1:100,000. Samples were washed three times with PBS, then coverslips were placed in a chamber (A7816, Thermo Fisher Scientific, Inc.) with 600 µl of imaging buffer (10% (w/v) glucose in 50 mM Tris (JT4109-02, Avantor), 50 mM NaCl (S271-500, Thermo Fisher Scientific, Inc.), 10 mM cysteamine hydrochloride (M6500-25G, Sigma-Aldrich, Inc.), 50 mM thioethylene glycol (M3148-25ML, Sigma-Aldrich, Inc.), 2 mM cyclooctatetraene (138924-1G, Sigma-Aldrich, Inc.), 2.5 mM protocatechuic acid (37580-25G-F, Sigma-Aldrich, Inc.), and 50 nM

protocatechuate 3,4-Dioxygenase (P8279-25UN, Sigma-Aldrich, Inc.), pH 8.0) topped with a layer of mineral oil (124020010, Acros Organics). Channels were merged and images were aligned using ImageJ software (Rasband, 1997-2018; Schneider et al., 2012). Photoshop (Photoshop CC 20.0.3, Adobe) was used to invert colors and select blue areas to show dynein-microtubule localization. The Coloc 2 Fiji 2.0 plugin was applied to raw images to obtain Pearson's coefficients that represent co-localization as an expression of intensity correlations between channels (Rasband, 1997-2018; Schindelin et al., 2012; Schneider et al., 2012).

A similar protocol was followed during DNA-PAINT experiments with minor exceptions to meet established guidelines (Agasti et al., 2017; Jungmann et al., 2014; Wang et al., 2017). Immediately prior to super-resolution imaging, fluorophore-labeled DNA imager strands P1-Atto 655 or P7-Atto 655 (a gift from the Yin Lab, Harvard University, Cambridge, MA) were diluted separately to 2 to 10 nM in imaging buffer (500 mM NaCl in PBS) to independently visualize microtubules or dynein IC, respectively.

2.3.7 Speckle processing and individual microtubule analysis

Images were processed using MetaMorph 7.8 (Molecular Devices) low-pass and Laplace filters, as described previously (Lee and Suter, 2008). Individual microtubule translocation events and rates were measured by producing montages from processed images and tracing internal fluorescent speckles over time. Velocities of five microtubules extending from the growth cone transition zone into the peripheral domain were averaged to calculate individual microtubule velocities for each cell.

2.3.8 Microtubule bulk velocity analysis

ImageJ tools were utilized for image processing and mass microtubule movement analysis, except as specified (Rasband, 1997-2018; Schneider et al., 2012). The line tool was used to trace a centerline from the distal tip of an axon to the leading edge of the growth cone on fluorescent image stacks. The region including the axon and growth cone was then cropped and straightened before applying Gaussian blur and Mexican hat filters for image processing. For taxol studies, processed image stacks were converted into kymographs, then lines of motion were traced on layers in GIMP 2.8.20 (GNU Image Manipulation Program). ImageJ KymoFlow software was utilized to transform traces into refined kymographs representing motion as a function of

position and time, then the ShearX plugin was applied to precisely align growth cone positions over time (Athamneh et al., 2017; Rasband, 1997-2018; Schneider et al., 2012). Resultant velocities were transferred to Excel (02981-002-423991, Microsoft) for analysis (Athamneh et al., 2017). For Noc and CilD experiments, standard ImageJ plugins were used to produce classical kymographs covering axon and growth cone regions and to trace velocities before transferring data to Excel (Rasband, 1997-2018; Schneider et al., 2012). Velocities from all types of studies were divided into 10 μm sections along the axon to calculate regional averages after initial processing and analysis.

2.3.9 Co-localization and microtubule extension analysis

MetaMorph 7.8 was used for conventional image processing and co-localization analysis. Images were sharpened with unsharp mask filters using the same settings for all growth cones analyzed. Thresholding was also performed similarly for all samples. Regions of interest were traced from the C domain boundary to the leading edge of the growth cone, and co-localization was determined by the percentage of overlap between channels. Individual microtubule lengths were traced from the C domain boundary into the P domain and averaged to determine an extension value for each growth cone.

2.3.10 MACF43 mRNA injections and +TIP analysis

GFP-MACF43 DNA in pCS2+ (a gift from the Lowery Lab, Boston College) was extracted from filter paper and transformed into DH5α cells by heat shock. DNA was purified with an E.Z.N.A. FastFilter Plasmid Kit (D6924, Omega Bio-tek, Inc.), and sequences were verified by the Purdue University Genomics Core Facility before linearizing the DNA with the NotI-HF enzyme (R3189S, New England BioLabs, Inc.) (Table 2.1).

Table 2.1. MACF Sequence Verification

Sequencing results from the Purdue University Genomics Core were compared to known sequences via BLAST software (National Center for Biotechnology Information, U.S. National Library of Medicine).

Feature	**Sequence (5'-3')**	**Match**	**Gaps**
SP6 (primer)	ATTTAGGTGACACTATAG	100%	0%
M13R (primer)	CATGGTCATAGCTGTTTCCTG	100%	0%
T3 (primer)	TCCCTTTAGTGAGGGTTAAT	100%	0%
MACF43 (dystonin) (MACF18 Overlap)	GAAACTGTCCCCCAGACACACAGACCTACACCCCGAGCAGGTTCTCGGCCATCCACAGCGAAGCCTTCAAAAATCCCCACGCCCCAGAGGAAATCACCTGCCAGCAAATTGGACAAGTCCTCAAAGAGATGA	100%	0%

GFP-MACF43 mRNA was obtained via mMESSAGE mMACHINE SP6 kits (AM1340, Thermo Fisher Scientific, Inc.). RNA was mixed with TE buffer (AM9860, Ambion) to achieve 0.8 to 1 mg/ml GFP-MACF43, spun at 13,000 g for 30 min, and stored on ice before injecting it into *Aplysia* neurons. Microinjection pipettes were prepared using a Narishige PP830 vertical system and chilled to 4°C before use. Cells recovered for 5 h at 14°C before acute treatments, as described by pharmacological methods. U-track MATLAB software was used to analyze microtubule dynamics (R2018b, The MathWorks, Inc.) (Applegate et al., 2011; Jaqaman et al., 2008).

2.3.11 Western blot

Aplysia central nervous system (CNS) tissue was homogenized with an Omni Mixer Homogenizer (17105, Omni International, Inc.) in a mixture of buffer (50 mM Tris-HCl, 150 mM NaCl, 1 mM EGTA, 1% Triton X-100, pH 7.5), 0.5 mM Pefabloc SC Plus (11873601, Roche Molecular Systems, Inc.), and 1% protease inhibitor cocktail (P8340, Sigma-Aldrich, Inc.) with one PhosSTOP tablet (PHOSS-RO, Roche, Ltd.). The lysis mixture was then spun at 10,000 g for 30 min at 4°C before collecting the supernatant. Proteins were separated using

sodium dodecyl sulfate-polyacrylamide gel electrophoresis (SDS-PAGE) with 5% gel and transferred to a polyvinylidene difluoride (PVDF) membrane. The membrane was blocked with 5% dry milk in PBS for 1 h at room temperature. It was then washed three times for 5 min with PBS and three times for 5 min with 0.1% triton in PBS (PBST) before it was incubated with antibodies against DHC1 diluted to 1:200 in 0.05% PBST with 0.1% dry milk overnight at 4°C. The membrane was subsequently washed with PBS, then 0.1% PBST and incubated with secondary antibodies (A21088, Thermo Fisher Scientific, Inc.) diluted to 1:1000 in 0.05% PBST with 0.1% dry milk for 1 h at room temperature. Final washes with PBS, then 0.1% PBST were performed before imaging the membrane with an Odyssey (LI-COR, Inc.) detection system.

2.3.12 Data analysis and display

Data were gathered and analyzed as described throughout the document. SAS 9.4 (SAS Institute, Inc.), SPSS Statistics 25.0 (IBM), and Excel software were used for statistical analyses. GraphPad Prism 7.0d (GraphPad Software, Inc.) and Canvas Draw 5 (Canvas GFX, Inc.) were used for data displays.

CHAPTER 3. EFFECTS OF TAXOL ON NEURITE ELONGATION AND MICROTUBULE TRANSLOCATION DYNAMICS

3.1 Introduction

Microtubule polymerization and translocation are essential for neurite growth. However, the distinct contributions of microtubule assembly and translocation to axonal elongation have not been fully quantified. This experimental series examined how microtubule assembly and translocation affect neurite elongation by quantifying neurite, individual microtubule, and mass microtubule movements when microtubule polymerization was pharmacologically enhanced by low doses of taxol.

3.2. Results and Discussion

3.2.1 Taxol dose responses in *Aplysia* neurons

Previous studies have demonstrated low-doses of taxol mildly stabilize microtubules so they spend more time polymerizing and less time in catastrophe (Witte et al., 2008). Conversely, high concentrations disturb dynamics and cause microtubules to break under actomyosin retrograde forces (Dehmelt et al., 2003; Letourneau et al., 1987; Waterman-Storer and Salmon, 1997). This study built upon prior research by testing the hypothesis that enhancing microtubule polymerization with low taxol concentrations increases neurite growth rates in *Aplysia* bag cell neurons.

Cells were cultured on hemolymph mixed with poly-L-lysine to determine taxol concentrations that increase and decrease neurite growth rates in *Aplysia* neurons. Neurite velocities were measured during chronic taxol treatments via phase microscopy pre- and post-treatment. Taxol was bath applied to separate samples at 1, 5, 10, 50, or 100 nM or 1 μM concentrations with treatments ranging from 4 to 24 h to determine dose responses. Optimal treatment time ranged from 4 to 10 h, with 5 nM taxol increasing neurite growth rates and 1 μM taxol decreasing them (Fig. 3.1).

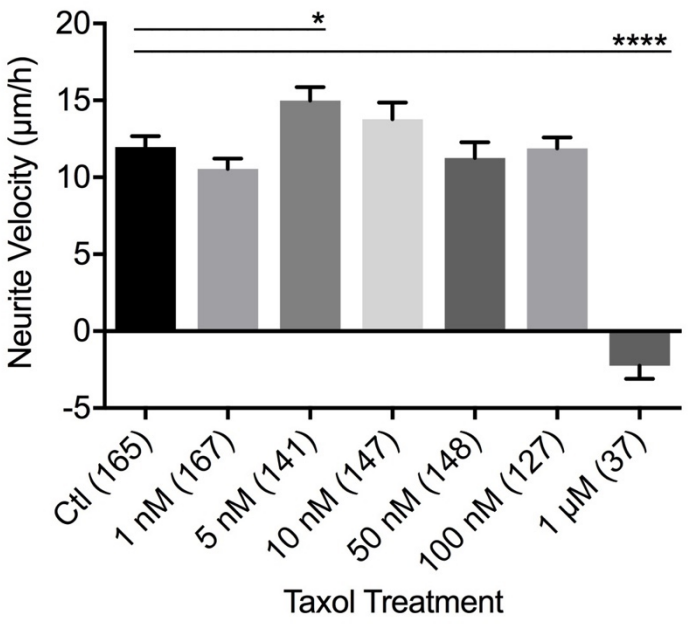

Figure 3.1. Low taxol concentrations increase neurite growth rates

Aplysia bag cell neurons were treated with DMSO (control (ctl)), 1, 5, 10, 50, or 100, nM or 1 μM taxol for 4 h to determine dose responses. 5 nM taxol increased neurite growth rates; 1 μM taxol decreased neurite growth rates. Parenthetical numbers represent neurites. Quantifications represent mean±s.e.m. with comparisons to controls for three independent experiments; ****$p<0.0001$, *$p<0.05$ (one-way ANOVA with Tukey's post hoc test).

Consistent with studies in other model systems, the results indicated mild microtubule stabilization increases neurite extension, but overstabilization compromises microtubule dynamics (Erturk et al., 2007; Sengottuvel et al., 2011; Witte et al., 2008). These studies built upon previous outgrowth investigations by analyzing neurite velocities to reveal that low taxol concentrations increase neurite growth rates and high concentrations reduce them; control growth rates were 12.0±0.7 μm/h, and 5 nM taxol increased them to 15.0±0.9 μm/h, while 1 μM taxol reduced them to -2.2±0.9 μm/h (mean±s.e.m.) (Fig. 3.1). These results implied mild microtubule stabilization enhances microtubule polymerization, which causes an increase in neurite growth rates. They also raised questions about the underlying mechanisms driving microtubule assembly and translocation during neurite outgrowth that are addressed later in the study. Specifically, these results spurred curiosity about whether microtubule assembly or

translocation has a stronger influence on neurite outgrowth and whether microtubule assembly must precede translocation to lay tracks for motor protein activity.

Drugs that attenuate microtubule dynamics inhibit both microtubule and F-actin polymerization, and they prevent axon branching but not elongation (Dent and Kalil, 2001). To determine whether enhancing microtubule dynamics promotes axon branching and elongation in *Aplysia* neurites, these characteristics were analyzed after treating cells with an array of taxol concentrations (Fig. 3.2 A, C). Axon branching after treatment increased by 0.2±0.1 branch points in controls versus 0.4±0.1 branch points in cells treated with 1 nM taxol, but the length of the longest neurite in each cell before and after treatment was similar in both groups (mean±s.e.m.) (Fig. 3.2 A, C). The change in the number of neurites before and after treatment was also similar for controls and cells treated with low taxol concentrations (Fig. 3.2 B). High taxol concentrations decreased all three characteristics (Fig. 3.2 A-C). Additional testing is required to determine the cause of decreased neurite branch points in 10 nM taxol samples compared to controls and higher concentration groups, but it may be partially due to variability in taxol effectiveness, which became apparent during subsequent acute taxol studies. The time-course effectiveness of taxol in *Aplysia* cells, which was revealed during neurite velocity experiments that showed 4 to10 h treatments were the most effective, may also be a factor. Results from this study indicate that enhancing microtubule polymerization promotes axon branching but not extension. Microtubules may be more receptive to taxol treatments during neurite initiation than during subsequent axonal growth. These findings strengthen the hypothesis that microtubules polymerize to explore the growth cone periphery before directing neurite growth (Dent and Kalil, 2001; Kalil and Dent, 2014; Lee and Suter, 2008; Tanaka et al., 1995).

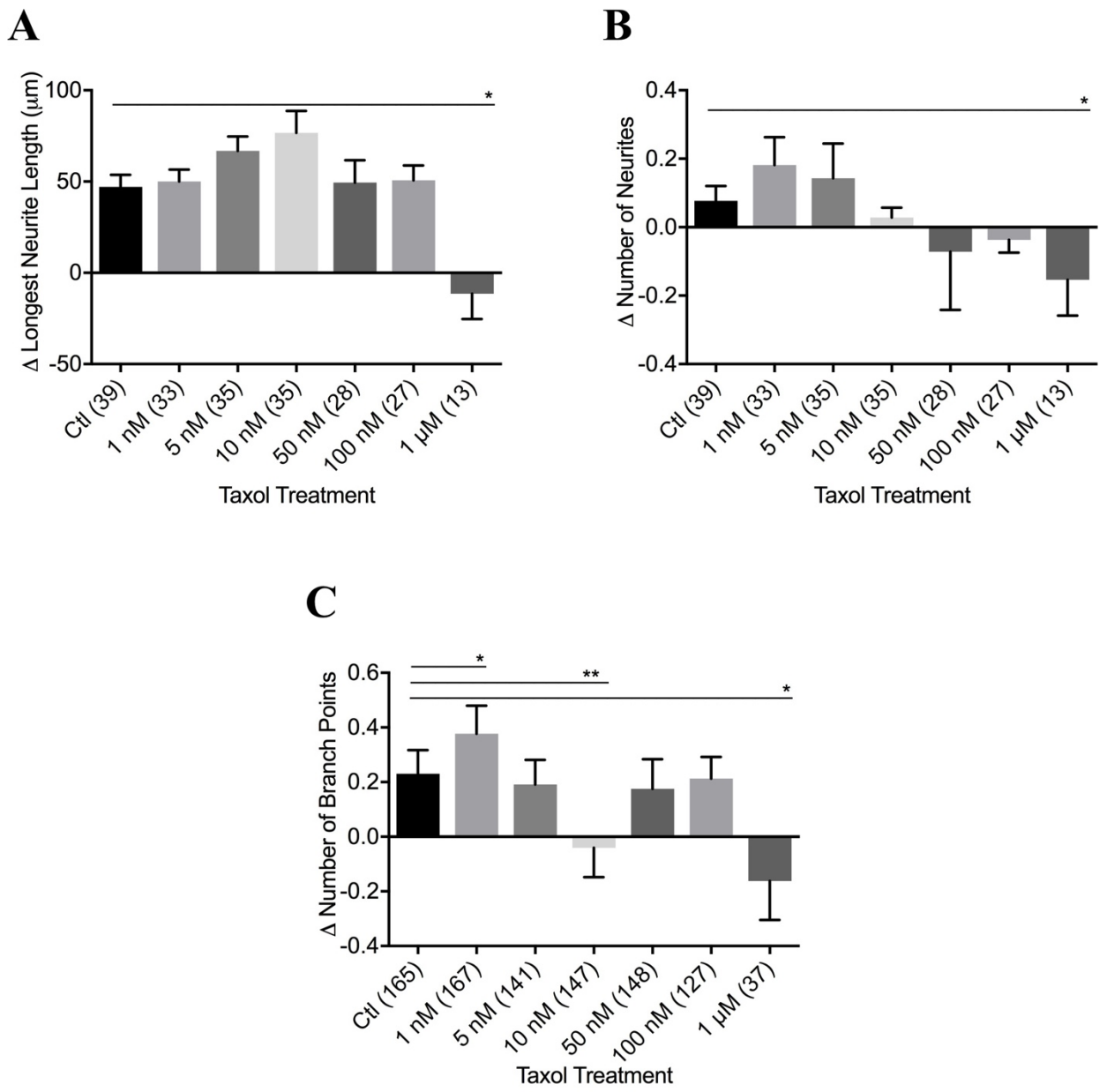

Figure 3.2. Neurite growth characteristics during taxol treatments

Changes in (A) the length of the longest neurite, (B) number of neurites, and (C) number of branch points in *Aplysia* bag cell neurons were calculated by measuring differences between pre- and post-treatment values. 1 nM taxol increased the number of branch points (C) but did not alter the length of the longest neurite or the number of neurites (A, B). 1 μM taxol reduced all three characteristics (A-C). Parenthetical numbers represent neurons in (A, B) and neurites in (C). Quantifications represent mean±s.e.m. with comparisons to controls for three independent experiments employing 4 h treatments; **$p<0.01$, *$p<0.05$ (one-way ANOVA with Tukey's post hoc test).

Chronic taxol treatments did not reveal a threshold concentration that simultaneously increased neurite growth rates, branching, elongation, and number of neurites (Figs 3.1, 3.2). However, concentrations between 1 and 10 nM were most effective for increasing the parameters of interest for this study. These concentrations were initially tested in subsequent fluorescent, live-cell microscopy experiments before selecting 5 nM taxol for acute treatment studies to determine whether individual and bulk microtubule translocations increase with stabilized microtubule dynamics.

3.2.2 Mass microtubule movements under enhanced microtubule assembly conditions

Previous studies employed the microtubule assembly inhibitor Noc to demonstrate a strong correlation between bulk microtubule and neurite velocities (Athamneh et al., 2017). To determine whether bulk microtubule translocation increases when microtubules are mildly stabilized with taxol, neurons were microinjected with rhodamine tubulin and allowed to recover for at least 1 h before time-lapse imaging. Fluorescent and DIC images of microtubules and neurites were then collected for 15 min at 15-20 s intervals following 30 min, 5 nM taxol treatments (Fig. 3.3 A). ImageJ was utilized to process fluorescent images and produce kymographs that were traced in Gimp 2.8.20 (Rasband, 1997-2018; Schneider et al., 2012). Traces were transformed into velocity maps with the ImageJ KymoFlow algorithm to obtain positional bulk microtubule flow rates along the axon and growth cone (Fig. 3.3 B) (Athamneh et al., 2017; Rasband, 1997-2018; Schneider et al., 2012).

While mass microtubule velocity was noticeably higher in the region from 10 to 20 μm proximal to the transition zone in taxol cells than in controls, average velocities from 0 to 30 μm proximal to the transition zone were similar for both groups, with 4.4±2.4 μm/h in controls and 4.1±2.1 μm/h in taxol cells (mean±s.e.m.) (Fig. 3.3 C, D). Bulk microtubule velocities in the transition zone were also nearly the same: 6.7 μm/h in controls and 6.0 μm/h in taxol-treated cells, respectively (Fig. 3.3 C).

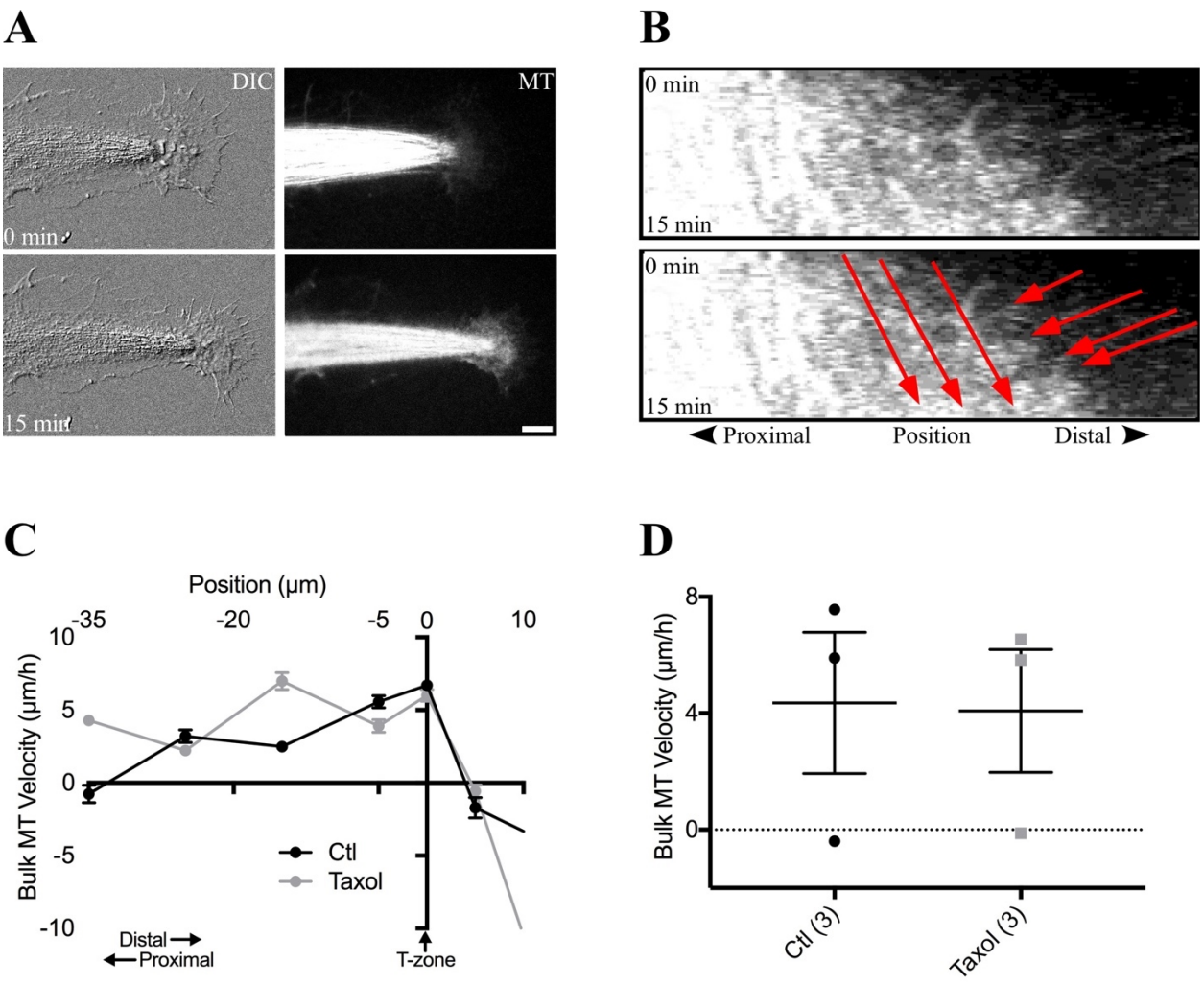

Figure 3.3. Low-dose taxol does not alter mass microtubule velocity in *Aplysia* neurites

(A) DIC images of a control (ctl) neurite with rhodamine-labeled microtubules (MT) at time 0 and 15 min later. Scale: 10 µm. (B) The velocity map of microtubules in (A) displays characteristic retrograde movement in the growth cone peripheral domain and anterograde movement in the central domain. The duplicated kymograph includes traces that measure motion. (C) Bulk microtubule velocity as a function of distance from the transition zone set at the origin in control (ctl) and 5 nM taxol cells. Velocities are plotted as mean±s.e.m. for 10 µm regions along the axon. (D) Bulk microtubule velocity from 0 to 30 µm proximal to the transition zone (mean±s.e.m.). Parenthetical numbers represent neurons. Data are from three independent experiments.

Although small sample sizes prevented statistical analysis, a tentative hypothesis may be formulated from experimental data. Observations indicate mild microtubule assembly enhancement does not immediately alter mass microtubule movements. Increasing bulk anterograde microtubule movements requires a sufficient increase in microtubule assembly; otherwise, actin retrograde forces continue to sweep microtubules backward. Because bulk and individual microtubule movements uniquely contribute to axonal growth, the next series of experiments examined the effects of microtubule stabilization on individual microtubule movements to determine whether stabilization increases forward translocations.

3.2.3 Individual microtubule translocation and assembly under mild microtubule stabilization conditions

Prior investigations revealed individual microtubule forward translocation increases in growth cones responding to adhesion molecules, but these studies did not fully characterize how individual microtubule movements contribute to axonal advance (Lee and Suter, 2008; Schaefer et al., 2008b). This series of experiments tested the hypothesis that microtubule assembly is required for individual forward microtubule translocation and that both processes contribute to the increased neurite growth rates observed during chronic taxol treatments. Individual microtubule FSM was used to test these predictions. Neurons were microinjected with rhodamine tubulin before performing fluorescent and DIC imaging, as described for mass microtubule movement studies (Fig. 3.4 A, B). Low-pass and Laplacian-transformation filters were used to process images and produce montages in MetaMorph 7.8, and individual microtubule-forward, microtubule-backward, and microtubule-pause events were identified by tracing speckles across frames with the MetaMorph multi-line tool (Fig. 3.4 C).

Although individual microtubule translocation rates increased with acute 5 nM taxol applications, neurite growth rates were unchanged (Fig. 3.4 D, E). Individual microtubule translocation events were not significantly different following taxol treatments, but there was a tradeoff of retraction and pause events for forward translocation (Fig. 3.4 F-H). These tradeoffs in individual microtubule translocations may explain the increase in microtubule translocation rates when microtubule assembly is mildly enhanced (Fix 3.4 E-H).

Figure 3.4. Low-dose taxol increases individual microtubule velocity

Cultured neurons were treated with DMSO (control (ctl)) or 5 nM taxol to analyze microtubule-neurite relationships. (A) DIC image of a growth cone after DMSO treatment. (B) Rhodamine-labeled microtubules inside (A). (C) Time-lapse montage of the red-boxed microtubule in (B) at 15 s intervals. (D) Neurite velocity was unchanged by 5 nM taxol after 15 min, but (E) microtubule (MT) velocity increased. (F-H) Forward, backward, and pause events are depicted as percentages of total microtubule events. Parenthetical numbers represent neurons; (E-H) depict averages of five microtubules for each neuron. Quantifications represent mean±s.e.m. for three independent experiments; *$p<0.05$ (Mann-Whitney test).

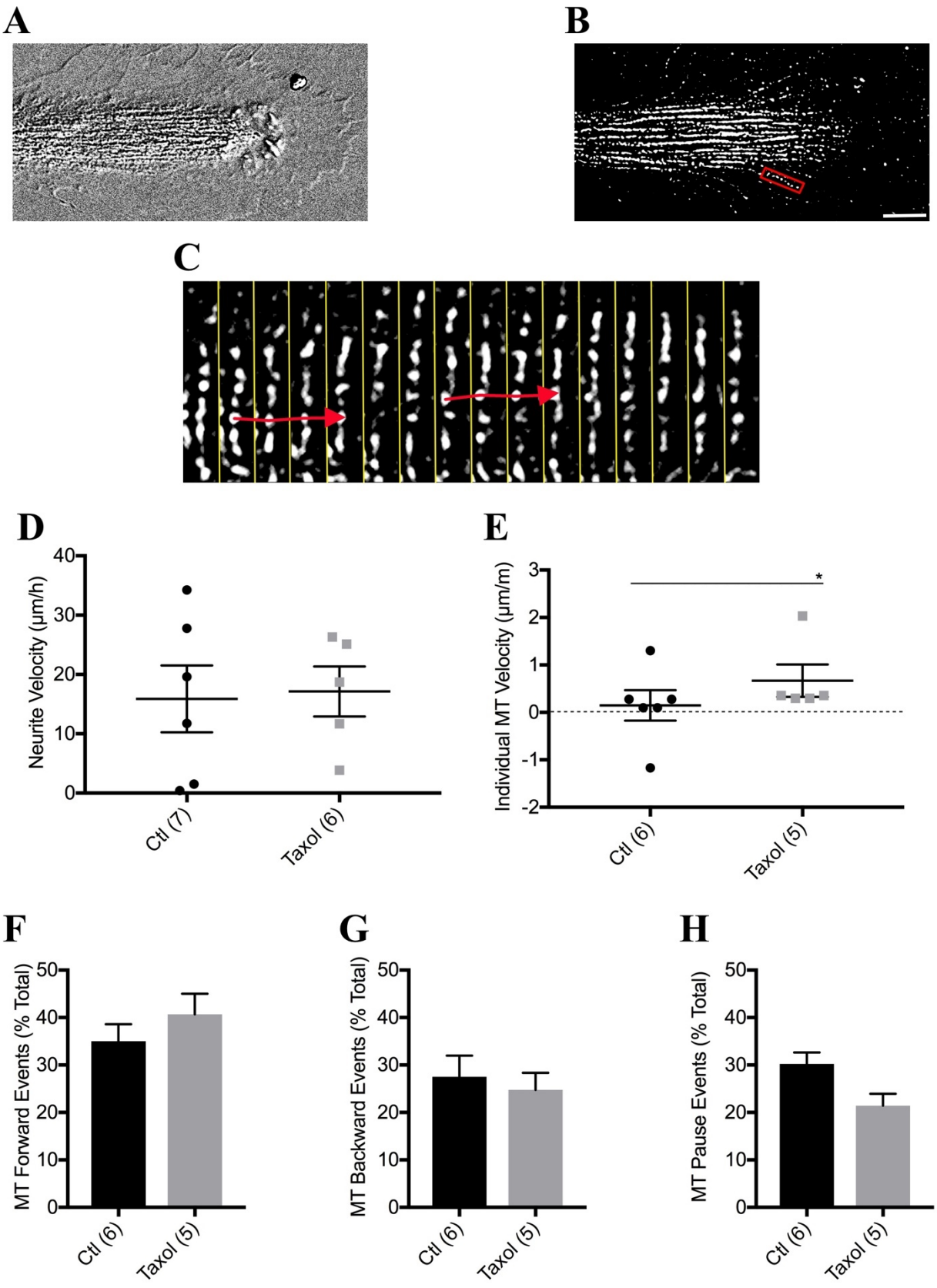
A
B
C
D
Neurite Velocity (µm/h)
40
30
20
10
0
Ctl (7)
Taxol (6)
E
Individual MT Velocity (µm/m)
3
2
1
0
-1
-2
*
Ctl (6)
Taxol (5)
F
MT Forward Events (% Total)
50
40
30
20
10
0
Ctl (6)
Taxol (5)
G
MT Backward Events (% Total)
50
40
30
20
10
0
Ctl (6)
Taxol (5)
H
MT Pause Events (% Total)
50
40
30
20
10
0
Ctl (6)
Taxol (5)

The increase in individual microtubule velocity and associated increase in forward translocation and decrease in retrograde translocation during mild microtubule stabilization suggests microtubule translocation and assembly contribute interdependently to neurite elongation. The unpredicted similarity between control and taxol neurite growth rates may be attributed to a time-course effect of taxol. Therefore, longer taxol treatments are predicted to increase neurite growth rates by inducing increased microtubule assembly, which will lay additional tracks for microtubule translocation.

3.3 Study Limitations

Additional testing is required to validate preliminary conclusions because small sample sizes and high variability restricted data analysis during this experimental series. Another limitation to this investigation was that it accounted for microtubule assembly indirectly by assuming low concentrations of taxol increased microtubule polymerization rather than measuring assembly directly by FSM. It is reasonable to assume low-dose taxol induced assembly because taxol is a proven microtubule stabilizer; however, the precise contributions of microtubule assembly were not quantified during this study due to experimental constraints (Jordan and Kamath, 2007). To partially address this issue, MACF43 was employed to track microtubule assembly during experiments described later in this work.

3.4 Conclusion

Taxol dose characteristics in *Aplysia* neurons were determined during this study. Consistent with prior studies, low taxol concentrations increased neurite velocities and high concentrations decreased them during chronic treatments (Erturk et al., 2007; Sengottuvel et al., 2011; Witte et al., 2008). However, 5 nM taxol produced unpredicted results during acute treatments. Although low-dose taxol increased individual microtubule translocations, it did not significantly increase neurite growth rates or mass microtubule velocities. Considering prior investigations that demonstrated individual microtubules explore the growth cone periphery through assembly and translocation, a possible explanation for the rate disparity is that individual microtubule forward translocation and assembly are prerequisites for mass microtubule and axon anterograde movement. Mass microtubule and neurite growth velocities are expected to increase with longer

taxol treatments because they should follow increases in individual microtubule velocity and forward translocations.

CHAPTER 4. DYNEIN-MICROTUBULE LOCALIZATION

A version of this chapter has been submitted to a peer-reviewed journal for publication.

4.1 Introduction

A battery of MAPs regulate microtubule dynamics and movements to mediate numerous cellular functions, including growth cone steering and advance (Hur et al., 2012; Kalil and Dent, 2014; Wong and Hashimoto, 2017). Dynein is an important MAP and minus-end directed motor protein (Reck-Peterson et al., 2018). Previous experiments revealed $p150^{Glued}$ recruits dynein to microtubule plus ends, where it tethers microtubules to actin, other microtubules, and the cellular membrane (Duellberg et al., 2013; Duellberg et al., 2014; Hendricks et al., 2012; Perlson et al., 2013; Yogev et al., 2017). They also demonstrated that dynein moves microtubules forward against actomyosin retrograde forces in the growth cone and drives mass microtubule movements that contribute to neurite elongation (Grabham et al., 2007; Roossien et al., 2014). Because mass microtubule movements represent the coordinated motion of microtubules cross-linked with MAPs, this study tested the hypothesis that microtubule assembly and dynein interactions are required for microtubule translocation and neurite growth.

4.2 Results and Discussion

4.2.1 Innovating a no-cost device enabled dual-system experimentation

Before testing the hypothesis, a no-cost device was designed to facilitate dual-system conventional and super-resolution imaging. Prior to constructing this device, mechanical differences in imaging systems necessitated separate sample preparations for conventional and super-resolution imaging, resulting in unnecessary monetary and time expenditures. A collaborative effort with Dr. Donghan Ma and the Purdue University Project Machine Shop produced a microscope stage holder that enables imaging a single sample on two unique systems (Fig. 4.1). This device made it possible to inspect samples and experiment with them via

conventional means before initiating super-resolution experiments, which increased experimental throughput by 100% and decreased super-resolution imaging false starts by 50%.

Figure 4.1. Innovation: setting the stage

Prior to innovation, the traditional stage holder (A) supported only the sample configuration depicted in (A') and limited imaging exclusively to a conventional microscopy system (A'', B''). After implementing a no-cost solution, the modified stage holder (B) allowed configurations in (A', A'') and (B', B'') and enabled dual-system imaging on super-resolution (C) and conventional microscopy (A", B") apparatuses during a single experiment.

A

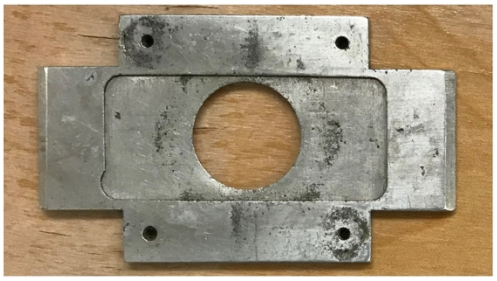

B

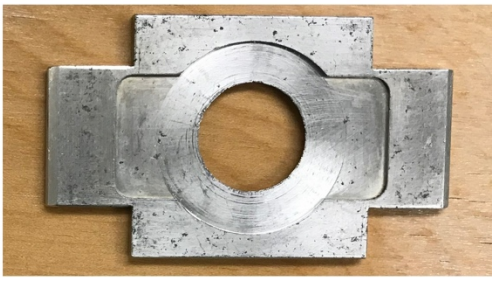

A’

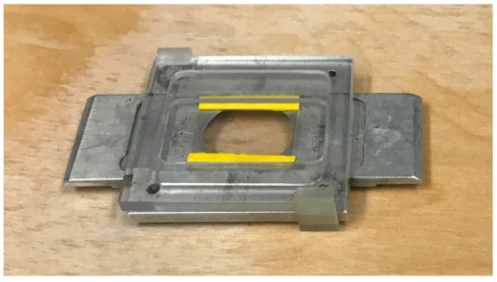

B’

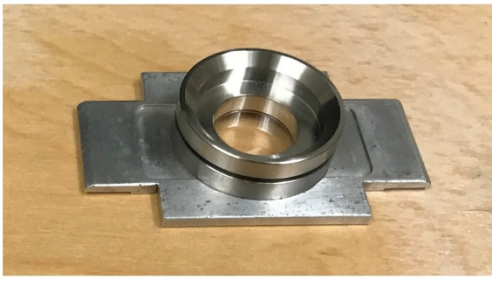

A’’

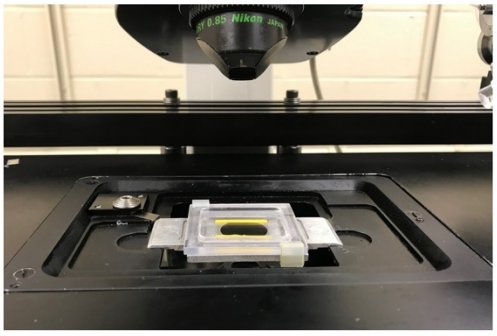

B’’

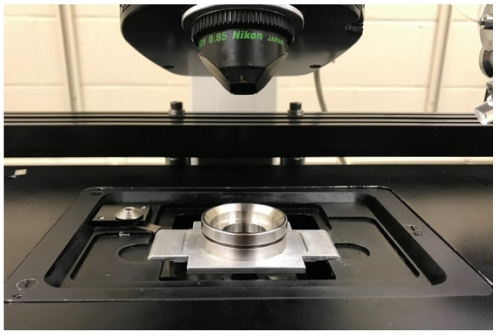

C

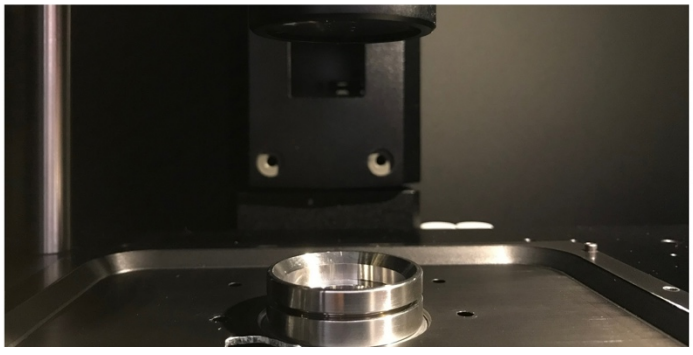

4.2.2 Inhibiting microtubule assembly disrupts dynein-microtubule interactions

Because disrupting microtubule assembly blocks microtubule associations with +TIPs, and +TIPs recruit dynein to microtubule plus ends, both conventional and single-molecule switching nanoscopy (SMSN) imaging of microtubules and dynein were performed to determine whether microtubule assembly is required for dynein-microtubule interactions (Coles and Bradke, 2015; Duellberg et al., 2014; Erdogan et al., 2017; Kapitein and Hoogenraad, 2015). After validating antibodies with a western blot, dynein heavy chain-1 (DHC1) and α-tubulin in bag cell neurons were immunolabeled following 5 min applications of 10 μM ciliobrevin D (CilD), 1 μM nocodazole (Noc), or both inhibitors in combination (Figs 4.2 and 4.3).

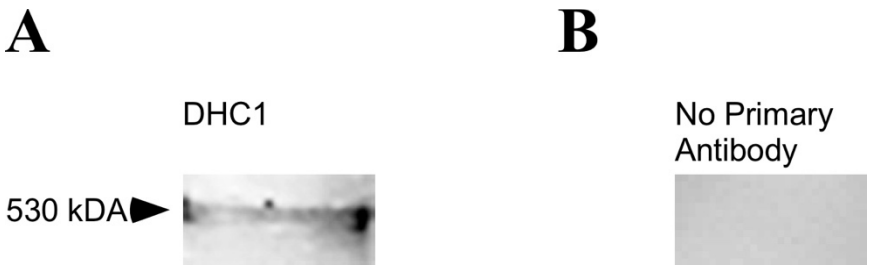

Figure 4.2. Western blot of DHC1 antibody using *Aplysia* CNS proteins

(A) Antibody detects the 532 kDA DHC1 in *Aplysia* CNS lysate. (B) The band is absent in the no primary antibody control.

While fewer microtubules extended beyond the C domain in Noc growth cones than in controls, microtubules in growth cones treated with either CilD alone or in combination with Noc extended farther than microtubules in growth cones treated only with Noc (Fig. 4.3 A-E). Dynein was detected along microtubules in control and CilD-treated growth cones, whereas a significant fraction of dynein signals was not associated with microtubules when assembly was inhibited with either Noc alone or in combination with CilD (Fig. 4.3 A-D, F).

Dynein-microtubule co-localization and microtubule extension were quantified for each experimental condition (Fig. 4.3 E, F). Control and CilD growth cones displayed similar co-localization values: 30.2±2.0% for controls and 29.0±2.2% for CilD (mean±s.e.m.) (Fig. 4.3 F). Noc and combination treatment groups had values of 8.8±1.4% and 10.0±1.0%, respectively,

which were significantly lower than those for control or CilD groups (mean±s.e.m.) (Fig. 4.3 F). Microtubule extension into the P domain differed significantly among all groups: it was 10.1±0.6 μm in control, 8.1±0.5 μm in CilD, 2.4±0.4 μm in Noc, and 5.1±0.4 μm in CilD-Noc growth cones (mean±s.e.m.) (Fig. 4.3 E). The similar co-localization values for control and CilD groups, along with the threefold decrease in co-localization for Noc- and CilD-Noc-treated neurons compared to controls, suggest microtubule assembly is required for proper dynein-microtubule interactions. Furthermore, the noncumulative negative effects of microtubule assembly and dynein inhibition indicate that microtubule assembly is required for dynein-mediated microtubule translocation and that these processes are interdependent (Fig. 4.3 E, F).

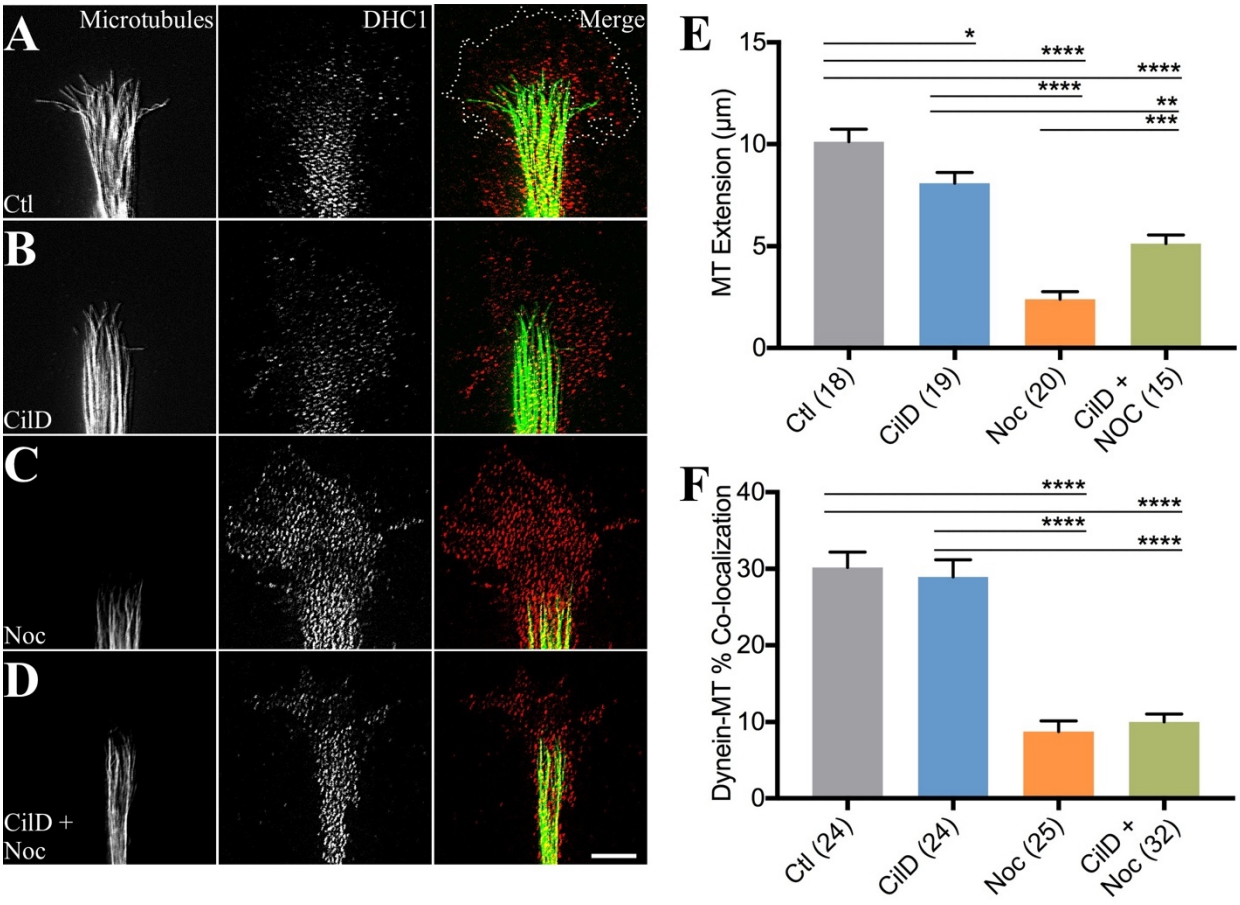

Figure 4.3. Inhibiting microtubule dynamics decreases dynein-microtubule co-localization

Cultured neurons were treated with 10 μM CilD, 1 μM Noc, or mixed CilD-Noc for 5 min before formaldehyde fixation and immunolabeling with antibodies against α-tubulin and DHC1 (A-D). Representative images of (A) control (ctl), (B) CilD, (C) Noc, (D) CilD and Noc growth cones are shown. The white trace in (A) indicates the region analyzed in (E, F). Scale bar: 10 μm. (E) Microtubule (MT) extension beyond the C domain boundary. (F) Dynein-microtubule co-localization from the C domain boundary to the leading edge of the growth cone. Parenthetical numbers represent neurites. Quantifications display mean±s.e.m. for three independent experiments; ****$p<0.0001$, ***$p<0.001$, **$p<0.01$, *$p<0.05$ (one-way ANOVA with Tukey's post hoc test).

4.2.3 Super-resolution imaging confirms dynein-microtubule interactions

SMSN was performed to confirm co-localization data and obtain additional insights into dynein-microtubule associations (Fig. 4.4). Although SMSN analysis was limited by low sample sizes, super-resolution imaging revealed dynein localizes along control and CilD microtubules, which had Pearson's coefficients representing channel intensity correlations of 0.10 and 0.06, respectively (Fig. 4.4 E", F). Much less dynein localization occurred along CilD-Noc (0.03 Pearson's coefficient) and Noc (0.01 Pearson's coefficient) microtubules (Fig. 4.4 E", F). These data should be further analyzed by applying computational strategies, such as artificial neural network accelerated localization microscopy (ANNA-PALM) software, after acquiring additional SMSN images. ANNA-PALM reconstructs super-resolution images with sparse molecule localization, which is characteristic of dynein, and improves spatial resolution (Ouyang et al., 2018). Although additional studies and computational applications are required for data analysis, SMSN validated initial co-localization findings and exposed an exciting area for future exploration wherein dynein-microtubule relationships may be resolved at the nanoscale level.

Figure 4.4. SMSN of dynein-microtubule localization

Neurons were fixed with formaldehyde and immunolabeled with antibodies against α-tubulin and DHC1 following 5 min applications of 10 μM CilD, 1 μM Noc, or combined CilD-Noc. (A-D) Representative images of microtubules (green) and dynein (red) in (A) control (ctl); (B) CilD; (C) Noc; (D) CilD and Noc growth cones. The dashed box represents the cropped regions displayed in (E). (E) Enlarged regions from (A-D). (E') Colors in (E) were inverted in Photoshop to clearly discern dynein (cyan) and microtubules (magenta). (E") The color isolation tool was then used to select and retain blue regions before desaturating magenta regions to pinpoint areas of dynein-microtubule co-localization with minimal image processing. Rectangles in (E") outline regions where dynein localized along microtubules in control and CilD growth cones. These regions were not readily discernable in cells treated with Noc or Noc-CilD. (F) To confirm observations from (E"), the Coloc 2 Fiji 2.0 plugin was applied to raw images from (E) to obtain Pearson's coefficients that represent intensity correlations between channels (Rasband, 1997-2018; Schindelin et al., 2012; Schneider et al., 2012). Scale bars: 2 μm.

SMSN imaging and reconstructions were performed by Dr. Donghan Ma (Huang Lab, Purdue University, West Lafayette, IN).

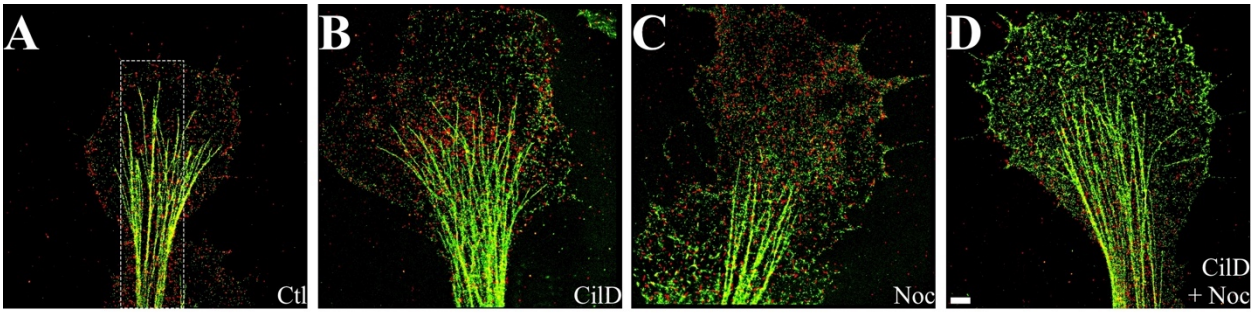
A
Ctl
B
CilD
C
Noc
D
CilD
+ Noc

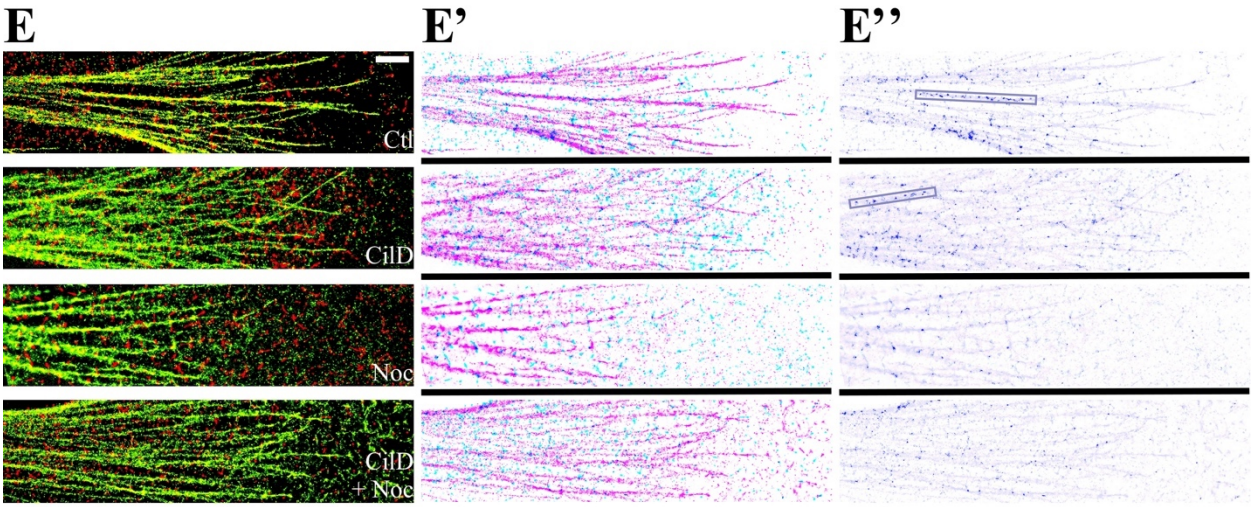
E
E'
E''
Ctl
CilD
Noc
CilD
+ Noc

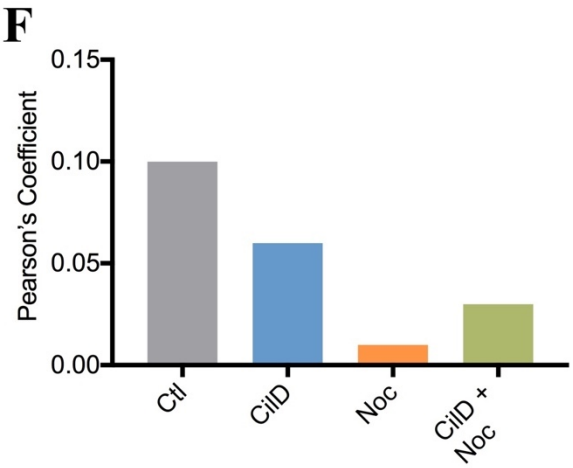
F
Pearson's Coefficient
0.15
0.10
0.05
0.00
Ctl
CilD
Noc
CilD +
Noc

4.2.4 Dynein intermediate chain labeling confirms heavy chain studies

To provide further confirmation of dynein-microtubule interactions, dynein ICs and α-tubulin were immunolabeled after performing the same drug applications that were administered during DHC experiments. Additional studies are required for data analysis, and antibodies must be validated by western blot, but conventional and SMSN imaging indicate dynein IC antibodies are an effective tool for refining dynein-microtubule co-localization measurements from DHC investigations (Figs 4.5, 4.6). Dynein IC antibody employment in future *Aplysia* growth cone model system studies will fine-tune understanding of the many regulators involved in microtubule dynamics and axonal elongation.

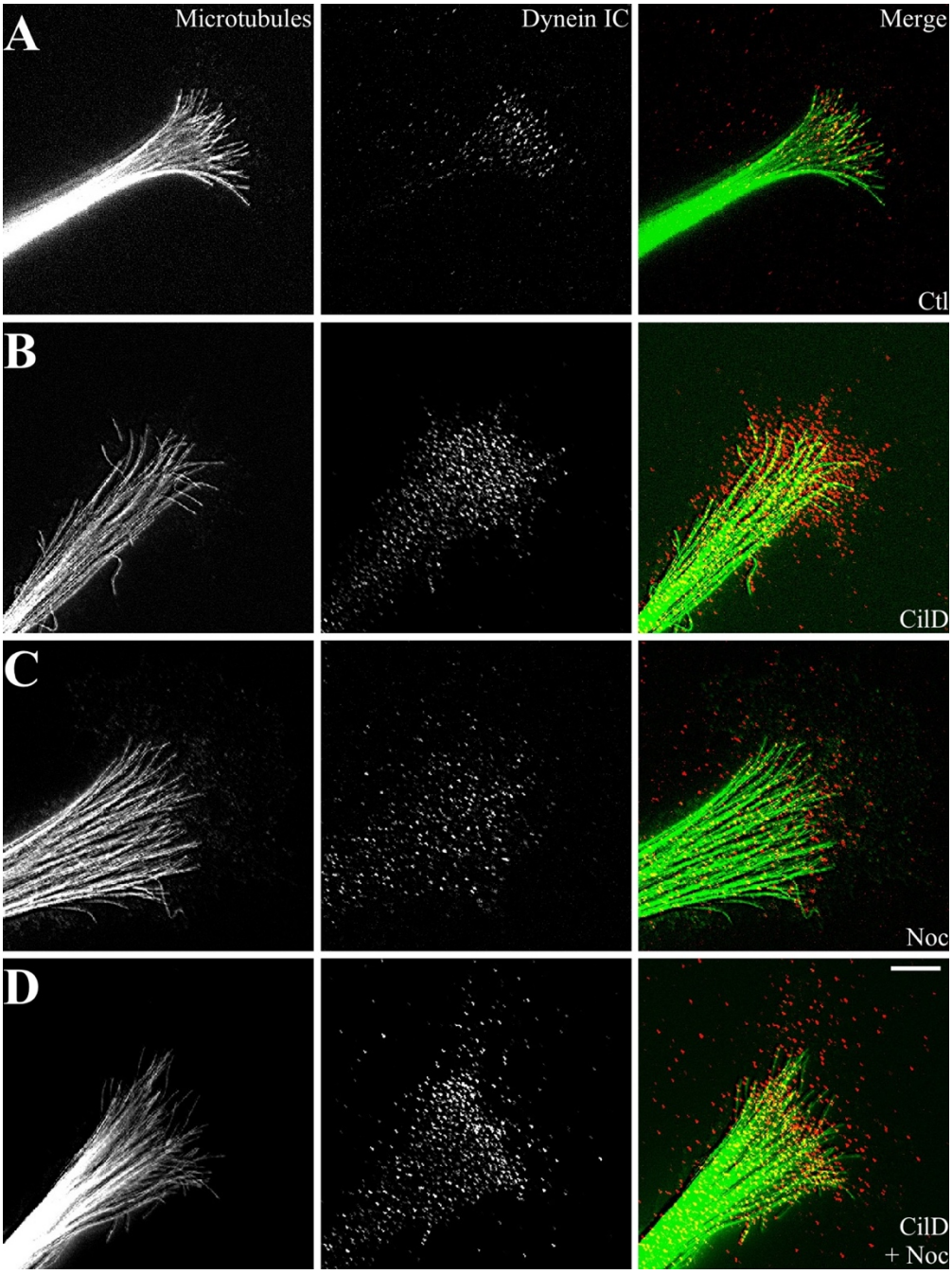

Figure 4.5. Dynein IC labeling confirms co-localization studies

Neurons were treated with 10 μM CilD, 1 μM Noc, or mixed CilD-Noc for 5 min before formaldehyde fixation and immunolabeling with antibodies against α-tubulin and dynein IC. Images of (A) control (ctl), (B) CilD, (C) Noc, (D) CilD and Noc growth cones are displayed. Additional studies are required for data analysis, but preliminary data indicate dynein IC antibodies may be used to refine dynein-microtubule co-localization measurements. Scale bar: 10 μm.

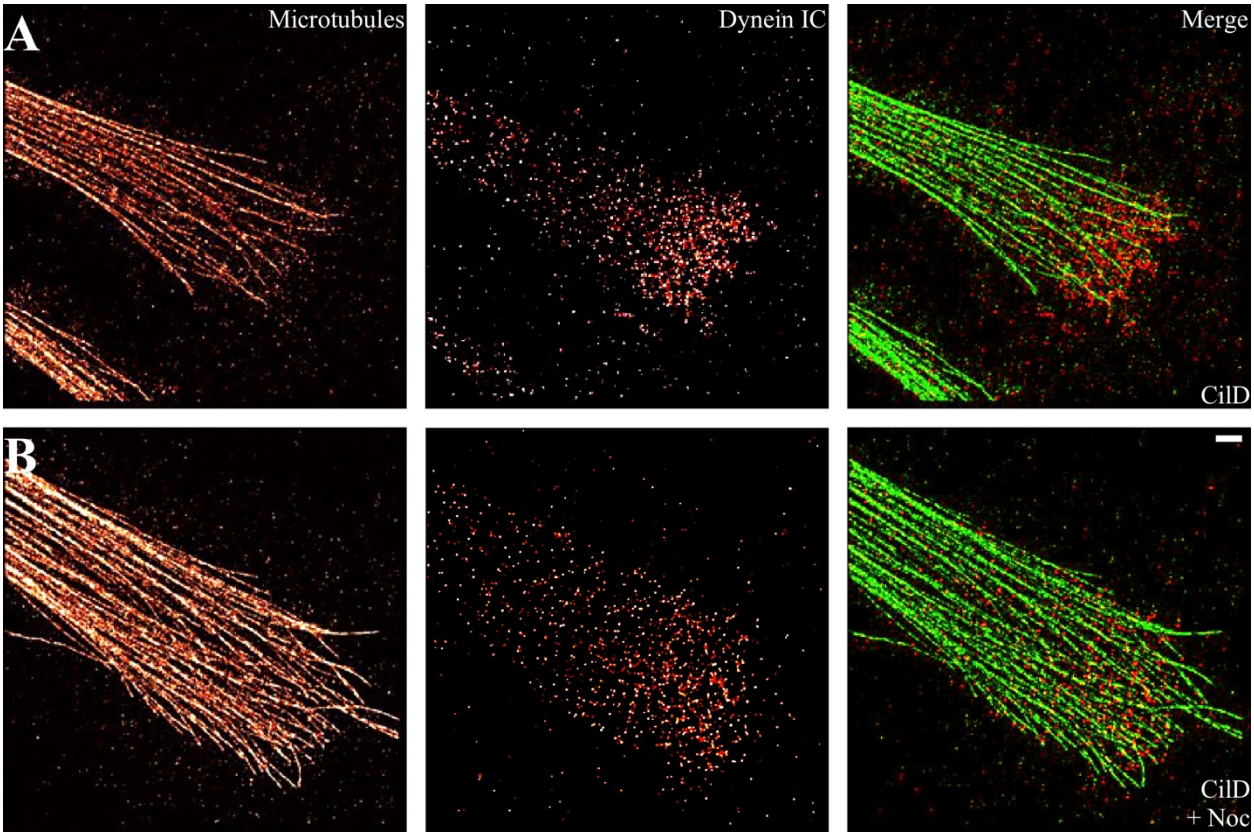

Figure 4.6. SMSN of dynein IC and microtubules

Growth cones were immunolabeled with antibodies against α-tubulin and dynein IC after 5 min, 10 μM CilD or combined 10 μM CilD and 1 μM Noc treatments. SMSN images show dynein IC and microtubules in (A) CilD and (B) CilD-Noc growth cones. Scale bar: 2 μm.

SMSN imaging and reconstructions were performed by Dr. Donghan Ma (Huang Lab, Purdue University, West Lafayette, IN).

4.2.5 PAINT-ing microtubules and dynein

Precision medicine offers encouraging prospects for tailoring neurological drug therapies to meet patient needs; however, determining which molecules to target and predicting patient responses limit progression in this field (Tan et al., 2016). Understanding the mechanisms by which neurons alter and maintain their molecular makeup is fundamental to realizing the potential of precision medicine for treating neurological diseases (Tan et al., 2016). To assist with this effort, DNA points accumulation for imaging in nanoscale topography (DNA-PAINT)

techniques were employed to achieve ultra-resolution imaging of dynein and microtubule interactions.

DNA-PAINT uses DNA molecules as labeling and imaging probes to accomplish high multiplexing, overcome photobleaching, and optimize localization (Schnitzbauer et al., 2017). It exploits super-resolution capabilities by using dyes that bind transiently with, and dissociate quickly from, targets to enable nanoscale precision (Hysolli, 2018; Nieves et al., 2018; Schnitzbauer et al., 2017). Two complementary single-stranded DNA oligomers, a docking strand and an imager strand, are used to visualize a target of interest (Schnitzbauer et al., 2017). Because docking strands are conjugated to secondary antibodies, conventional and PAINT sample-preparation protocols are interchangeable with minor modifications. Imager strands are conjugated to organic dyes and diffuse freely in imaging buffer, making them undetectable in the unbound state (Jungmann et al., 2014). Cameras detect them when they bind transiently to a complementary docking strand, where they remain stationary for an extended time (Jungmann et al., 2014).

Consistent with prior experiments, DNA-PAINT produced super-resolution reconstructions of microtubules (Fig. 4.7 A) (Auer et al., 2018; Nieves et al., 2018). However, it was not as effective for dynein reconstructions (Fig. 4.7 B). A combination of factors may have precluded dynein visualization with PAINT, including labeling techniques, imaging buffers, and imager strands. The natural sparsity of motor protein molecules is also suspected to have limited DNA-PAINT applications during dynein studies. Further testing will determine whether PAINT technology may be used to refine dynein-microtubule relationships.

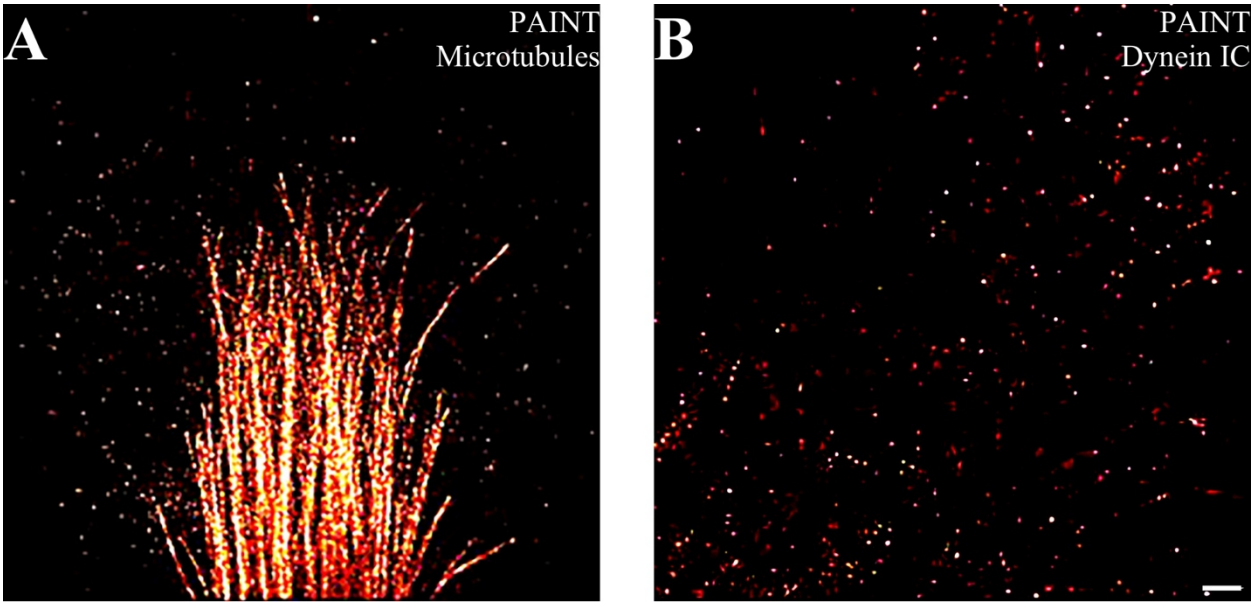

Figure 4.7. DNA-PAINT imaging of dynein IC and microtubules

Super-resolution PAINT images of (A) microtubules labeled with DNA-conjugated P7 secondary antibodies and P7-Atto 655 imager strands and (B) dynein IC labeled with DNA-conjugated P1 secondary antibodies and P1-Atto 655 imager strands in separate cells. Growth cones were immunolabeled with primary antibodies against (A) α-tubulin and (B) dynein IC. PAINT produced microtubule reconstructions but provided insufficient data for informative dynein reconstructions. Scale bar: 2 μm.

PAINT imaging and reconstructions were performed by Dr. Donghan Ma (Huang Lab, Purdue University, West Lafayette, IN).

Although DNA-PAINT did not reveal new details during these experiments, the investigations paved the way for employing this powerful tool in future neuronal studies. With ever-improving DNA-PAINT technologies, the spectrum of labeling capabilities will continue to expand. PAINT promises to increase the number of neuronal proteins that may be imaged simultaneously. It also has the potential to specifically and simultaneously label multiple subunits in complex proteins, such as dynein, to fully define molecular interactions.

4.3 Study Limitations

This study provided significant insights into dynein-microtubule interactions, but it is important to acknowledge the limitations of fluorescence microscopy and co-localization analysis. Errors are introduced during co-localization quantifications because molecules in the same subcellular region are not necessarily bound, fluorescent displays are artifact-prone, and image acquisition and measurement techniques are not standardized (Barlow et al., 2010; Moser et al., 2017). To mitigate these factors, images were acquired using the same acquisition and emission settings during all conventional microscopy experiments. Images were also processed using the same settings for each sample, and image thresholding was performed with minimal differences among samples. Additionally, super-resolution imaging was conducted to confirm co-localization.

4.4 Conclusion

Dampening microtubule dynamics reduced both dynein-microtubule co-localization and microtubule extension beyond the C domain (Fig. 4.3 E, F). Dynein inhibition also disturbed microtubule extension less than blocking microtubule assembly and did not significantly impact dynein-microtubule co-localization (Fig. 4.3 E, F). These findings, combined with the knowledge that CilD locks dynein in a weakly-bound transition state on microtubules, suggest microtubule assembly is required for dynein to affect microtubule forward translocation through motor activity and plus-end binding activity (Roossien et al., 2015). The results also unveiled new possibilities for precisely resolving details of dynein-microtubule interactions with SMSN.

CHAPTER 5. MICROTUBULE ASSEMBLY AND DYNEIN-MEDIATED TRANSLOCATION DURING NEURITE ELONGATION

A version of this chapter has been submitted to a peer-reviewed journal for publication.

5.1 Introduction

Early studies employing microtubule-assembly inhibitors and microtubule-stabilizing agents suggested microtubule assembly at the distal end of the axon is the driving force for axonal elongation (Bamburg et al., 1986; Letourneau and Ressler, 1984). More recently, individual microtubule translocation and bulk microtubule movement were detected in advancing growth cones and elongating neurites (Athamneh et al., 2017; Lee and Suter, 2008; Schaefer et al., 2002). Bulk microtubule movements occur at slower speeds than individual sliding and correlate with neurite elongation (Athamneh et al., 2017). These mass microtubule movements differ from individual sliding that initiates new neurites because they are more closely related to cell migration and represent the flow of a meshwork of cross-linked microtubules, actin, and motor proteins (Baas and Yu, 1996; Chang et al., 1998; Hutchins and Wray, 2014; Lu et al., 2013; Lu and Gelfand, 2017). Studies have demonstrated that both neurite elongation and docked mitochondrial movement, an indicator of bulk microtubule advance, decrease when microtubule assembly is blocked with Noc (Athamneh et al., 2017). Similar effects have occurred when dynein is disrupted, which raises questions about how microtubule assembly, dynein activity, and microtubule translocation are related and how they contribute to neurite elongation (Roossien et al., 2014). In the present study, the contributions of these processes were investigated by inhibiting microtubule assembly with Noc, dynein with CilD, or both in combination before analyzing neurite growth, microtubule translocation and dynamics, and axonal tension. Inhibiting microtubule assembly and dynein activity did not have additive effects on neurite growth and had partial compensatory effects on microtubule movements, suggesting microtubule dynamics and translocation are interdependent processes. Specifically, this study indicates microtubule assembly is required for dynein to generate individual and bulk microtubule movements during neurite elongation.

5.2 Results

5.2.1 Dynein inhibition attenuates neurite growth rate reductions caused by blocking microtubule assembly

This experimental series tested the hypothesis that dynein-driven microtubule movement and microtubule assembly are interdependent processes in neurite elongation. Dynein was chronically inhibited with 10 μM CilD, microtubule assembly dynamics were blocked with 1 μM Noc, or dynein and microtubule assembly were inhibited simultaneously with mixed CilD-Noc treatments for 6 h in cultured *Aplysia californica* bag cell neurons (Fig. 5.1 A-D). Neurite elongation rates were measured with phase contrast microscopy, revealing Noc alone decreased neurite velocity from 4.4±0.5 μm/h to -2.9±0.3 μm/h, whereas CilD and simultaneous CilD-Noc treatments reduced velocity to 0.0±0.3 μm/h and -1.1±0.1 μm/h, respectively (mean±s.e.m.) (Fig. 5.1 E). Although future tests with lower and higher concentrations of CilD and Noc will reveal precise details of dynein-microtubule contributions to neurite growth, the lack of an additive effect of the combination treatment in the present study suggests dynein activity and microtubule assembly are interdependent with respect to neurite elongation. Reduced variance in CilD-Noc neurites compared to other groups also indicates growth cone dynamics are largely influenced by both dynein activity and microtubule assembly (Fig. 5.1 E).

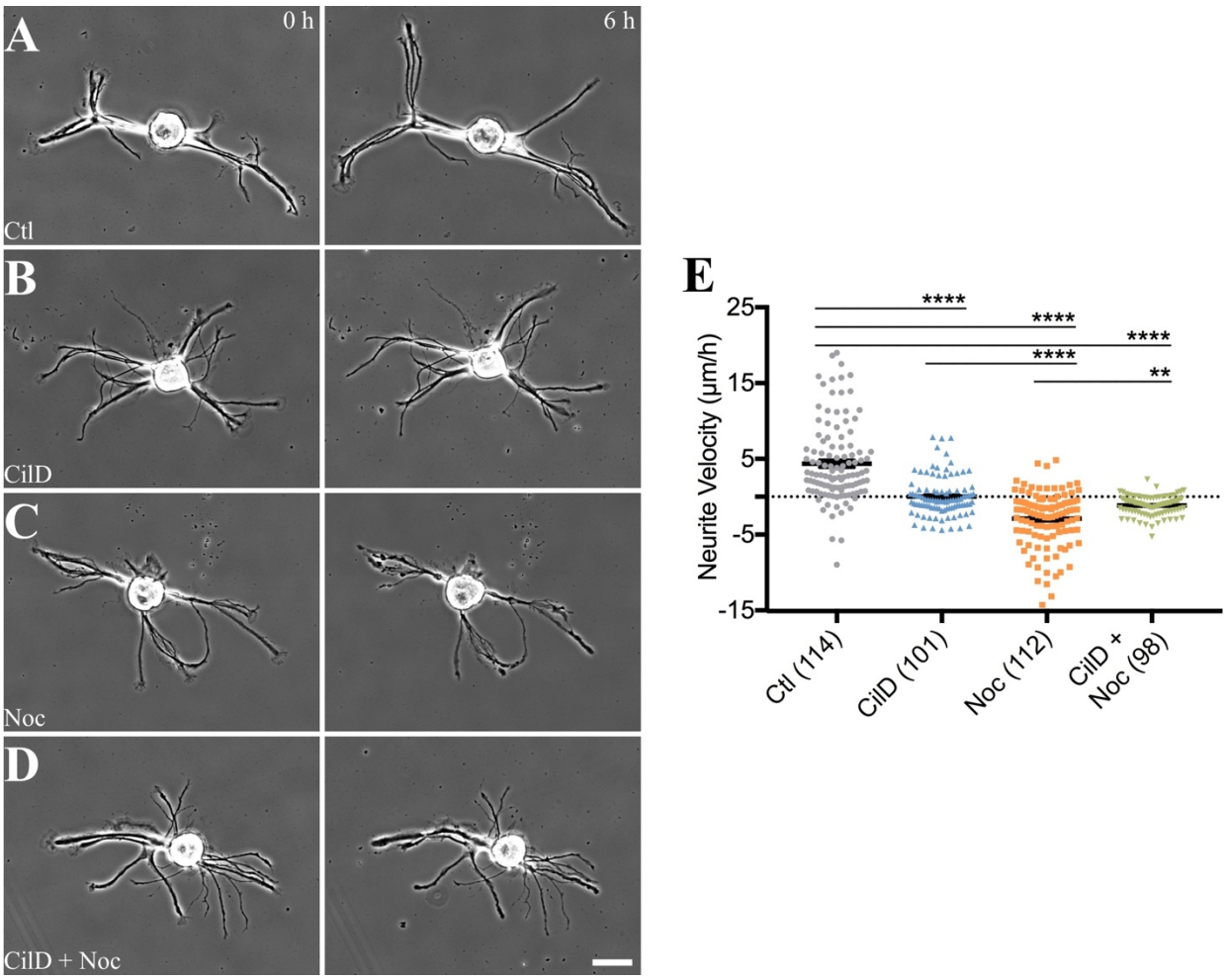

Figure 5.1. Combined CilD and Noc reduces neurite growth rates less than Noc alone

10 µM CilD and 1 µM Noc were applied separately or together to *Aplysia* bag cell neuronal cultures to disrupt dynein activity and microtubule assembly. CilD was applied 5 min prior to Noc in combined treatments to ensure dynein inhibition preceded microtubule assembly inhibition. (A-D) Phase contrast images of (A) control (ctl), (B) CilD, (C) Noc, (D) CilD and Noc neurons before and after 6 h chronic treatments. Scale bar: 50 µm. (E) Combination treatments reduced neurite elongation rates less than Noc alone. Parenthetical numbers represent neurites. Plots represent mean±s.e.m. for three independent experiments; ****$p<0.0001$, **$p<0.01$ (one-way ANOVA with Tukey's post hoc test).

5.2.2 Microtubule assembly and dynein activity cooperate in bulk and individual microtubule translocation

Previous studies revealed a high correlation between bulk microtubule velocity and neurite growth rates in both chick sensory and *Aplysia* bag cell neurons (Athamneh et al., 2017). The

present study tested the hypothesis that both dynein activity and microtubule assembly are required for bulk microtubule translocation and that these processes are interdependent. X-rhodamine-labeled tubulin was injected into bag cell neurons, and bulk microtubule motion was monitored for 15 min by FSM while tracking corresponding neurite velocity for 1.5 h by phase contrast microscopy (Fig. 5.2 A). Bulk microtubule translocation velocities were measured on kymographs spanning from the leading edge of the growth cone to 50 μm from the T zone (Fig. 5.2 A', B). Average bulk microtubule anterograde velocity was 7.3±1.4 μm/h in controls, but velocities were significantly lower in all three drug conditions: –2.1±0.7 μm/h for Noc, 0.0±0.7 μm/h for CilD, and 1.8±0.5 μm/h for CilD-Noc (mean±s.e.m.) (Fig. 5.2 C). Regression analysis revealed a strong correlation between neurite and bulk microtubule velocity, with an R^2 of 79%, which is consistent with previous studies (Fig. 5.4 B) (Athamneh et al., 2017). The reduction in bulk microtubule velocity when microtubule assembly or dynein activity were inhibited, the reduced variability in mass microtubule velocity in combination-treated cells compared to other treatment groups, and the high correlation between neurite and bulk microtubule velocity, suggest both microtubule dynamics and dynein activity are required for anterograde bulk microtubule translocation and neurite elongation.

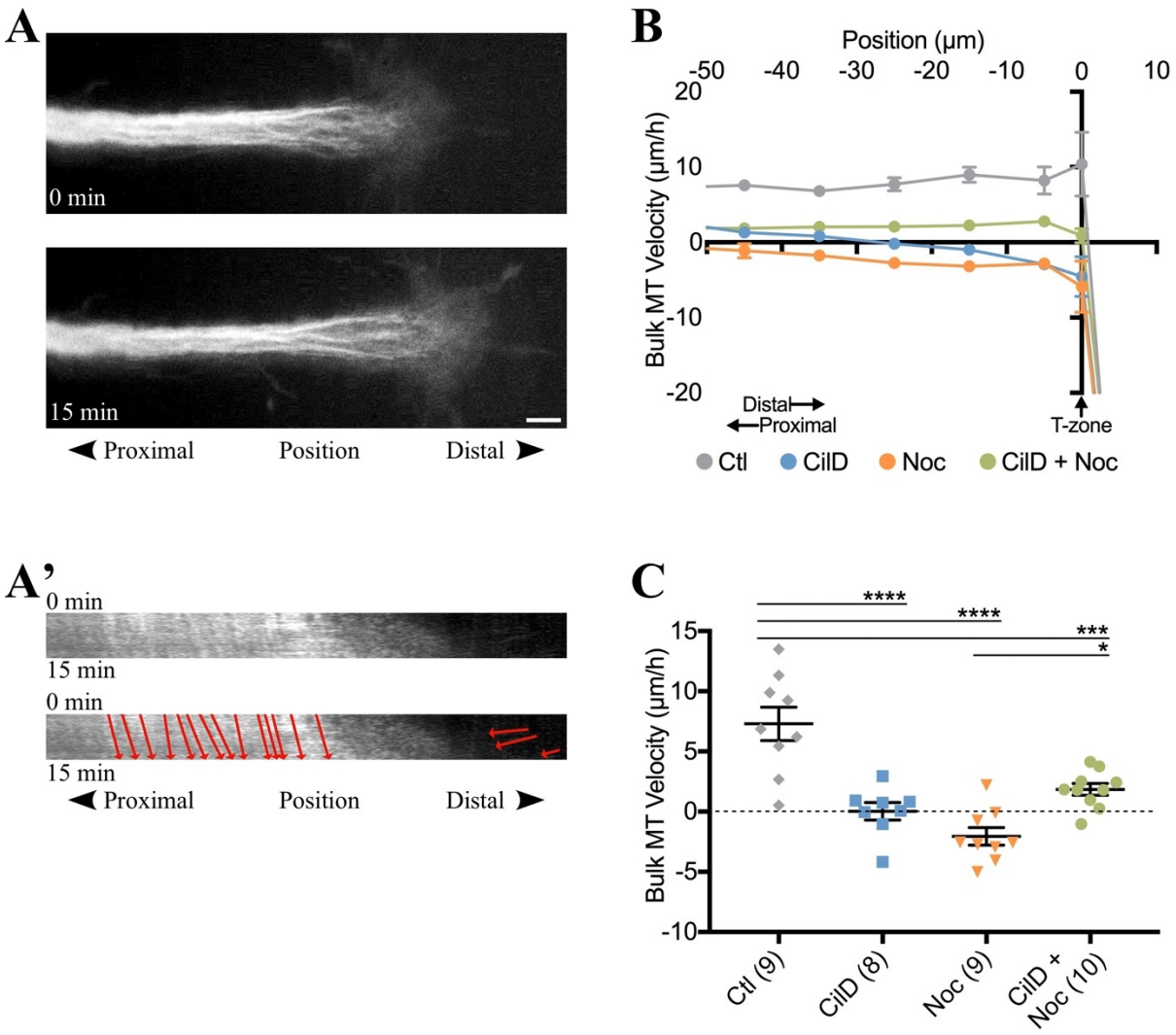

Figure 5.2. Bulk microtubule velocity depends on microtubule assembly and dynein activity

(A) Fluorescent images display microtubule distribution in a control neurite at time 0 and 15 min later. Scale: 10 µm. (A') The kymograph of the entire region in (A) displays anterograde bulk microtubule movement with characteristic retrograde velocity in the growth cone P domain and anterograde velocity in the C domain. The duplicated kymograph includes traces that indicate motion. (B) Bulk microtubule (MT) velocity as a function of distance from the transition zone set at the origin. Velocities are plotted as mean±s.e.m. for 10 µm regions along the neurite (ctl: control). (C) Bulk microtubule velocity from 10 to 50 µm proximal to the transition zone represented as mean±s.e.m.; ****$p<0.0001$, ***$p<0.001$, *$p<0.05$ (one-way ANOVA with Tukey's post hoc test). Parenthetical numbers represent neurons. Data in (B, C) are from eight independent experiments.

Previous FSM studies have revealed a significant increase in individual microtubule anterograde translocation in *Aplysia* growth cones responding to adhesion molecule apCAM (Lee and Suter, 2008; Schaefer et al., 2008a). However, these investigations did not fully define the extent to which individual microtubule assembly and movements contribute to growth cone and neurite advance. Because bulk microtubule motion represents the coordinated movement of microtubules cross-linked with MAPs, some of which preferentially bind to polymerizing microtubules, the present study tested the hypothesis that microtubule assembly and dynein activity are required for individual microtubule translocation that precedes mass microtubule and neurite movements (Leung et al., 1999; Miller and Suter, 2018; Sun et al., 2001; Wu et al., 2008). Individual microtubule analysis revealed acute Noc and CilD treatments reduced forward microtubule velocities in the T zone and P domain more than combined CilD-Noc treatments, which was consistent with chronic treatments and bulk analysis (Figs 5.1; 5.2; 5.3 F, G). Acute treatments also revealed neurite velocities followed the same trend; individual Noc and CilD treatments reduced growth rates more than the combination treatment (Fig. 5.3 A-E). These results indicate Noc and CilD do not have additive effects and microtubule assembly and dynein-mediated microtubule translocation are interdependent processes required for neurite outgrowth. The reduced variances in neurite and individual microtubule velocities in combination treatment groups also strengthens the idea that growth cone dynamics depend upon both microtubule assembly and dynein activity (Fig. 5.3 E, G).

To further analyze individual microtubule behavior, percentages of microtubule forward, backward, and pause events were calculated, which revealed all drug treatments reduced forward and increased backward events (Fig. 5.3 H-J). Forward translocation occurred 6.7% more often in CilD than in Noc neurites and 11.9% more frequently in combined CilD-Noc than Noc neurites (Fig. 5.3 H). Retrograde translocation frequency was 36% higher in Noc and 23% higher in CilD growth cones compared to those in combination-treatment groups (Fig. 5.3 I). Pause frequency was 13% higher in combination treatment groups compared to all other groups (Fig. 5.3 J). Regression analysis revealed individual microtubule velocity correlates less with neurite velocity than bulk microtubule velocity (Fig. 5.4). These results indicate microtubule assembly and dynein-mediated anterograde translocation contribute to axonal growth in an interdependent manner and strengthen the hypothesis that individual microtubule translocation precedes mass microtubule movements associated with neurite advance.

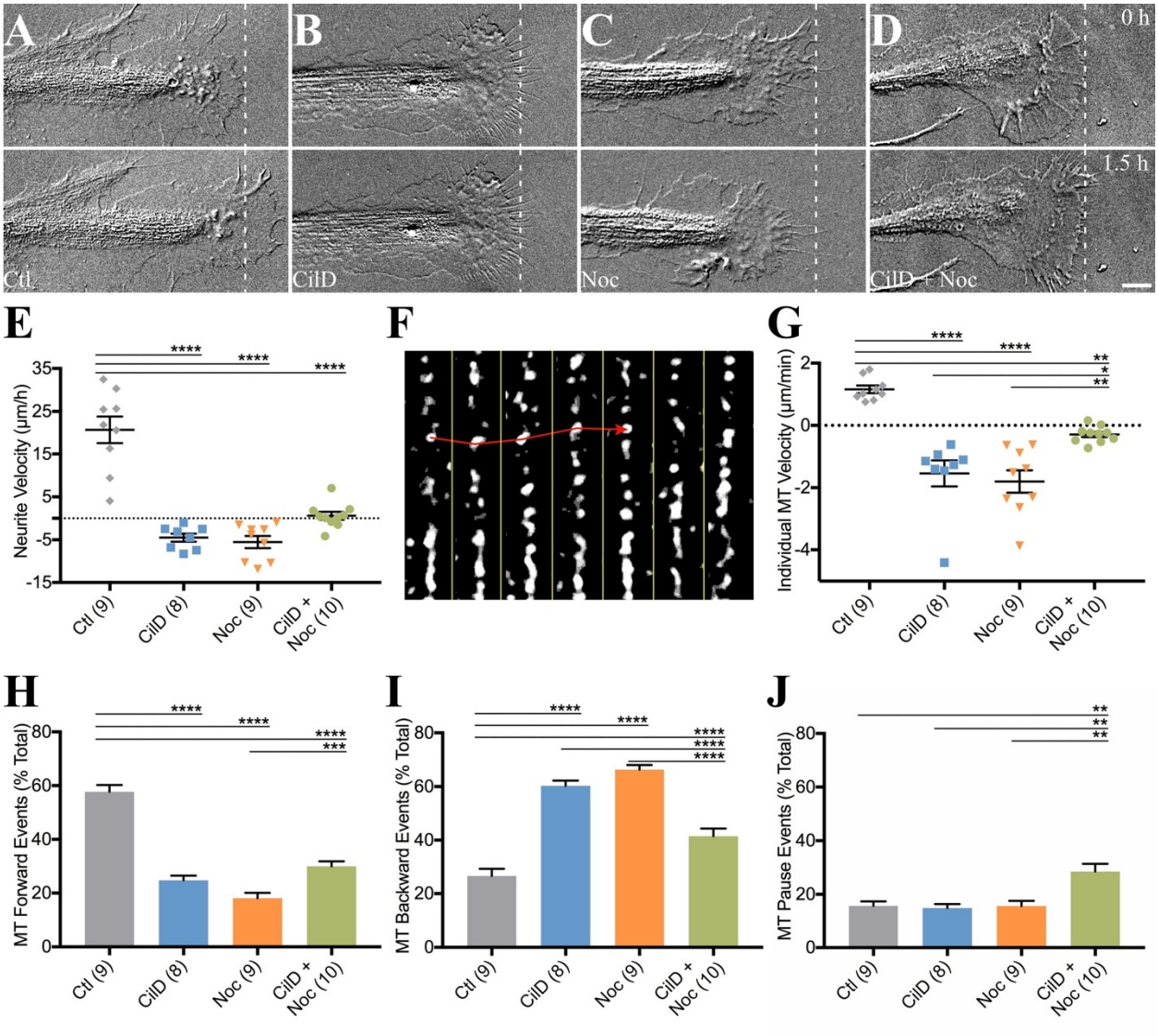

Figure 5.3. Microtubule dynamics and dynein activity are interdependent processes in individual microtubule translocation

(A-D) DIC images portray growth cone morphology and extension before and after 1.5 h treatments with (A) DMSO (control (ctl)), (B) CilD, (C) Noc, (D) CilD and Noc. Scale bar: 10 μm. (E) CilD and Noc significantly reduced neurite growth rates, but the combination treatment had a lesser effect. (F) Time-lapse montage of an individual microtubule labeled with rhodamine tubulin at 15 s intervals. (G) Individual microtubule (MT) velocity. (H-J) Forward, backward, and pause events depicted as percentages of total microtubule events. Quantifications represent mean±s.e.m. from eight independent experiments; ****$p<0.0001$, ***$p<0.001$, **$p<0.01$, *$p<0.05$ ((E, G-I): one-way ANOVA with Tukey's post hoc test; (J): Mann-Whitney test). (G-J) depict averages of five microtubules for each neuron. Parenthetical numbers represent neurons.

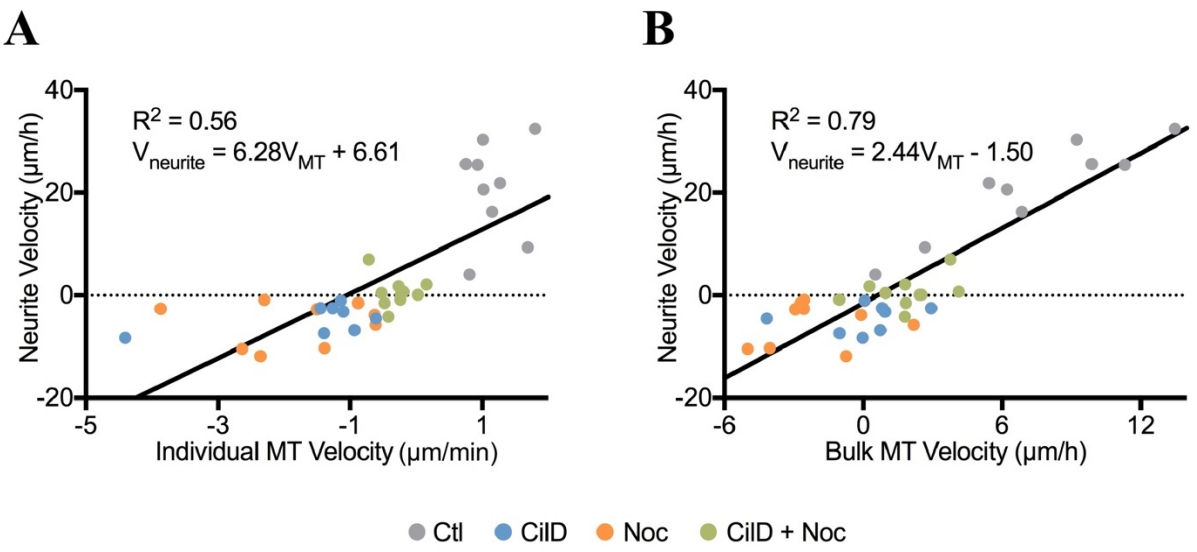

Figure 5.4. Neurite velocity correlates more with bulk than individual microtubule velocity

(A) Regression analysis of average individual microtubule (MT) velocity versus axon velocity. Each point represents the velocity of one neurite and the average velocity of five individual microtubules. (B) Regression analysis of bulk microtubule velocity versus neurite velocity. Each point represents the axonal velocity of one neurite and the average bulk microtubule velocity from 10 to 50 µm proximal to the T zone. Data are from eight independent experiments.

5.2.3 Microtubule assembly inhibition disrupts MACF43-microtubule associations

Next, the study explored whether dynein inhibition affects microtubule assembly rates. Bag cell neurons were microinjected with mRNA encoding a 43-residue fragment of GFP-tagged microtubule-actin-crosslinking-factor (GFP-MACF43). MACF tracks microtubule growth ends by interacting with end-binding proteins via associations at its C-terminal domains, as described previously (Leung et al., 1999; Sun et al., 2001). Dynein inhibition did not significantly impact MACF comet dynamics (Fig. 5.5 A, B, E-G). Microtubule growth velocity was 8.0±0.4 µm/min in control growth cones and 8.2±0.4 µm/min in CilD-treated growth cones; microtubule growth lengths were the same at 2.2±0.1 µm (mean±s.e.m.) (Fig. 5.5 E, F). Although statistically significant, the difference between control and CilD microtubule lifetimes was small: 17.1±0.3 s versus 16.2±0.3 s (mean±s.e.m.) (Fig. 5.5 G). Noc abolished the GFP-MACF43 signal in less than 5 min because MACF43 preferentially binds to growing microtubules (Fig. 5.5 C, D).

These findings indicate dynein inhibition does not significantly affect microtubule growth, whereas microtubule assembly disruption inhibits associations between +TIPs and microtubules.

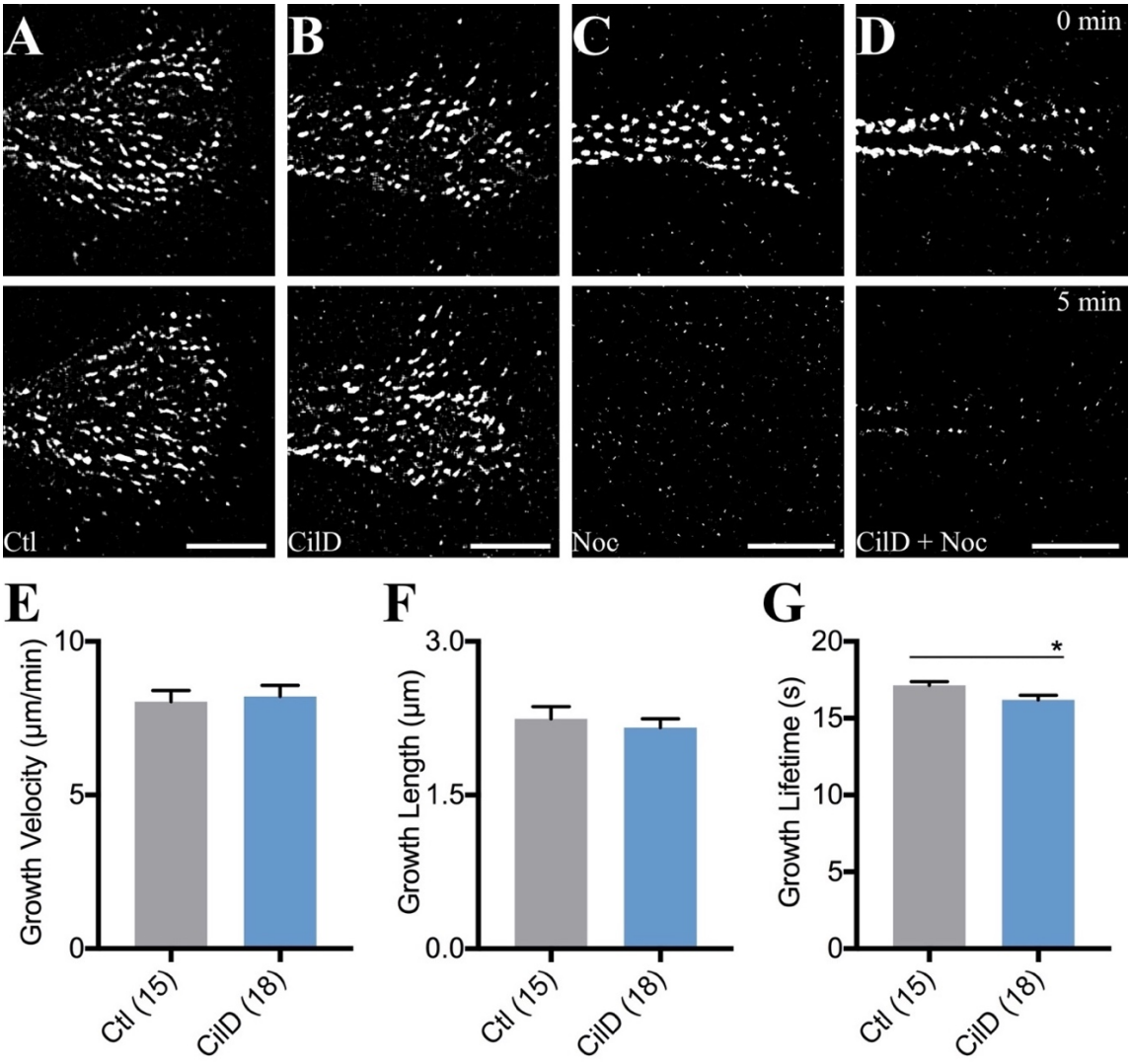

Figure 5.5. Dynein inhibition does not affect microtubule growth rates

The +TIP GFP-MACF43 was expressed to measure microtubule assembly rates, growth lengths, and growth lifetimes. The top images display MACF43 comets in (A) control (ctl), (B) CilD, (C) Noc, (D) CilD and Noc growth cones at time 0; the bottom images show the same growth cones 5 min later. MACF43 comets disappeared immediately when microtubule assembly was inhibited (C, D). (E-G) Microtubule growth velocity, length, and lifetime for 2 min following drug application. Data are depicted as mean±s.e.m. from nine independent experiments; *$p<0.05$ (Mann-Whitney test). Parenthetical numbers represent neurites. Scale bars: 10 µm.

5.2.4 Increases in axonal tension induced by dynein inhibition depend on microtubule dynamics

Disrupting dynein with CilD or blocking microtubule assembly with Noc increases axonal tension in chick DRG axons by similar amounts (Athamneh et al., 2017; Roossien et al., 2014). If separate mechanisms cause a rise in tension during individual treatments, simultaneous inhibition of dynein activity and microtubule assembly is expected to cause an increase in tension compared to individual treatments. Conversely, if microtubule assembly and dynein activity are cooperative, dynein inhibition is expected to compensate for a rise in tension caused by microtubule assembly inhibition. To test these possibilities during the present study, the Miller Lab (Michigan State University, East Lansing, MI) conducted a series of experiments in which chick DRG growth cones were attached to force-calibrated needles, and forces were allowed to stabilize before CilD and Noc were added sequentially to culture medium. Tension levels doubled upon CilD treatment. Rather than rising more, tension decreased significantly following subsequent Noc treatment. These biophysical results further support the conclusion that microtubule assembly and dynein-mediated microtubule movement are interdependent processes.

5.3 Discussion

The necessity of microtubule assembly for axonal elongation is well established (Coles and Bradke, 2015; Kapitein and Hoogenraad, 2015; Letourneau and Ressler, 1984; Voelzmann et al., 2016). While assembly alone was once considered crucial for outgrowth, recent studies highlight the importance of individual microtubule sliding during neurite initiation, rapid sliding along growing axons, translocation in advancing growth cones responding to adhesion substrates and traction forces, and bulk motion during axonal elongation (Athamneh et al., 2017; Baas and Black, 1990; Baas et al., 1991; Bamburg et al., 1986; del Castillo et al., 2015; Lee and Suter, 2008; Lu et al., 2013; Schaefer et al., 2008a). Although microtubule assembly and translocation have generally been viewed as independent processes, the observation that disruption of microtubule assembly blocks bulk translocation of docked mitochondria in a manner similar to the disruption of dynein raised questions about whether and how microtubule assembly, dynein activity, and microtubule translocation are interlinked (Athamneh et al., 2017; Roossien et al., 2014).

This study demonstrated that concurrently attenuating microtubule assembly and dynein activity does not have additive effects on neurite elongation rates, which further suggests the two processes are interdependent (Fig. 5.1). Because disrupting microtubule assembly blocks microtubule associations with +TIPs and +TIPs recruit dynein to microtubule plus ends, growth cones and microtubules were imaged after inhibiting microtubule assembly and dynein activity to determine whether microtubule assembly is required for dynein-microtubule interactions (Coles and Bradke, 2015; Erdogan et al., 2017; Kapitein and Hoogenraad, 2015). Treatments affected bulk and individual microtubule movements in a manner similar to how they affected neurite behavior. Inhibiting either microtubule assembly or dynein activity reduced microtubule translocation (Figs 5.2, 5.3). Inhibiting both processes also reduced individual microtubule translocation less than inhibiting microtubule assembly alone, implying microtubule assembly is required for dynein-mediated translocation. Consistent with a previous study, there was a strong correlation between bulk forward microtubule translocation and neurite elongation rates (Fig. 5.4 B) (Athamneh et al., 2017). The present study also revealed individual microtubule translocation velocity in neurons treated with combined CilD-Noc was less negative than in neurons treated with either CilD or Noc alone (Fig. 5.3 G). The higher percentage of retrograde microtubule events that occurred in isolated treatment groups compared to combination treatment samples, and the increase in microtubule pausing in combination versus individual treatment growth cones indicates microtubule assembly and dynein activity are interrelated (Fig. 5.3 I, J). Furthermore, the higher frequency of forward microtubule translocation events in CilD growth cones compared to those treated with Noc strengthens the idea that microtubule assembly is required for translocation (Fig. 5.3 H). Additional studies are required to completely explain the mechanism, but the significant increase in individual microtubule retrograde movements with CilD and Noc, along with the increase in paused microtubules with combination treatments, suggests different mechanisms exist that link microtubules to retrograde actin flow.

This study built upon previous biophysical experiments to further investigate relationships between microtubule dynamics and dynein-driven translocation with respect to axonal tension. Classical studies demonstrated microtubule disruption increases axonal tension and led to the longstanding idea that microtubule assembly generates a pushing force that counteracts actomyosin contraction to drive neurite elongation (Athamneh et al., 2017; Buxbaum and Heidemann, 1992; Joshi et al., 1985). Recent studies have shown inhibiting dynein induces bulk

microtubule retraction and increases axonal tension (Athamneh et al., 2017; Roossien et al., 2014). Additionally, they enabled a working model in which tension increases when dynein is inhibited because it is unable to counteract actomyosin contractile forces (Ahmad et al., 2000; Roossien et al., 2014). In the present study, the Miller Lab (Michigan State University, East Lansing, MI) found axonal tension increased with CilD; however, tension decreased dramatically upon subsequent Noc addition. While additional studies are required to fully explain this response, one possibility is microtubules uncouple from the actin cytoskeleton because fewer dynein molecules link them to surrounding structures. Together these results suggest the possibility that tension increases when microtubule assembly is disrupted partially because dynein-mediated force generation decreases. Incorporating microtubule assembly enhancers and dynein knockout techniques into future biophysical experiments will provide insight into the strength of this explanation.

5.4 Study Limitations

Testing throughout this study relied extensively upon applications of pharmacological agents. A concern with this approach is the increased potential for confounding variables compared to alternative techniques. Unknown causes may have contributed to the effects observed during this project, but an abundance of caution was applied during experimentation and data analysis to ensure the highest levels of accuracy. Strict adherence to consistent testing conditions and quantification methods maintained factors other than microtubule assembly and dynein-mediated translocation as constant as possible. Although a multitude of variables affect neuronal growth, the relationships identified during this work are reasonable due to careful experimental design and cautious data interpretations.

Another limitation was individual microtubule translocation could be measured only in the T zone and P domain because microtubule density was too high for speckle analysis in other regions. Furthermore, microtubule growth velocities were measured by tracking MACF43, but assembly rates were not quantified directly via FSM analysis. Thus, the behavior of the individual microtubules analyzed may not fully represent the population of microtubules driving axonal elongation. Future SMSN experiments should further clarify individual microtubule behavior.

5.5 Conclusion

This study concludes with a model that suggests normal dynein-microtubule interactions counteract actin retrograde flow, slide microtubules forward, and balance neurite tension to drive neurite elongation (Fig. 5.6). Dynein pulls microtubules forward in the C and P domains while the actomyosin contractile system pulls microtubules forward in the C domain and pushes them backward in the P domain via microtubule-actin linkers, such as MACF (Fig. 5.6 B). In the axon and growth cone, dynein pushes microtubules apart and counterbalances actomyosin contractile forces. When dynein is inhibited, microtubule-actin linkers continue to pull microtubules forward in the C domain and push them backward in the P domain, but dynein no longer pulls microtubules forward in either domain (Fig. 5.6 C). Meanwhile, retrograde actomyosin forces in the P domain and along the axon cause axonal retraction because dynein ceases to sufficiently counter these forces and slide microtubules forward. When microtubule assembly is blocked, microtubules are still pulled forward in the C domain because dynein-actin coupling persists; however, the loss of MACF and other +TIP interactions causes microtubule-actin uncoupling and reduces dynein recruitment to microtubule plus ends (Fig. 5.6 D). This activity decreases dynein pushing forces along the axon and in the growth cone, which allows actomyosin to pull microtubules rearward and results in increased axonal tension, slowed axonal growth, and more microtubule backward sliding. Simultaneous microtubule assembly and dynein inhibition disrupts microtubule-actin coupling for three reasons: it reduces microtubule extension into the P domain, abolishes microtubule binding with MACF and other actin cross-linkers, and decreases dynein cross-linkages between microtubules and actin (Fig. 5.6 E). In this case, neurites remain nearly stationary rather than retracting because the loss of connectivity results in more paused microtubules and a drop in axonal tension. In summary, this model underscores the interdependent relationship between microtubule assembly and dynein-driven microtubule translocation in neurite elongation, and it shows microtubule assembly affects axonal growth primarily by enabling dynein and microtubule-actin cross-linkers to mediate microtubule motion.

Figure 5.6. Microtubule assembly and dynein-mediated translocation are interdependent activities required for neurite elongation

(A) Schematic of the growth cone domains and primary cytoskeletal elements. (B) Normal dynein-microtubule interactions counter non-muscle myosin II-driven actin retrograde flow, slide microtubules forward, and balance neurite tension to promote axonal growth. Dynein pulls microtubules forward in the C and P domains. The actomyosin contractile system pulls microtubules forward in the C domain and pushes it backward in the P domain via microtubule-actin linkers, such as MACF. In the axon (not depicted) and growth cone, dynein pushes microtubules apart and counters actomyosin contractile forces. (C) CilD treatments cause axonal retraction. MACF continues to mediate microtubule forward pulling in the C domain and backward pulling in the P domain; however, dynein does not pull microtubules forward in either domain. Additionally, dynein no longer sufficiently slides microtubules forward or counters retrograde actomyosin forces along the neurite and in the growth cone P domain. (D) Noc causes neurite retraction. Dynein-actin coupling continues and enables forward microtubule pulling, but microtubules and actin uncouple and dynein is not recruited to microtubule plus ends due to a loss of +TIP interactions. This decreases dynein pushing forces in the axon and growth cone, allowing actomyosin to move microtubules backward. Axonal tension rises, neurite growth slows, and microtubule backward sliding increases. (E) Concurrent CilD and Noc treatments cause forward and backward microtubule movements to decrease. This is caused by microtubule-actin uncoupling due to three factors: reduced microtubule extension into the P domain, abolished MACF cross-linking activity, and decreased dynein cross-linkages between microtubules and actin. The loss of connectivity causes microtubules to pause, neurite tension to drop, and neurites to remain nearly stationary. The figure excludes many linker and accessory molecules to emphasize proteins examined during this study.

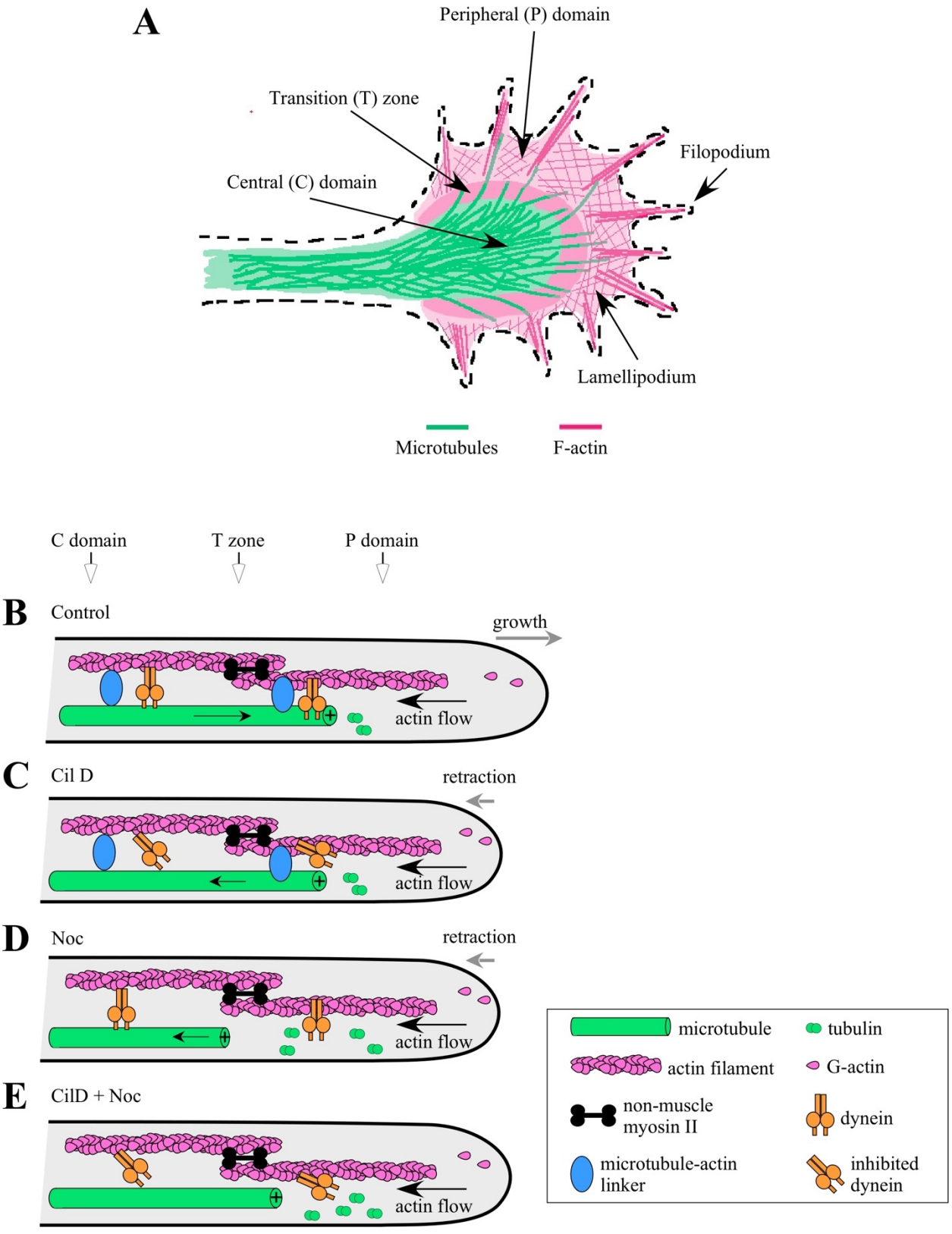
A
Peripheral (P) domain
Transition (T) zone
Filopodium
Central (C) domain
Lamellipodium
Microtubules
F-actin
C domain
T zone
P domain
B
Control
growth
actin flow
C
Cil D
retraction
actin flow
D
Noc
retraction
actin flow
E
CilD + Noc
actin flow
microtubule
tubulin
actin filament
G-actin
non-muscle myosin II
dynein
microtubule-actin linker
inhibited dynein

CHAPTER 6. FINAL THOUGHTS AND FUTURE RESEARCH

6.1 Final Thoughts

This body of work presented a new model of microtubule-dynein interactions in neuronal growth cones (Fig. 5.6). The proposed framework shows microtubule assembly affects microtubule anterograde translocation primarily by facilitating dynein motor and plus-end binding activities. It depicts dynein-microtubule interactions driving neurite elongation by counteracting actin retrograde flow, sliding microtubules forward, and balancing neurite tension.

Live- and fixed-cell experimentation demonstrated the strength of the model. Pharmacological agents were used to test the framework over a spectrum of conditions that enhanced or inhibited dynein activity and microtubule assembly. The deeper understanding of dynein-microtubule interactions resulting from this work provides a firm foundation for future microtubule-motor protein studies.

6.2 Future Research

Future endeavors should continue to pursue richer knowledge about dynein-microtubule interactions. To precisely define dynein-microtubule spatiotemporal relations, live-cell SMSN microtubule imaging should be conducted while applying the same treatment schemes described in this study. Super-resolution imaging of microtubules treated with taxol, Noc, and CilD alone and in various combinations will provide details about microtubule dynamics that conventional imaging cannot fully capture. Additionally, SMSN imaging of microtubules, dynein, and F-actin in fixed cells should be accomplished to further test the proposed model and determine details of dynein linkages with microtubules and F-actin. Experiments from this study should also be repeated while employing different CilD and Noc doses to test the model under milder and more intense dynein and microtubule inhibition. Based on data from the present study, linear relationships between drug concentrations and microtubule and neurite behaviors are expected.

Dynein knockout strategies should be employed during conventional and super-resolution imaging experiments to further define how dynein influences microtubules and neurite growth. To start, clustered regularly interspaced short palindromic repeats (CRISPR) and CRISPR-

associated protein 9 (Cas9) (CRISPR-Cas9) technology should be used to generate dynein knockouts in *Aplysia* neurons (Cong et al., 2013). This technique could be implemented immediately and efficiently due to the many digital and commercial tools available for construct design (Adli, 2018).

Attention should be directed toward clarifying the influences of non-muscle myosin II on microtubule dynamics and translocation. This task is important because targeting myosin holds the potential to deliver neuronal regeneration solutions (Hur et al., 2012). Furthermore, motor protein studies have traditionally focused on intracellular cargo transport, but increased attention has been given to their role in organizing cytoskeletal filaments (Ahmad et al., 2000; Vale, 2003). *Aplysia* neuronal studies have demonstrated this role by revealing that non-muscle myosin II is essential for severing actin bundles and regulating the shape and structure of the growth cone central domain (Burnette et al., 2008). Additionally, exposing *Aplysia* neurons to blebbistatin, an inhibitor that binds to the myosin II motor domain, enables long actin bundles to proliferate in the growth cone periphery and obscure the transition zone (Allingham et al., 2005; Medeiros et al., 2006). These results indicate that myosin inhibition is necessary for regulating growth cone guidance and actin retrograde flow (Medeiros et al., 2006; Turney and Bridgman, 2005). Data also suggest myosin inhibition both reorganizes actin and microtubules and frees microtubules from compressed states to facilitate their advancement toward the growth cone periphery and promote axonal motility (Hur et al., 2011).

Myosin-dynein-microtubule studies will address two rational explanations for why neuronal tension rises when microtubule assembly is inhibited: microtubule assembly disruption inhibits dynein force generation, or microtubule assembly inhibition leads to myosin activation via the guanine nucleotide exchange factor H1 (GEF-H1) signaling pathway (de Rooij et al., 2018; Miller and Suter, 2018; Takano et al., 2017). The first hypothesis was strengthened during the present work, but the second remains largely untested. Future experimentation is expected to reveal that both hypotheses are relevant and will help determine the relative influences of dynein force generation and myosin activation on neuronal force balance.

To begin testing these hypotheses, blebbistatin may be added to the existing treatment arsenal (Allingham et al., 2005). Incorporating myosin inhibition into proven live- and fixed-cell approaches should be a seamless process. Mechanisms driving myosin, dynein, MAP, and microtubule interactions may be investigated by light microscopy, FSM, and biophysical

analysis, as described in this report. Moreover, antibodies against *Aplysia* non-muscle myosin II heavy chain (NMIIHC), myosin II regulatory light chain (RLC), and phosphorylated-RLC (pRLC) have been validated during previous studies (Medeiros et al., 2006; Yang et al., 2013). NMIIHC antibodies were also verified as an effective tool under local laboratory conditions (Fig. 6.1).

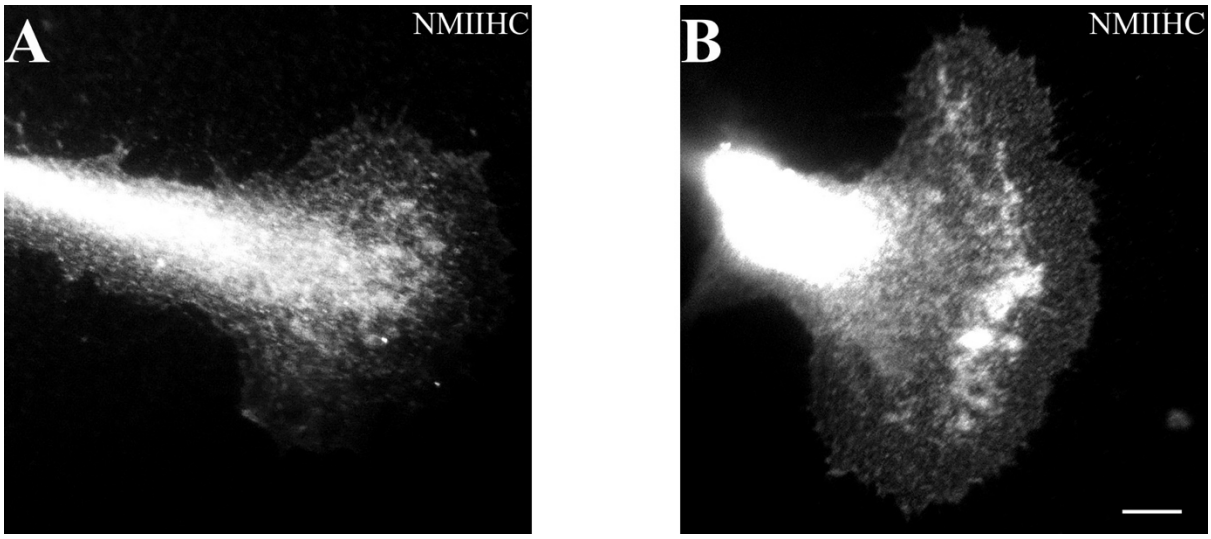

Figure 6.1. Non-muscle myosin II heavy chain labeling in *Aplysia* growth cones

Neurons were fixed with formaldehyde and immunolabeled with antibodies against NMIIHC. (A, B) Images display NMIIHC in growth cones from separate samples. Scale bar: 10 μm.

This project improved the framework for understanding dynein-microtubule interactions and proposed a new myosin-microtubule venture. Examining how myosin localization and activation influences dynein-microtubule associations will extend the reach of promising research into controlling microtubule dynamics and growth cone motility through myosin inhibition (Hur et al., 2011; Hur and Zhou, 2010). Through continuous, incremental improvements from projects such as these and collective, multidisciplinary efforts, essential knowledge about growth cone and microtubule dynamics will be obtained to actualize the goal of solving neuronal disorders.

REFERENCES

Adli, M. (2018). The CRISPR tool kit for genome editing and beyond. *Nature Communications, 9*(1), 1-13.

Agasti, S. S., Wang, Y., Schueder, F., Sukumar, A., Jungmann, R., & Yin, P. (2017). DNA-barcoded labeling probes for highly multiplexed Exchange-PAINT imaging. *Chemical Science, 8*(4), 3080-3091.

Ahmad, F. J., Hughey, J., Wittmann, T., Hyman, A., Greaser, M., & Baas, P. W. (2000). Motor proteins regulate force interactions between microtubules and microfilaments in the axon. *Nature Cell Biology, 2*(5), 276-280.

Akhmanova, A., & Steinmetz, M. O. (2008). Tracking the ends: a dynamic protein network controls the fate of microtubule tips. *Nature Reviews Molecular Cell Biology, 9*(4), 309-322.

Akhmanova, A., & Steinmetz, M. O. (2010). Microtubule plus TIPs at a glance. *Journal of Cell Science, 123*(20), 3415-3419.

Akhmanova, A., & Steinmetz, M. O. (2015). Control of microtubule organization and dynamics: Two ends in the limelight. *Nature Reviews Molecular Cell Biology, 16*(12), 711-726.

Al-Bassam, J., Kim, H., Brouhard, G., Van Oijen, A., Harrison, S. C., & Chang, F. (2010). CLASP promotes microtubule rescue by recruiting tubulin dimers to the microtubule. *Developmental Cell, 19*(2), 245-258.

Al-Bassam, J., Kim, H., Flor-Parra, I., Lal, N., Velji, H., & Chang, F. (2012). Fission yeast Alp14 is a dose-dependent plus end-tracking microtubule polymerase. *Molecular Biology of the Cell, 23*(15), 2878-2890.

Allan, V. J. (2011). Cytoplasmic dynein. *Biochemical Society Transactions, 39*(5), 1169-1178.

Allingham, J. S., Smith, R., & Rayment, I. (2005). The structural basis of blebbistatin inhibition and specificity for myosin II. *Nature Structural & Molecular Biology, 12*(4), 378-379.

Almeida, T. B., Carnell, A. J., Barsukov, I. L., & Berry, N. G. (2017). Targeting SxIP-EB1 interaction: An integrated approach to the discovery of small molecule modulators of dynamic binding sites. *Scientific Reports, 7*(1), 1-12.

Alushin, G. M., Lander, G. C., Kellogg, E. H., Zhang, R., Baker, D., & Nogales, E. (2014). High-resolution microtubule structures reveal the structural transitions in alpha beta-tubulin upon GTP hydrolysis. *Cell, 157*(5), 1117-1129.

Alves-Silva, J., Sánchez-Soriano, N., Beaven, R., Klein, M., Parkin, J., Millard, T. H., ... & Prokop, A. (2012). Spectraplakins promote microtubule-mediated axonal growth by functioning as structural microtubule-associated proteins and EB1-dependent plus TIPs (tip interacting proteins). *Journal of Neuroscience, 32*(27), 9143-9158.

Applegate, K. T., Besson, S., Matov, A., Bagonis, M. H., Jaqaman, K., & Danuser, G. (2011). PlusTipTracker: Quantitative image analysis software for the measurement of microtubule dynamics. *Journal of Structural Biology, 176*(2), 168-184.

Applewhite, D. A., Grode, K. D., Keller, D., Zadeh, A., Slep, K. C., & Rogers, S. L. (2010). The spectraplakin short stop is an actin-microtubule cross-linker that contributes to organization of the microtubule network. *Molecular Biology of the Cell, 21*(10), 1714-1724.

Athamneh, A. I. M., He, Y. P., Lamoureux, P., Fix, L., Suter, D. M., & Miller, K. E. (2017). Neurite elongation is highly correlated with bulk forward translocation of microtubules. *Scientific Reports, 7*(1), 1-13.

Auer, A., Schlichthaerle, T., Woehrstein, J. B., Schueder, F., Strauss, M. T., Grabmayr, H., & Jungmann, R. (2018). Nanometer-scale multiplexed super-resolution imaging with an economic 3D-DNA-PAINT microscope. *Chemphyschem, 19*(22), 3024-3034.

Ayaz, P., Munyoki, S., Geyer, E. A., Piedra, F. A., Vu, E. S., Bromberg, R., … & Rice, L. M. (2014). A tethered delivery mechanism explains the catalytic action of a microtubule polymerase. *Elife, 3*, 1-47.

Ayaz, P., Ye, X. C., Huddleston, P., Brautigam, C. A., & Rice, L. M. (2012). A TOG: Alpha beta-tubulin complex structure reveals conformation-based mechanisms for a microtubule polymerase. *Science, 337*(6096), 857-860.

Baas, P. W., & Ahmad, F. J. (1993). The transport-properties of axonal microtubules establish their polarity orientation. *Journal of Cell Biology, 120*(6), 1427-1437.

Baas, P. W., & Ahmad, F. J. (2013). Beyond taxol: Microtubule-based treatment of disease and injury of the nervous system. *Brain, 136*(10), 2937-2951.

Baas, P. W., & Black, M. M. (1990). Individual microtubules in the axon consist of domains that differ in both composition and stability. *Journal of Cell Biology, 111*(2), 495-509.

Baas, P. W., & Lin, S. (2011). Hooks and comets: The story of microtubule polarity orientation in the neuron. *Developmental Neurobiology, 71*(6), 403-418.

Baas, P. W., & Yu, W. Q. (1996). A composite model for establishing the microtubule arrays of the neuron. *Molecular Neurobiology, 12*(2), 145-161.

Baas, P. W., Deitch, J. S., Black, M. M., & Banker, G. A. (1988). Polarity orientation of microtubules in hippocampal-neurons - uniformity in the axon and nonuniformity in the dendrite. *Proceedings of the National Academy of Sciences of the United States of America, 85*(21), 8335-8339.

Baas, P. W., Rao, A. N., Matamoros, A. J., & Leo, L. (2016). Stability properties of neuronal microtubules. *Cytoskeleton, 73*(9), 442-460.

Baas, P. W., Slaughter, T., Brown, A., & Black, M. M. (1991). Microtubule dynamics in axons and dendrites. *Journal of Neuroscience Research, 30*(1), 134-153.

Bamburg, J. R., Bray, D., & Chapman, K. (1986). Assembly of microtubules at the tip of growing axons. *Nature, 321*(6072), 788-790.

Barlow, A. L., MacLeod, A., Noppen, S., Sanderson, J., & Guerin, C. J. (2010). Colocalization analysis in fluorescence micrographs: Verification of a more accurate calculation of Pearson's correlation coefficient. *Microscopy and Microanalysis, 16*(6), 710-724.

Belmont, L. D., & Mitchison, T. J. (1996). Identification of a protein that interacts with tubulin dimers and increases the catastrophe rate of microtubules. *Cell, 84*(4), 623-631.

Bieling, P., Kandels-Lewis, S., Telley, I. A., Van Dijk, J., Janke, C., & Surrey, T. (2008). CLIP-170 tracks growing microtubule ends by dynamically recognizing composite EB1/tubulin-binding sites. *Journal of Cell Biology, 183*(7), 1223-1233.

Bieling, P., Laan, L., Schek, H., Munteanu, E. L., Sandblad, L., Dogterom, M., ... & Surrey, T. (2007). Reconstitution of a microtubule plus-end tracking system in vitro. *Nature, 450*(7172), 1100-1105.

Bonnet, C., Boucher, D., Lazereg, S., Pedrotti, B., Islam, K., Denoulet, P., & Larcher, J. C. (2001). Differential binding regulation of microtubule-associated proteins MAP1A, MAP1B, and MAP2 by tubulin polyglutamylation. *Journal of Biological Chemistry, 276*(16), 12839-12848.

Bray, D., & Bunge, M. B. (1981). Serial analysis of microtubules in cultured rat sensory axons. *Journal of Neurocytology, 10*(4), 589-605.

Broderick, M. J. F., & Winder, S. J. (2005). Spectrin, alpha-actinin, and dystrophin. M. F. Richards, D. S. Eisenberg, & P. S. Kim (Eds.), *Fibrous Proteins: Coiled-Coils, Collagen and Elastomers* (Vol. 70, pp. 203-246). Cambridge, MA: Acedemic Press.

Brouhard, G. J., & Rice, L. M. (2018). Microtubule dynamics: An interplay of biochemistry and mechanics. *Nature Reviews Molecular Cell Biology, 19*(7), 451-463.

Brouhard, G. J., Stear, J. H., Noetzel, T. L., Al-Bassam, J., Kinoshita, K., Harrison, S. C., Howard, J., & Hyman, A. A. (2008). XMAP215 is a processive microtubule polymerase. *Cell, 132*(1), 79-88.

Buey, R. M., Diaz, J. F., & Andreu, J. M. (2006). The nucleotide switch of tubulin and microtubule assembly: A polymerization-driven structural change. *Biochemistry, 45*(19), 5933-5938.

Burnette, D. T., Ji, L., Schaefer, A. W., Medeiros, N. A., Danuser, G., & Forscher, P. (2008). Myosin II activity facilitates microtubule bundling in the neuronal growth cone neck. *Developmental Cell, 15*(1), 163-169.

Burton, P. R., & Paige, J. L. (1981). Polarity of axoplasmic microtubules in the olfactory nerve of the frog. *Proceedings of the National Academy of Sciences of the United States of America-Biological Sciences, 78*(5), 3269-3273.

Buxbaum, R. E., & Heidemann, S. R. (1992). An absolute rate theory model for tension control of axonal elongation. *Journal of Theoretical Biology, 155*(4), 409-426.

Candeias, V., & Diabo, R. (2018). Here are five priorities for better cooperation on mental health. Retrieved from https://www.weforum.org/agenda/2018/11/five-ways-mental-health-care-better-depression/

Carter, A. P. (2013). Crystal clear insights into how the dynein motor moves. *Journal of Cell Science, 126*(3), 705-713.

Chang, S. H., Rodionov, V. I., Borisy, G. G., & Popov, S. V. (1998). Transport and turnover of microtubules in frog neurons depend on the pattern of axonal growth. *Journal of Neuroscience, 18*(3), 821-829.

Chen, H. J., Lin, C. M., Lin, C. S., Perez-Olle, R., Leung, C. L., & Liem, R. K. H. (2006). The role of microtubule actin cross-linking factor 1 (MACF1) in the Wnt signaling pathway. *Genes & Development, 20*(14), 1933-1945.

Cole, D. G. (2003). The intraflagellar transport machinery of Chlamydomonas reinhardtii. *Traffic, 4*(7), 435-442.

Coles, C. H., & Bradke, F. (2015). Coordinating neuronal actin-microtubule dynamics. *Current Biology, 25*(15), R677-R691.

Conde, C., & Caceres, A. (2009). Microtubule assembly, organization and dynamics in axons and dendrites. *Nature Reviews Neuroscience, 10*(5), 319-332.

Cong, L., Ran, F. A., Cox, D., Lin, S. L., Barretto, R., Habib, N., … & Zang, F. (2013). Multiplex genome engineering using CRISPR/Cas systems. *Science, 339*(6121), 819-823.

Conn, P. J., & Kaczmarek, L. K. (1989). The bag cell neurons of *Aplysia* - a model for the study of the molecular mechanisms involved in the control of prolonged animal behaviors. *Molecular Neurobiology, 3*(4), 237-273.

Coombes, C. E., Yamamoto, A., Kenzie, M. R., Odde, D. J., & Gardner, M. K. (2013). Evolving tip structures can explain age-dependent microtubule catastrophe. *Current Biology, 23*(14), 1342-1348.

Coquelle, F. M., Caspi, M., Cordelieres, F. P., Dompierre, J. P., Dujardin, D. L., Koifman, C., … & De Mey, J. R. (2002). LIS1, CLIP-170's key to the dynein/dynactin pathway. *Molecular and Cellular Biology, 22*(9), 3089-3102.

Coue, M., Lombillo, V. A., & McIntosh, J. R. (1991). Microtubule depolymerization promotes particle and chromosome movement *in vitro*. *Journal of Cell Biology, 112*(6), 1165-1175.

Davenport, R. W., Dou, P., Rehder, V., & Kater, S. B. (1993). A sensory role for neuronal growth cone filopodia. *Nature, 361*(6414), 721-724.

De Groot, C. O., Jelesarov, I., Damberger, F. F., Bjelic, S., Scharer, M. A., Bhavesh, N. S., … & Akhmanova, A. (2010). Molecular insights into mammalian end-binding protein heterodimerization. *Journal of Biological Chemistry, 285*(8), 5802-5814.

De Rooij, R., Kuhl, E., & Miller, K. E. (2018). Modeling the axon as an active partner with the growth cone in axonal elongation. *Biophysical Journal, 115*(9), 1783-1795.

Dehmelt, L., Nalbant, P., Steffen, W., & Halpain, S. (2006). A microtubule-based, dynein-dependent force induces local cell protrusions: Implications for neurite initiation. *Brain Cell Biology, 35*(1), 39-56.

Dehmelt, L., Smart, F. M., Ozer, R. S., & Halpain, S. (2003). The role of microtubule-associated protein 2c in the reorganization of microtubules and lamellipodia during neurite initiation. *Journal of Neuroscience, 23*(29), 9479-9490.

Del Castillo, U., Winding, M., Lu, W., & Gelfand, V. I. (2015). Interplay between kinesin-1 and cortical dynein during axonal outgrowth and microtubule organization in Drosophila neurons. *Elife, 4*, 1-20.

Dent, E. W., & Gertler, F. B. (2003). Cytoskeletal dynamics and transport in growth cone motility and axon guidance. *Neuron, 40*(2), 209-227.

Dent, E. W., & Kalil, K. (2001). Axon branching requires interactions between dynamic microtubules and actin filaments. *Journal of Neuroscience, 21*(24), 9757-9769.

Desai, A., & Mitchison, T. J. (1997). Microtubule polymerization dynamics. *Annual Review of Cell and Developmental Biology, 13*(1), 83-117.

Desai, A., Verma, S., Mitchison, T. J., & Walczak, C. E. (1999). Kin I kinesins are microtubule-destabilizing enzymes. *Cell, 96*(1), 69-78.

Dimitrov, A., Quesnoit, M., Moutel, S., Cantaloube, I., Pous, C., & Perez, F. (2008). Detection of GTP-tubulin conformation in vivo reveals a role for GTP remnants in microtubule rescues. *Science, 322*(5906), 1353-1356.

Dixit, R., Barnett, B., Lazarus, J. E., Tokito, M., Goldman, Y. E., & Holzbaur, E. L. F. (2009). Microtubule plus-end tracking by CLIP-170 requires EB1. *Proceedings of the National Academy of Sciences,* 106(2), 492-497.

Djinovic-Carugo, K., Gautel, M., Ylanne, J., & Young, P. (2002). The spectrin repeat: A structural platform for cytoskeletal protein assemblies. *FEBS Letters, 513*(1), 119-123.

Dogterom, M., & Yurke, B. (1997). Measurement of the force-velocity relation for growing microtubules. *Science, 278*(5339), 856-860.

Du, Y. Q., English, C. A., & Ohi, R. (2010). The kinesin-8 Kif18A dampens microtubule plus-end dynamics. *Current Biology, 20*(4), 374-380.

Duellberg, C., Fourniol, F. J., Maurer, S. P., Roostalu, J., & Surrey, T. (2013). End-binding proteins and Ase1/PRC1 define local functionality of structurally distinct parts of the microtubule cytoskeleton. *Trends in Cell Biology, 23*(2), 54-63.

Duellberg, C., Trokter, M., Jha, R., Sen, I., Steinmetz, M. O., & Surrey, T. (2014). Reconstitution of a hierarchical +TIP interaction network controlling microtubule end tracking of dynein. *Nature cell biology, 16*(8), 804-11.

Erdogan, B., Cammarata, G. M., Lee, E. J., Pratt, B. C., Francl, A. F., Rutherford, E. L., & Lowery, L. A. (2017). The microtubule plus-end-tracking protein TACC3 promotes persistent axon outgrowth and mediates responses to axon guidance signals during development. *Neural Development, 12*(1), 1-10.

Ersfeld, K., Wehland, J., Plessmann, U., Dodemont, H., Gerke, V., & Weber, K. (1993). Characterization of the Tubulin Tyrosine Ligase. *Journal of Cell Biology, 120*(3), 725-732.

Erturk, A., Hellal, F., Enes, J., & Bradke, F. (2007). Disorganized microtubules underlie the formation of retraction bulbs and the failure of axonal regeneration. *Journal of Neuroscience, 27*(34), 9169-9180.

Ferreira, J. G., Pereira, A. J., Akhmanova, A., & Maiato, H. (2013). Aurora B spatially regulates EB3 phosphorylation to coordinate daughter cell adhesion with cytokinesis. *Journal of Cell Biology, 201*(5), 709-724.

Firestone, A. J., Weinger, J. S., Maldonado, M., Barlan, K., Langston, L. D., O'Donnell, M., … & Chen, J. K. (2012). Small-molecule inhibitors of the AAA plus ATPase motor cytoplasmic dynein. *Nature, 484*(7392), 125-129.

Gallo, G. (2011). The neuronal actin cytoskeleton and the protrusion of lamellipodia and filopodia. In G. Gallo & L. M. Lanier (Eds.), *Neurobiology of Actin: From Neurulation to Synaptic Function* (Vol. 5, pp. 7-22). New York, NY: Springer.

Geraldo, S., & Gordon-Weeks, P. R. (2009). Cytoskeletal dynamics in growth-cone steering. *Journal of cell science, 122*(20), 3595-604.

Gomez, T. M., & Letourneau, P. C. (2014). Actin dynamics in growth cone motility and navigation. *Journal of Neurochemistry, 129*(2), 221-234.

Gouveia, S. M., & Akhmanova, A. (2010). Cell and molecular biology of microtubule plus end tracking proteins: End binding proteins and their partners. In K. W. Jeon (Ed.), *International Review of Cell and Molecular Biology* (Vol. 285, pp. 1-74). San Diego, CA: Elsevier.

Gouveia, S. M., Leslie, K., Kapitein, L. C., Buey, R. M., Grigoriev, I., Wagenbach, M., ... & Steinmetz, M. O. (2010). In vitro reconstitution of the functional interplay between MCAK and EB3 at microtubule plus ends. *Current Biology, 20*(19), 1717-1722.

Grabham, P. W., Seale, G. E., Bennecib, M., Goldberg, D. J., & Vallee, R. B. (2007). Cytoplasmic dynein and LIS1 are required for microtubule advance during growth cone remodeling and fast axonal outgrowth. *Journal of Neuroscience, 27*(21), 5823-5834.

Grego, S., Cantillana, V., & Salmon, E. D. (2001). Microtubule treadmilling in vitro investigated by fluorescence speckle and confocal microscopy. *Biophysical Journal, 81*(1), 66-78.

Gundersen, G. G., Khawaja, S., & Bulinski, J. C. (1987). Postpolymerization detyrosination of alpha-tubulin - a mechanism for subcellular differentiation of microtubules. *Journal of Cell Biology, 105*(1), 251-264.

Gupta, K. K., Alberico, E. O., Nathke, I. S., & Goodson, H. V. (2014). Promoting microtubule assembly: A hypothesis for the functional significance of the plus TIP network. *Bioessays, 36*(9), 818-826.

Gupta, M. L., Carvalho, P., Roof, D. M., & Pellman, D. (2006). Plus end-specific depolymerase activity of Kip3, a kinesin-8 protein, explains its role in positioning the yeast mitotic spindle. *Nature Cell Biology, 8*(9), 913-923.

Hafner, J., Mayr, M. I., Mockel, M. M., & Mayer, T. U. (2014). Pre-anaphase chromosome oscillations are regulated by the antagonistic activities of Cdk1 and PP1 on Kif18A. *Nature Communications, 5*(4397), 1-14.

Hayashi, I., & Ikura, M. (2003). Crystal structure of the amino-terminal microtubule-binding domain of end-binding protein 1 (EB1). *Journal of Biological Chemistry,* 278(38), 36430-36434.

He, Y. P., Ren, Y., Wu, B. B., Decourt, B., Lee, A. C., Taylor, A., & Suter, D. M. (2015). Src and cortactin promote lamellipodia protrusion and filopodia formation and stability in growth cones. *Molecular Biology of the Cell, 26*(18), 3229-3244.

Heidemann, S. R., Lamoureux, P., & Buxbaum, R. E. (1990). Growth cone behavior and production of traction force. *Journal of Cell Biology, 111*(5), 1949-1957.

Heidemann, S. R., Landers, J. M., & Hamborg, M. A. (1981). Polarity orientation of axonal microtubules. *Journal of Cell Biology, 91*(3), 661-665.

Hendricks, A. G., Lazarus, J. E., Perlson, E., Gardner, M. K., Odde, D. J., Goldman, Y. E., & Holzbaur, E. L. F. (2012). Dynein tethers and stabilizes dynamic microtubule plus ends. *Current Biology, 22*(7), 632-637.

Honnappa, S., Gouveia, S. M., Weisbrich, A., Damberger, F. F., Bhavesh, N. S., Jawhari, H., ... & Jelesarov, I. (2009). An EB1-binding motif acts as a microtubule tip localization signal. *Cell, 138*(2), 366-376.

Houseweart, M. K., & Cleveland, D. W. (1999). Cytoskeletal linkers: New MAPs for old destinations. *Current Biology, 9*(22), R864-R866.

Howard, J., & Hyman, A. A. (2007). Microtubule polymerases and depolymerases. *Current Opinion in Cell Biology, 19*(1), 31-35.

Howard, J., Zanic, M., & Gardner, M. (2011). The depolymerizing kinesins Kip3 (kinesin-8) and MCAK (kinesin-13) are catastrophe factors that destabilize microtubules by different mechanisms. *Molecular Biology of the Cell, 147*(5), 1092-1103.

Huang, F., Hartwich, T. M. P., Rivera-Molina, F. E., Lin, Y., Duim, W. C., Long, J. J., ... & Davidson, M. W. (2013). Video-rate nanoscopy using sCMOS camera-specific single-molecule localization algorithms. *Nature Methods, 10*(7), 653-658.

Huang, J., Roberts, A. J., Leschziner, A. E., & Reck-Peterson, S. L. (2012). Lis1 acts as a "clutch" between the ATPase and microtubule-binding domains of the dynein motor. *Cell, 150*(5), 975-986.

Hubbert, C., Guardiola, A., Shao, R., Kawaguchi, Y., Ito, A., Nixon, A., Yoshida, M., Wang, X. F., & Yao, T. P. (2002). HDAC6 is a microtubule-associated deacetylase. *Nature, 417*(6887), 455-458.

Hunter, A. W., Caplow, M., Coy, D. L., Hancock, W. O., Diez, S., Wordeman, L., & Howard, J. (2003). The kinesin-related protein MCAK is a microtubule depolymerase that forms an ATP-hydrolyzing complex at microtubule ends. *Molecular Cell, 11*(2), 445-457.

Hunyadi, V., Chretien, D., & Janosi, I. M. (2005). Mechanical stress induced mechanism of microtubule catastrophes. *Journal of Molecular Biology, 348*(4), 927-938.

Hur, E. M., & Zhou, F. Q. (2010). GSK3 signalling in neural development. *Nature Reviews Neuroscience, 11*(8), 539-551.

Hur, E. M., Saijilafu, & Zhou, F. Q. (2012). Growing the growth cone: Remodeling the cytoskeleton to promote axon regeneration. *Trends in Neurosciences, 35*(3), 164-174.

Hur, E. M., Yang, I. H., Kim, D. H., Byun, J., Saijilafu, Xu, W. L., Nicovich, P. R., … & Zhou, F. Q. (2011). Engineering neuronal growth cones to promote axon regeneration over inhibitory molecules. *Proceedings of the National Academy of Sciences of the United States of America, 108*(12), 5057-5062.

Hussmann, F., Drummond, D. R., Peet, D. R., Martin, D. S., & Cross, R. A. (2016). Alp7/TACC-Alp14/TOG generates long-lived, fast-growing MTs by an unconventional mechanism. *Scientific Reports, 6*(20653), 1-15.

Hutchins, B. I., & Wray, S. (2014). Capture of microtubule plus-ends at the actin cortex promotes axophilic neuronal migration by enhancing microtubule tension in the leading process. *Frontiers in Cellular Neuroscience, 8*(400), 1-8.

Hyman, A. A., Chretien, D., Arnal, I., & Wade, R. H. (1995). Structural changes accompanying GTP hydrolysis in microtubules - information from a slowly hydrolyzable analog guanylyl-(alpha,beta)-methylene-diphosphonate. *Journal of Cell Biology, 128*(1), 117-125.

Hysolli, E. (2018). PAINT-ing the future of fluorescence imaging. Retrieved from https://wyss.harvard.edu/paint-ing-the-future-of-fluorescence-imaging/

Iimori, M., Ozaki, K., Chikashige, Y., Habu, T., Hiraoka, Y., Maki, T., Hayashi, I., Obuse, C., & Matsumoto, T. (2012). A mutation of the fission yeast EB1 overcomes negative regulation by phosphorylation and stabilizes microtubules. *Experimental Cell Research, 318*(3), 262-275.

Inoue, S., & Salmon, E. D. (1995). Force generation by microtubule assembly disassembly in mitosis and related movements. *Molecular Biology of the Cell, 6*(12), 1619-1640.

Insel, T. (2015). Mental health awareness month: By the numbers. Retrieved from https://www.nimh.nih.gov/about/directors/thomas-insel/blog/2015/mental-health-awareness-month-by-the-numbers.shtml

Insel, T. R. (2008). Assessing the economic costs of serious mental illness. *American Journal of Psychiatry, 165*(6), 663-665.

Janke, C., & Bulinski, J. C. (2011). Post-translational regulation of the microtubule cytoskeleton: mechanisms and functions. *Nature Reviews Molecular Cell Biology, 12*(12), 773-786.

Janson, M. E., De Dood, M. E., & Dogterom, M. (2003). Dynamic instability of microtubules is regulated by force. *Journal of Cell Biology, 161*(6), 1029-1034.

Jaqaman, K., Loerke, D., Mettlen, M., Kuwata, H., Grinstein, S., Schmid, S. L., & Danuser, G. (2008). Robust single-particle tracking in live-cell time-lapse sequences. *Nature Methods, 5*(8), 695-702.

Jefferson, J. J., Leung, C. L., & Liem, R. K. H. (2004). Plakins: Goliaths that link cell junctions and the cytoskeleton. *Nature Reviews Molecular Cell Biology, 5*(7), 542-553.

Jordan, M. A., & Kamath, K. (2007). How do microtubule-targeted drugs work? An overview. *Current Cancer Drug Targets, 7*(8), 730-742.

Joshi, H. C., Chu, D., Buxbaum, R. E., & Heidemann, S. R. (1985). Tension and compression in the cytoskeleton of PC-12 neurites. *Journal of Cell Biology, 101*(3), 697-705.

Jungmann, R., Avendano, M. S., Woehrstein, J. B., Dai, M. J., Shih, W. M., & Yin, P. (2014). Multiplexed 3D cellular super-resolution imaging with DNA-PAINT and Exchange-PAINT. *Nature Methods, 11*(3), 313-318.

Kalil, K., & Dent, E. W. (2014). Branch management: Mechanisms of axon branching in the developing vertebrate CNS. *Nature Reviews Neuroscience, 15*(1), 7-18.

Kapitein, L. C., & Hoogenraad, C. C. (2015). Building the neuronal microtubule cytoskeleton. *Neuron, 87*(3), 492-506.

Kapur, M., Wang, W., Maloney, M. T., Millan, I., Lundin, V. F., Tran, T. A., & Yang, Y. M. (2012). Calcium tips the balance: A microtubule plus end to lattice binding switch operates in the carboxyl terminus of BPAG1n4. *Embo Reports, 13*(11), 1021-1029.

Khawaja, S., Gundersen, G. G., & Bulinski, J. C. (1988). Enhanced stability of microtubules enriched in detyrosinated tubulin is not a direct function of detyrosination level. *Journal of Cell Biology, 106*(1), 141-149.

King, S. M., Barbarese, E., Dillman, J. F., PatelKing, R. S., Carson, J. H., & Pfister, K. K. (1996). Brain cytoplasmic and flagellar outer arm dyneins share a highly conserved M(r) 8,000 light chain. *Journal of Biological Chemistry, 271*(32), 19358-19366.

Komarova, Y. A., Akhmanova, A. S., Kojima, S., Galjart, N., & Borisy, G. G. (2002). Cytoplasmic linker proteins promote microtubule rescue in vivo. *Journal of Cell Biology, 159*(4), 589-599.

Komarova, Y., De Groot, C. O., Grigoriev, I., Gouveia, S. M., Munteanu, E. L., Schober, J. M., … & Borisy, G. G.(2009). Mammalian end binding proteins control persistent microtubule growth. *Journal of Cell Biology, 184*(5), 691-706.

Konishi, Y., & Setou, M. (2009). Tubulin tyrosination navigates the kinesin-1 motor domain to axons. *Nature Neuroscience, 12*(5), 559-567.

Korobova, F., & Svitkina, T. (2008). Arp2/3 complex is important for filopodia formation, growth cone motility, and neuritogenesis in neuronal cells. *Molecular Biology of the Cell, 19*(4), 1561-1574.

Koshland, D. E., Mitchison, T. J., & Kirschner, M. W. (1988). Polewards chromosome movement driven by microtubule depolymerization in vitro. *Nature, 331*(6156), 499-504.

Kumar, P., & Wittmann, T. (2012). +TIPs: SxIPping along microtubule ends. *Trends Cell Biology, 22*(8), 418-28.

Kumar, P., Chimenti, M. S., Pemble, H., Schonichen, A., Thompson, O., Jacobson, M. P., & Wittmann, T. (2012). Multisite phosphorylation disrupts arginine-glutamate salt bridge networks required for binding of cytoplasmic linker-associated protein 2 (CLASP2) to end-binding protein 1 (EB1). *Journal of Biological Chemistry, 287*(21), 17050-17064.

Laan, L., Pavin, N., Husson, J., Romet-Lemonne, G., Van Duijn, M., Lopez, M. P., Vale, R. D., Julicher, F., Reck-Peterson, S. L., & Dogterom, M. (2012). Cortical dynein controls microtubule dynamics to generate pulling forces that position microtubule asters. *Cell, 148*(3), 502-514.

Lacroix, B., Van Dijk, J., Gold, N. D., Guizetti, J., Aldrian-Herrada, G., Rogowski, K., Gerlich, D. W., & Janke, C. (2010). Tubulin polyglutamylation stimulates spastin-mediated microtubule severing. *Journal of Cell Biology, 189*(6), 945-954.

Lamoureux, P., Buxbaum, R. E., & Heidemann, S. R. (1989). Direct evidence that growth cones pull. *Nature, 340*(6229), 156-162.

Lansbergen, G., Komarova, Y., Modesti, M., Wyman, C., Hoogenraad, C. C., Goodson, H. V., ... & Grosveld, F. (2004). Conformational changes in CLIP-170 regulate its binding to microtubules and dynactin localization. *Journal of Cell Biology, 166*(7), 1003-1014.

Lazarus, J. E., Moughamian, A. J., Tokito, M. K., & Holzbaur, E. L. F. (2013). Dynactin subunit p150(Glued) is a neuron-specific anti-catastrophe factor. *Plos Biology, 11*(7), 1-12.

Ledizet, M., & Piperno, G. (1987). Identification of an acetylation site of Chlamydomonas alpha-tubulin. *Proceedings of the National Academy of Sciences of the United States of America, 84*(16), 5720-5724.

Lee, A. C., & Suter, D. M. (2008). Quantitative analysis of microtubule dynamics during adhesion-mediated growth cone guidance. *Developmental Neurobiology, 68*(12), 1363-1377.

Letourneau, P. C., & Ressler, A. H. (1984). Inhibition of neurite initiation and growth by taxol. *The Journal of cell biology*, *98*(4), 1355-62.

Letourneau, P. C., Shattuck, T. A., & Ressler, A. H. (1987). Pull and push in neurite elongation - observations on the effects of different concentrations of cytochalasin-B and taxol. *Cell Motility and the Cytoskeleton, 8*(3), 193-209.

Leung, C. L., Sun, D. M., Zheng, M., Knowles, D. R., & Liem, R. K. H. (1999). Microtubule actin cross-linking factor (MACF): A hybrid of dystonin and dystrophin that can interact with the actin and microtubule cytoskeletons. *Journal of Cell Biology, 147*(6), 1275-1285.

Lewis, A. K., & Bridgman, P. C. (1992). Nerve growth cone lamellipodia contain two populations of actin-filaments that differ in organization and polarity. *Journal of Cell Biology, 119*(5), 1219-1243.

Liem, R. K. H. (2016). Cytoskeletal integrators: The spectrin superfamily. *Cold Spring Harbor Perspectives in Biology, 8*(10), 1-12.

Lowery, L. A., & Van Vactor, D. (2009). The trip of the tip: Understanding the growth cone machinery. *Nature Reviews Molecular Cell Biology, 10*(5), 332-343.

Lu, W., & Gelfand, V. I. (2017). Moonlighting motors: Kinesin, dynein, and cell polarity. *Trends in Cell Biology, 27*(7), 505-514.

Lu, W., Fox, P., Lakonishok, M., Davidson, M. W., & Gelfand, V. I. (2013). Initial neurite outgrowth in *Drosophila* neurons is driven by kinesin-powered microtubule sliding. *Current Biology, 23*(11), 1018-1023.

Lu, W., Lakonishok, M., & Gelfand, V. I. (2015). Kinesin-1-powered microtubule sliding initiates axonal regeneration in Drosophila cultured neurons. *Molecular Biology of the Cell, 26*(7), 1296-1307.

Magoski, N. S. (2017). Electrical synapses and neuroendocrine cell function. In J. Jing (Ed.), *Network Functions and Plasticity: Perspectives from Studying Neuronal Electrical Coupling in Microcircuits* (pp.137-160). Cambridge, MA: Acedemic Press.

Mallavarapu, A., & Mitchison, T. (1999). Regulated actin cytoskeleton assembly at filopodium tips controls their extension and retraction. *Journal of Cell Biology, 146*(5), 1097-1106.

Mandelkow, E. M., Milligan, R. A., Trinczek, B., Obermann, H., Marx, A., & Mandelkow, E. (1991). Microtubule dynamics and microtubule caps. *Journal of Muscle Research and Cell Motility, 12*(5), 496-497.

Marx, A., Godinez, W. J., Tsimashchuk, V., Bankhead, P., Rohr, K., & Engel, U. (2013). Xenopus cytoplasmic linker-associated protein 1 (XCLASP1) promotes axon elongation and advance of pioneer microtubules. *Molecular Biology of the Cell, 24*(10), 1544-1558.

McKenney, R. J., Huynh, W., Tanenbaum, M. E., Bhabha, G., & Vale, R. D. (2014). Activation of cytoplasmic dynein motility by dynactin-cargo adapter complexes. *Science, 345*(6194), 337-341.

McKenney, R. J., Vershinin, M., Kunwar, A., Vallee, R. B., & Gross, S. P. (2010). LIS1 and NudE induce a persistent dynein force-producing state. *Cell, 141*(2), 304-314.

McMurray, C. T. (2000). Neurodegeneration: Diseases of the cytoskeleton? *Cell Death and Differentiation, 7*(10), 861-865.

McNally, F. J., & Vale, R. D. (1993). Identification of katanin, an ATPase that severs and disassembles stable microtubules. *Cell, 75*(3), 419-429.

Medeiros, N. A., Burnette, D. T., & Forscher, P. (2006). Myosin II functions in actin-bundle turnover in neuronal growth cones. *Nature Cell Biology, 8*(3), 215-226.

Millecamps, S., & Julien, J. P. (2013). Axonal transport deficits and neurodegenerative diseases. *Nature Reviews Neuroscience, 14*(3), 161-176.

Miller, K. E., & Suter, D. M. (2018). An integrated cytoskeletal model of neurite outgrowth. *Frontiers in Cellular Neuroscience, 12*, 1-19.

Mimori-Kiyosue, Y., Grigoriev, I., Lansbergen, G., Sasaki, H., Matsui, C., Severin, F., ... & Akhmanova, A. (2005). CLASP1 and CLASP2 bind to EB1 and regulate microtubule plus-end dynamics at the cell cortex. *Journal of Cell Biology, 168*(1), 141-153.

Mitchison, T., & Kirschner, M. (1984a). Dynamic instability of microtubule growth. *Nature. 312*(5991), 237-242.

Mitchison, T., & Kirschner, M. (1984b). Microtubule assembly nucleated by isolated centrosomes. *Nature, 312*(5991), 232-237.

Mitchison, T., & Kirschner, M. (1988). Cytoskeletal dynamics and nerve growth. *Neuron, 1*(9), 761-772.

Moores, C. A., Yu, M., Guo, J., Beraud, C., Sakowicz, R., & Milligan, R. A. (2002). A mechanism for microtubule depolymerization by KinI kinesins. *Molecular Cell, 9*(4), 903-909.

Moroz, L. (2011). *Aplysia*. *Current Biology*, *21*(2), R60-R61.

Moroz, L. L., Edwards, J. R., Puthanveettil, S. V., Kohn, A. B., Hla, T., Heyland, A., ... & Jezzini, S. (2006). Neuronal transcriptome of *Aplysia*: Neuronal compartments and circuitry. *Cell, 127*(7), 1453-1467.

Moser, B., Hochreiter, B., Herbst, R., & Schmid, J. A. (2017). Fluorescence colocalization microscopy analysis can be improved by combining object-recognition with pixel-intensity-correlation. *Biotechnology Journal, 12*(1), 1-8.

Myers, K. A., Tint, I., Nadar, C. V., He, Y., Black, M. M., & Baas, P. W. (2006). Antagonistic forces generated by cytoplasmic dynein and myosin-II during growth cone turning and axonal retraction. *Traffic, 7*(10), 1333-1351.

Nawrotek, A., Knossow, M., & Gigant, B. (2011). The determinants that govern microtubule assembly from the atomic structure of GTP-tubulin. *Journal of Molecular Biology, 412*(1), 35-42.

Nehlig, A., Molina, A., Rodrigues-Ferreira, S., Honore, S., & Nahmias, C. (2017). Regulation of end-binding protein EB1 in the control of microtubule dynamics. *Cellular and Molecular Life Sciences, 74*(13), 2381-2393.

Nieves, D. J., Gaus, K., & Baker, M. A. B. (2018). DNA-based super-resolution microscopy: DNA-PAINT. *Genes, 9*(12), 1-14.

Noordstra, I., Liu, Q. Y., Nijenhuis, W., Hua, S. S., Jiang, K., Baars, M., … & Akhmanova, A. (2016). Control of apico-basal epithelial polarity by the microtubule minus-end-binding protein CAMSAP3 and spectraplakin ACF7. *Journal of Cell Science, 129*(22), 4278-4288.

North, B. J., Marshall, B. L., Borra, M. T., Denu, J. M., & Verdin, E. (2003). The human Sir2 ortholog, SIRT2, is an NAD(+)-dependent tubulin deacetylase. *Molecular Cell,* 11(2), 437-444.

Omotade, O. F., Pollitt, S. L., & Zheng, J. Q. (2017). Actin-based growth cone motility and guidance. *Molecular and Cellular Neuroscience, 84*, 4-10.

O'Toole, M., Lamoureux, P., & Miller, K. E. (2015). Measurement of subcellular force generation in neurons. *Biophysical Journal, 108*(5), 1027-1037.

Ouyang, W., Aristov, A., Lelek, M., Hao, X., & Zimmer, C. (2018). Deep learning massively accelerates super-resolution localization microscopy. *Nature Biotechnology, 36*(5), 460-468.

Perlson, E., Hendricks, A. G., Lazarus, J. E., Ben-Yaakov, K., Gradus, T., Tokito, M., & Holzbaur, E. L. F. (2013). Dynein interacts with the neural cell adhesion molecule (NCAM180) to tether dynamic microtubules and maintain synaptic density in cortical neurons. *Journal of Biological Chemistry, 288*(39), 27812-27824.

Pfister, K. (2016). *The neuronal cytoskeleton, motor proteins, and organelle trafficking in the axon*. Cambridge, MA: Elsevier.

Pfister, K. K., Shah, P. R., Hummerich, H., Russ, A., Cotton, J., Annuar, A. A., King, S. M., & Fisher, E. M. C. (2006). Genetic analysis of the cytoplasmic dynein subunit families. *Plos Genetics* 2, 11-26.

Pollard, T., Earnshaw, W., Lippincott-Schwartz, J., & Johnson, G. (2017). *Cell Biology* (3th ed.). Cambridge, MA: Elsevier.

Portran, D., Schaedel, L., Xu, Z. J., Thery, M., & Nachury, M. V. (2017). Tubulin acetylation protects long-lived microtubules against mechanical ageing. *Nature Cell Biology, 19*(4), 391-398.

Rasband, W. S. (2018). ImageJ (1.51m9) [Software]. Retrieved from https://imagej.nih.gov/ij/

Ravelli, R. B. G., Gigant, B., Curmi, P. A., Jourdain, I., Lachkar, S., Sobel, A., & Knossow, M. (2004). Insight into tubulin regulation from a complex with colchicine and a stathmin-like domain. *Nature, 428*(6979), 198-202.

Raybin, D., & Flavin, M. (1975). Enzyme tryosylating alpha-tubulin and its role in microtubule assembly. *Biochemical and Biophysical Research Communications, 65*(3), 1088-1095.

Reck-Peterson, S. L., Redwine, W. B., Vale, R. D., & Carter, A. P. (2018). The cytoplasmic dynein transport machinery and its many cargoes. *Nature Reviews Molecular Cell Biology, 19*(6), 382-398.

Rice, L. M., Montabana, E. A., & Agard, D. A. (2008). The lattice as allosteric effector: Structural studies of alpha beta- and gamma-tubulin clarify the role of GTP in microtubule assembly. *Proceedings of the National Academy of Sciences of the United States of America, 105*(14), 5378-5383.

Roberts, A. J., Kon, T., Knight, P. J., Sutoh, K., & Burgess, S. A. (2013). Functions and mechanics of dynein motor proteins. *Nature Reviews Molecular Cell Biology, 14*(11), 713-726.

Rochlin, M. W., Wickline, K. M., & Bridgman, P. C. (1996). Microtubule stability decreases axon elongation but not axoplasm production. *Journal of Neuroscience, 16*(10), 3236-3246.

Roossien, D. H., Lamoureux, P., & Miller, K. E. (2014). Cytoplasmic dynein pushes the cytoskeletal meshwork forward during axonal elongation. *Journal of Cell Science, 127*(16), 3593-3602.

Roossien, D. H., Lamoureux, P., Van Vactor, D., & Miller, K. E. (2013). Drosophila growth cones advance by forward translocation of the neuronal cytoskeletal meshwork in vivo. *Plos One, 8*(11), 1-12.

Roossien, D. H., Miller, K. E., & Gallo, G. (2015). Ciliobrevins as tools for studying dynein motor function. *Frontiers in Cellular Neuroscience, 9*, 1-10.

Roper, K., & Brown, N. H. (2003). Maintaining epithelial integrity: A function for gigantic spectraplakin isoforms in adherens junctions. *Journal of Cell Biology, 162*(7), 1305-1315.

Roper, K., Gregory, S. L., & Brown, N. H. (2002). The ‘spectraplakins': Cytoskeletal giants with characteristics of both spectrin and plakin families. *Journal of Cell Science, 115*(22), 4215-4225.

Sainath, R., & Gallo, G. (2015). The dynein inhibitor ciliobrevin D inhibits the bidirectional transport of organelles along sensory axons and impairs NGF-mediated regulation of growth cones and axon branches. *Developmental Neurobiology, 75*(7), 757-777.

Schaefer, A. W., Kabir, N., & Forscher, P. (2002). Filopodia and actin arcs guide the assembly and transport of two populations of microtubules with unique dynamic parameters in neuronal growth cones. *Journal of Cell Biology, 158*(1), 139-152.

Schaefer, A. W., Schoonderwoert, V. T., Ji, L., Mederios, N., Danuser, G., & Forscher, P. (2008). Coordination of actin filament and microtubule dynamics during neurite outgrowth. *Dev Cell, 15*(1), 146-162.

Schindelin, J., Arganda-Carreras, I., Frise, E., Kaynig, V., Longair, M., Pietzsch, T., ... & Tinevez, J. Y. (2012). Fiji: An open-source platform for biological-image analysis. *Nature Methods, 9*(7), 676-682.

Schneider, C. A., Rasband, W. S., & Eliceiri, K. W. (2012). NIH image to ImageJ: 25 years of image analysis. *Nature Methods, 9*(7), 671-675.

Schnitzbauer, J., Strauss, M. T., Schlichthaerle, T., Schueder, F., & Jungmann, R. (2017). Super-resolution microscopy with DNA-PAINT. *Nature Protocols, 12*(6), 1198-1228.

Sengottuvel, V., Leibinger, M., Pfreimer, M., Andreadaki, A., & Fischer, D. (2011). Taxol facilitates axon regeneration in the mature CNS. *Journal of Neuroscience, 31*(7), 2688-2699.

Siglin, A. E., Sun, S. J., Moore, J. K., Tan, S., Poenie, M., Lear, J. D., … & Williams, J. C. (2013). Dynein and dynactin leverage their bivalent character to form a high-affinity interaction. *Plos One, 8*(4), 1-15.

Slep, K. C., Rogers, S. L., Elliott, S. L., Ohkura, H., Kolodziej, P. A., & Vale, R. D. (2005). Structural determinants for EB1-mediated recruitment of APC and spectraplakins to the microtubule plus end. *Journal of Cell Biology, 168*(4), 587-598.

Song, Y. Y., & Brady, S. T. (2015). Post-translational modifications of tubulin: Pathways to functional diversity of microtubules. *Trends in Cell Biology, 25*(3), 125-136.

Sonnenberg, A., Rojas, A. M., & De Pereda, J. M. (2007). The structure of a tandem pair of spectrin repeats of plectin reveals a modular organization of the plakin domain. *Journal of Molecular Biology, 368*(5), 1379-1391.

Stahnisch, F. W., & Nitsch, R. (2002). Santiago Ramon y Cajal's concept of neuronal plasticity: The ambiguity lives on. *Trends in Neurosciences, 25*(11), 589-591.

Steinmetz, M. O., Kammerer, R. A., Jahnke, W., Goldie, K. N., Lustig, A., & Van Oostrum, J. (2000). Op18/stathmin caps a kinked protofilament-like tubulin tetramer. *Embo Journal, 19*(4), 572-580.

Stiess, M., Maghelli, N., Kapitein, L. C., Gomis-Ruth, S., Wilsch-Brauninger, M., Hoogenraad, … ., & Bradke, F. (2010). Axon extension occurs independently of centrosomal microtubule nucleation. *Science, 327*(5966), 704-707.

Stumpff, J., Von Dassow, G., Wagenbach, M., Asbury, C., & Wordeman, L. (2008). The kinesin-8 motor Kif18A suppresses kinetochore movements to control mitotic chromosome alignment. *Developmental Cell, 14*(2), 252-262.

Sudo, H., & Baas, P. W. (2010). Acetylation of microtubules influences their sensitivity to severing by katanin in neurons and fibroblasts. *Journal of Neuroscience, 30*(21), 7215-7226.

Sun, D. M., Leung, C. L., & Liem, R. K. H. (2001). Characterization of the microtubule binding domain of microtubule actin crosslinking factor (MACF): Identification of a novel group of microtubule associated proteins. *Journal of Cell Science, 114*(1), 161-172.

Suozzi, K. C., Wu, X. Y., & Fuchs, E. (2012). Spectraplakins: Master orchestrators of cytoskeletal dynamics. *Journal of Cell Biology, 197*(4), 465-475.

Suter, D. M., & Forscher, P. (1998). An emerging link between cytoskeletal dynamics and cell adhesion molecules in growth cone guidance. *Current Opinion in Neurobiology, 8*(1), 106-116.

Suter, D. M., & Forscher, P. (2000). Substrate-cytoskeletal coupling as a mechanism for the regulation of growth cone motility and guidance. *Journal of Neurobiology, 44*(2), 97-113.

Suter, D. M., & Miller, K. E. (2011). The emerging role of forces in axonal elongation. *Progress in Neurobiology, 94*(2), 91-101.

Suter, D. M., Schaefer, A. W., & Forscher, P. (2004). Microtubule dynamics are necessary for Src family kinase-dependent growth cone steering. *Current Biology, 14*(13), 1194-1199.

Szyk, A., Deaconescu, A. M., Spector, J., Goodman, B., Valenstein, M. L., Ziolkowska, N. E., … & Roll-Mecak, A. (2014). Molecular basis for age-dependent microtubule acetylation by tubulin acetyltransferase. *Cell, 157*(6), 1405-1415.

Takano, T., Wu, M. Y., Nakamuta, S., Naoki, H., Ishizawa, N., Namba, T., ... & Amano, M. (2017). Discovery of long-range inhibitory signaling to ensure single axon formation. *Nature Communications, 8*(33), 1-18.

Tamariz, E., & Varela-Echavarria, A. (2015). The discovery of the growth cone and its influence on the study of axon guidance. *Frontiers in Neuroanatomy, 9*, 1-9.

Tan, L., Jiang, T., & Yu, J. T. (2016). Toward precision medicine in neurological diseases. *Annals of Translational Medicine, 4*(6), 1-7.

Tanaka, E. M., & Kirschner, M. W. (1991). Microtubule behavior in the growth cones of living neurons during axon elongation *Journal of Cell Biology, 115*(2), 345-363.

Tanaka, E., Ho, T., & Kirschner, M. W. (1995). The role of microtubule dynamics in growth cone motility and axonal growth. *Journal of Cell Biology, 128*(1), 139-155.

Tanenbaum, M. E., Vale, R. D., & McKenney, R. J. (2013). Cytoplasmic dynein crosslinks and slides anti-parallel microtubules using its two motor domains. *Elife, 2*, 1-20.

Tanielian, T., Jaycox, L. H., Schell, T. L., Marshall, G. N., Burnam, M. A., Eibner, C., … & Viana, M. E. (2008). *Invisible wounds of war. Summary and recommendations for addressing psychological and cognitive injuries*. Retrieved from https://apps.dtic.mil/dtic/tr/fulltext/u2/a480992.pdf

Tokunaga, M., Imamoto, N., & Sakata-Sogawa, K. (2008). Highly inclined thin illumination enables clear single-molecule imaging in cells. *Nature Methods, 5*(2), 159-162.

Turney, S. G., & Bridgman, P. C. (2005). Laminin stimulates and guides axonal outgrowth via growth cone myosin II activity. *Nature Neuroscience, 8*(6), 717-719.

Urnavicius, L., Zhang, K., Diamant, A. G., Motz, C., Schlager, M. A., Yu, M. M., … & Carter, A. P. (2015). The structure of the dynactin complex and its interaction with dynein. *Science, 347*(6229), 1441-1446.

Vale, R. D. (2003). The molecular motor toolbox for intracellular transport. *Cell, 112*(4), 467-480.

Vallee, R. B., McKenney, R. J., & Ori-McKenney, K. M. (2012). Multiple modes of cytoplasmic dynein regulation. *Nature Cell Biology, 14*(3), 224-230.

Vallee, R. B., Seale, G. E., & Tsai, J. W. (2009). Emerging roles for myosin II and cytoplasmic dynein in migrating neurons and growth cones. *Trends in Cell Biology, 19*(7), 347-355.

Van der Vaart, B., Akhmanova, A., & Straube, A. (2009). Regulation of microtubule dynamic instability. *Biochemical Society Transactions, 37*(5), 1007-1013.

Van der Vaart, B., Manatschal, C., Grigoriev, I., Olieric, V., Gouveia, S. M., Bjelic, S., … & Akhmanova, A (2011). SLAIN2 links microtubule plus end-tracking proteins and controls microtubule growth in interphase. *Journal of Cell Biology, 193*(6), 1083-1099.

Van Dijk, J., Miro, J., Strub, J. M., Lacroix, B., Van Dorsselaer, A., Edde, B., & Janke, C. (2008). Polyglutamylation is a post-translational modification with a broad range of substrates. *Journal of Biological Chemistry, 283*(7), 3915-3922.

Varga, V., Helenius, J., Tanaka, K., Hyman, A. A., Tanaka, T. U., & Howard, J. (2006). Yeast kinesin-8 depolymerizes microtubules in a length-dependent manner. *Nature Cell Biology, 8*(9), 957-960.

Varga, V., Leduc, C., Bormuth, V., Diez, S., & Howard, J. (2009). Kinesin-8 motors act cooperatively to mediate length-dependent microtubule depolymerization. *Cell, 138*(6), 1174-1183.

Vasquez, R. J., Howell, B., Yvon, A. M. C., Wadsworth, P., & Cassimeris, L. (1997). Nanomolar concentrations of nocodazole alter microtubule dynamic instability in vivo and in vitro. *Molecular Biology of the Cell, 8*(6), 973-985.

Voelzmann, A., Hahn, I., Pearce, S. P., Sanchez-Soriano, N., & Prokop, A. (2016). A conceptual view at microtubule plus end dynamics in neuronal axons. *Brain Research Bulletin, 126*(3), 226-237.

Walker, R. A., Obrien, E. T., Pryer, N. K., Soboeiro, M. F., Voter, W. A., Erickson, H. P., & Salmon, E. D. (1988). Dynamic instability of individual microtubules analyzed by video light-microscopy - rate constants and transition frequencies. *Journal of Cell Biology, 107*(4), 1437-1448.

Wang, Y., Woehrstein, J. B., Donoghue, N., Dai, M. J., Avendano, M. S., Schackmann, R. C. J., ... & Lapan, S. W. (2017). Rapid sequential in situ multiplexing with DNA exchange imaging in neuronal cells and tissues. *Nano Letters, 17*(10), 6131-6139.

Waterman-Storer, C. M., & Salmon, E. D. (1997). Actomyosin-based retrograde flow of microtubules in the lamella of migrating epithelial cells influences microtubule dynamic instability and turnover and is associated with microtubule breakage and treadmilling. *Journal of Cell Biology, 139*(2), 417-434.

Waterman-Storer, C. M., & Salmon, E. D. (1998). How microtubules get fluorescent speckles. *Biophysical Journal, 75*(4), 2059-2069.

Watson, P., & Stephens, D. J. (2006). Microtubule plus-end loading of $p150^{Glued}$ is mediated by EB1 and CLIP-170 but is not required for intracellular membrane traffic in mammalian cells. *Journal of Cell Science, 119*(13), 2758-2767.

Webster, D. R., Wehland, J., Weber, K., & Borisy, G. G. (1990). Detyrosination of alpha-tubulin does not stabilize microtubules in vivo. *Journal of Cell Biology, 111*(1), 113-122.

Wickstead, B., & Gull, K. (2007). Dyneins across eukaryotes: A comparative genomic analysis. *Traffic, 8*(12), 1708-1721.

Wiese, C., & Zheng, Y. X. (2006). Microtubule nucleation: Gamma-tubulin and beyond. *Journal of Cell Science, 119*(20), 4143-4153.

Witte, H., Neukirchen, D., & Bradke, F. (2008). Microtubule stabilization specifies initial neuronal polarization. *Journal of Cell Biology, 180*(3), 619-632.

Wloga, D., & Gaertig, J. (2010). Post-translational modifications of microtubules. *Journal of Cell Science, 123*(20), 3447-3455.

Wloga, D., Joachimiak, E., & Fabczak, H. (2017). Tubulin post-translational modifications and microtubule dynamics. *International Journal of Molecular Sciences, 18*(10), 1-18.

Wloga, D., Webster, D. M., Rogowski, K., Bre, M. H., Levilliers, N., Jerka-Dziadosz, M., Janke, C., Dougan, S. T., & Gaertig, J. (2009). TTLL3 is a tubulin glycine ligase that regulates the assembly of cilia. *Developmental Cell, 16*(6), 867-876.

Wong, J. H., & Hashimoto, T. (2017). Novel Arabidopsis microtubule-associated proteins track growing microtubule plus ends. *Bmc Plant Biology, 17*(1), 1-11.

Wu, X. Y., Kodama, A., & Fuchs, E. (2008). ACF7 regulates cytoskeletal-focal adhesion dynamics and migration and has ATPase activity. *Cell, 135*(1), 137-148.

Xia, P., Liu, X., Wu, B., Zhang, S. Y., Song, X. Y., Yao, P. Y., … & Yao, X. B. (2014). Super-resolution imaging reveals structural features of EB1 in microtubule plus-end tracking. *Molecular Biology of the Cell, 25*(25), 4166-4173.

Yali, Z., Wang, D., & Kelsey, M. (2009). Preparation of *Aplysia* sensory-motor neuron cell cultures. *Journal of Visualized Experiments, 28*, 1-3.

Yang, Q., Zhang, X. F., Van Goor, D., Dunn, A. P., Hyland, C., Medeiros, N., & Forscher, P. (2013). Protein kinase C activation decreases peripheral actin network density and increases central nonmuscle myosin II contractility in neuronal growth cones. *Molecular Biology of the Cell, 24*(19), 3097-3114.

Ye, Y. H., Meyer, H. H., & Rapoport, T. A. (2001). The AAA ATPase Cdc48/p97 and its partners transport proteins from the ER into the cytosol. *Nature,* 414(6864), 652-656.

Yogev, S., Maeder, C. I., Cooper, R., Horowitz, M., Hendricks, A. G., & Shen, K. (2017). Local inhibition of microtubule dynamics by dynein is required for neuronal cargo distribution. *Nature Communications, 8*, 1-14.

Yu, W. Q., & Baas, P. W. (1994). Changes in microtubule number and length during axon differentiation. *Journal of Neuroscience, 14*(5), 2818-2829.

Zhang, J. M., Yue, J. P., & Wu, X. Y. (2017). Spectraplakin family proteins-cytoskeletal crosslinkers with versatile roles. *Journal of Cell Science, 130*(15), 2447-2457.

Zhang, R., Alushin, G. M., Brown, A., & Nogales, E. (2015). Mechanistic origin of microtubule dynamic instability and its modulation by EB proteins. *Cell, 162*(4), 849-859.

Zimniak, T., Stengl, K., Mechtler, K., & Westermann, S. (2009). Phosphoregulation of the budding yeast EB1 homologue Bim1p by Aurora/Ipl1p. *Journal of Cell Biology, 186*(3), 379-391.